NUREG/CR-6401
CNWRA 95-017

Faulting in the Yucca Mountain Region

Critical Review and Analyses of Tectonic Data from the Central Basin and Range

Prepared by
D. A. Ferrill, G. L. Stirewalt, D. B. Henderson, J. A. Stamatakos, A. P. Morris, K. H. Spivey, CNWRA
B. P. Wernicke, CIT

Center for Nuclear Waste Regulatory Analyses
Southwest Research Institute

Division of Geological and Planetary Science
California Institute of Technology

Prepared for
U.S. Nuclear Regulatory Commission

AVAILABILITY NOTICE

Availability of Reference Materials Cited in NRC Publications

Most documents cited in NRC publications will be available from one of the following sources:

1. The NRC Public Document Room, 2120 L Street, NW., Lower Level, Washington, DC 20555-0001

2. The Superintendent of Documents, U.S. Government Printing Office, P. O. Box 37082, Washington, DC 20402-9328

3. The National Technical Information Service, Springfield, VA 22161-0002

Although the listing that follows represents the majority of documents cited in NRC publications, it is not intended to be exhaustive.

Referenced documents available for inspection and copying for a fee from the NRC Public Document Room include NRC correspondence and internal NRC memoranda; NRC bulletins, circulars, information notices, inspection and investigation notices; licensee event reports; vendor reports and correspondence; Commission papers; and applicant and licensee documents and correspondence.

The following documents in the NUREG series are available for purchase from the Government Printing Office: formal NRC staff and contractor reports, NRC-sponsored conference proceedings, international agreement reports, grantee reports, and NRC booklets and brochures. Also available are regulatory guides, NRC regulations in the *Code of Federal Regulations*, and *Nuclear Regulatory Commission Issuances*.

Documents available from the National Technical Information Service include NUREG-series reports and technical reports prepared by other Federal agencies and reports prepared by the Atomic Energy Commission, forerunner agency to the Nuclear Regulatory Commission.

Documents available from public and special technical libraries include all open literature items, such as books, journal articles, and transactions. *Federal Register* notices, Federal and State legislation, and congressional reports can usually be obtained from these libraries.

Documents such as theses, dissertations, foreign reports and translations, and non-NRC conference proceedings are available for purchase from the organization sponsoring the publication cited.

Single copies of NRC draft reports are available free, to the extent of supply, upon written request to the Office of Administration, Distribution and Mail Services Section, U.S. Nuclear Regulatory Commission, Washington, DC 20555-0001.

Copies of industry codes and standards used in a substantive manner in the NRC regulatory process are maintained at the NRC Library, Two White Flint North, 11545 Rockville Pike, Rockville, MD 20852-2738, for use by the public. Codes and standards are usually copyrighted and may be purchased from the originating organization or, if they are American National Standards, from the American National Standards Institute, 1430 Broadway, New York, NY 10018-3308.

DISCLAIMER NOTICE

NUREG/CR-6401
CNWRA 95-017

Faulting in the Yucca Mountain Region

Critical Review and Analyses of Tectonic Data from the Central Basin and Range

Manuscript Completed: February 1996
Date Published: March 1996

Prepared by
D. A. Ferrill, G. L. Stirewalt, D. B. Henderson, J. Stamatakos, A. P. Morris, K. H. Spivey, CNWRA
B. P. Wernicke, CIT

Center for Nuclear Waste Regulatory Analyses
Southwest Research Institute
6220 Culebra Road
San Antonio, TX 78228-0510

Division of Geological and Planetary Science
California Institute of Technology
Pasadena, CA 91125

E. O'Donnell, NRC Project Manager

Prepared for
Division of Regulatory Applications
Office of Nuclear Regulatory Research
U.S. Nuclear Regulatory Commission
Washington, DC 20555-0001
NRC Job Code L2200

Disclaimer

NUREG–6401 is not a substitute for NRC regulations and compliance is not required. The approaches and/or methods described in this NUREG/CR are provided for information only. Publication of this report does not necessarily constitute NRC approval or agreement with the information contained herein.

ABSTRACT

Yucca Mountain, Nevada, has been proposed as the potential site for a high-level waste (HLW) repository. The tectonic setting of Yucca Mountain presents several potential hazards for a proposed repository, such as potential for earthquake seismicity, fault disruption, basaltic volcanism, magma channeling along pre-existing faults, and faults and fractures that may serve as barriers or conduits for groundwater flow. Characterization of geologic structures and tectonic processes will be necessary to assess compliance with regulatory requirements for the proposed high level waste repository. In this report, we specifically investigate fault slip, seismicity, contemporary stain, and fault-slip potential in the Yucca Mountain region with regard to Key Technical Uncertainties outlined in the License Application Review Plan (Sections 3.2.1.5 through 3.2.1.9 and 3.2.2.8). These investigations center on (i) alternative methods of determining the slip history of the Bare Mountain Fault, (ii) cluster analysis of historic earthquakes, (iii) crustal strain determinations from Global Positioning System measurements, and (iv) three-dimensional slip-tendency analysis. The goal of this work is to assess uncertainties associated with neotectonic data sets critical to the Nuclear Regulatory Commission and the Center for Nuclear Waste Regulatory Analyses' ability to provide prelicensing guidance and perform license application review with respect to the proposed HLW repository at Yucca Mountain.

Results from these investigations include the following. First, fission track thermochronometry and the patterns of alluvial fan sedimentation at Bare Mountain suggest that slip on the Bare Mountain Fault has been more recent and at a greater rate than suggested by trenching studies alone. These results point out the limitations of trenching studies in fault slip analysis and that alternative techniques need to be investigated in order to arrive at a robust estimate of fault slip. Second, analyses of earthquake seismicity illustrate the brevity of the historic seismic record and point out the uncertainty of predictions of future seismicity that are based on historic seismicity and the well-recognized importance of studies of paleoseismicity. Third, newly collected Global Positioning System measurements demonstrate that crustal strains in the Yucca Mountain and Death Valley region are measurable over very short periods of time (i.e., several years). These crustal strain measurements highlight that the Basin and Range is still tectonically active and that these measurements will be instrumental in assessing tectonic hazards such as potential seismicity and fault rupture. Fourth, slip tendency analysis shows that many faults in the Yucca Mountain region are favorably oriented for slip in the contemporary stress state. Improvements can be made in assessment of fault slip tendency through analyses of *in situ* stress at depth and improved knowledge of fault geometry.

CONTENTS

CONTENTS (Cont'd)

FIGURES

FIGURES (Cont'd)

TABLES

EXECUTIVE SUMMARY

The technical objectives of the Tectonic Processes in the Central Basin and Range Research Project are to support development of an adequate understanding of issues related to the tectonic activity of the Yucca Mountain (YM) region. The ultimate goal of the project is to provide timely prelicensing review and development of technical expertise in preparation for license application review of the proposed high-level nuclear waste (HLW) repository at YM. Because the proposed HLW repository is situated within the tectonically active central Basin and Range Province, characterizations of the contemporary tectonic setting of YM and of the potential for future tectonic events are critical to compliance evaluation with regard to long-term waste isolation and short-term safety and retrievability objectives specified in the Nuclear Regulatory Commission (NRC) regulation 10 CFR Part 60. Specific concerns outlined in 10 CFR Part 60 include structural deformation that may adversely affect the regional groundwater flow [60.122(c)(4)], structural deformation that may have occurred during the Quaternary Period [60.122(c)(11)], seismic events that could affect the site significantly [60.122(c)(12)], tectonic processes and features that may increase the frequency of occurrence or magnitude of earthquakes [60.122(c)(13)], and more frequent occurrence of earthquakes of higher magnitude than is typical of the area in which the geologic setting is located [60.122(c)(14)]. In addition, design criteria must be met to provide protection against natural phenomena such that the structures, systems, and components important to safety are designed so that natural phenomena and environmental conditions anticipated at the geologic repository operations area will not interfere with necessary safety functions [60.131(b)(1)].

The central Basin and Range Province is characterized by a complex system of extensional and strike-slip faults that have been active throughout the Cenozoic (last 65 Ma). Information concerning estimates of seismic risk, fault displacement, and structural deformation related to Basin and Range faulting in the YM region is necessary in order to adequately assess compliance with specific regulatory requirements as documented in License Application Review Plan (Nuclear Regulatory Commission, 1994), Sections 3.2.1.5 through 3.2.1.9 and 3.2.2.8. Key Technical Uncertainties (KTUs) relevant to these fault-related processes include uncertainties in (i) the structural and tectonic setting of YM, (ii) the spatial and temporal patterns of seismicity, (iii) the slip history of faults, (iv) the effects of seismicity and structural deformation on groundwater flow and transport, (v) the magnitude of fault slip and associated seismic shaking at surface and shallow subsurface locations, and (vi) the effects of structural deformation on rock-mass properties. All but the last of these KTUs require a safety review supported by independent tests, analyses, and other investigations. This report addresses these uncertainties by evaluating (i) faulting, (ii) seismicity, (iii) contemporary strain, and (iv) fault-slip potential in the YM region.

Faulting

Faulting within the YM region has been the subject of intense investigations by the Department of Energy (DOE). The DOE has primarily relied upon trenching studies in Quaternary alluvium for slip-rate estimates and fault-slip histories from which constraints on paleoseismicity and fault-displacement hazards will be generated. Investigations of paleoseismicity are necessary for seismic hazard prediction due to the long period of regulatory concern (10,000 yr) compared with the brevity of the historic seismic record (<200 yr) for the YM region.

In trenching studies, sites are chosen at locations where faults appear to cut datable sedimentary units. These studies rely upon discernible surface offsets (fault scarps and fault-line scarps) in alluvium to aid the investigators in locating trench sites. Trenches (approximately 1 to 3 m depth) are then excavated

perpendicular to the alluvial scarp, and interpretations about the fault-slip history are made from observations of offset sedimentary markers exposed in the trench walls. In addition to potential uncertainties associated with proper trench construction, numerous sources of technical uncertainty are associated with the interpretation of fault-slip history from trenching studies. These uncertainties include the distributed nature faulting in which the trench captures only part of the total fault slip; blind earthquakes that do not result in surface ruptures; fault orientation, especially the dip of the fault; the direction of fault slip; the nature of the fault-block deformation; and techniques used to date sedimentary markers.

Most of these uncertainties can cause underestimation of fault slip, slip rate, and recurrence of slip, and thus, effectively minimize the potential seismic hazard. Alternative techniques are therefore needed to independently assess fault-slip and fault-slip histories and to provide limiting constraints on the DOE's fault-slip estimates. In this report, the fault-slip history of the Bare Mountain Fault (BMF) is studied by two alternative techniques; apatite fission track thermochronometry (FTT) and an analysis of alluvial fan sedimentation related to the uplift of Bare Mountain (BM). The BMF was chosen because it is one of the key structures in the YM region, and may control fault slip on many of the faults within and surrounding YM.

Apatite FTT reveals that the BM block cooled through the 110 °C annealing temperature of apatite between 14 and 15 Ma, probably as the result of tectonic denudation of BM during the development of the Bullfrog Hills detachment system. Geological evidence in Crater Flat (Carr and Parrish, 1985) indicates that the BMF may have also played a significant role in the uplift of BM since 12 Ma. In addition, temperature-time diagrams show continued uplift of BM from the Middle Miocene to the present. Total uplift ranges between 2 and 3 km, depending on assumptions of the average geothermal gradient for Nevada since the Miocene. If a continental average geothermal gradient of 30 °C is assumed from the Pliocene to present, then the average uplift rate of BM for the last 4 m.y. is 0.24 mm/yr. A 0.24 mm/yr uplift rate corresponds to a fault-slip rate of 0.28 mm/yr, assuming an average BMF dip of 60°. This rate contrasts with the 0.015 mm/yr rate determined from trenching studies of the Tarantula Canyon alluvial fan (Pezzopane, 1995).

Analyses of the pattern of alluvial fan sedimentation around BM indicate movement of the BMF during Pleistocene and Holocene times. There is a general correlation between the ratios of fan area to sediment-source area, the amount of Holocene sedimentation at the fan heads, and dip of the BMF. Slip on the BMF appears to increase from north to south, with relatively little Holocene throw along the BMF at Tarantula Canyon, the location of a trenching site used to constrain the slip history of the BMF (Klinger and Anderson, 1994; Pezzopane, 1995). Moreover, in the vicinity of Tarantula Canyon, the BMF has relatively low dip angles (45 to 50°), such that the vertical offset of the trenched alluvium will be smaller than those on steeper portions of the fault for a given increment of horizontal extension. Collectively, these results suggest that fault-slip rates derived from trenching studies in the Tarantula Canyon fan are absolute minimum values and not representative of the BMF as a whole.

Seismicity

Earthquake activity in the YM region represents a significant risk to the proposed HLW repository, especially because YM is located near the intersection of two prominent seismic belts: the Intermountain Seismic Belt and the Walker Lane Seismic Belt. Although the YM region has not experienced a major historical earthquake, realistic predictions and probability assessment of future seismicity are hampered

by the brevity of the historical seismic record (<200 yr). Moreover, because YM is only 50 km from one of the most active faults in the western Basin and Range, the Death Valley-Furnace Creek (DVFC) fault system, there is a distinct possibility that clustered seismic activity associated with a large (M>7.5) earthquake on the fault system could directly impact YM.

The Ms 7.6 Landers earthquake sequence (1992) was studied as an analog to possible clustered seismic activity associated with a large magnitude event along the fault. In the Landers' sequence, King (1994) found that patterns of aftershocks occurred on optimally oriented faults in regions with as little as a 0.05 MPa increase in stress. The Big Bear shock (Ms=6.2), located 35 km to the west of the Landers' mainshock, and the Little Skull Mountain shock (M=5.4), located 15 km beyond YM to the east, are both considered to have been triggered aftershocks by the Landers' earthquake (Hill et al., 1993; King et al., 1994). Given the areal extent of the affected region around the Landers' earthquake (>50 km), these results suggest that a similar earthquake on the DVFC fault system could potentially trigger significant seismic activity at YM and BM.

Contemporary Strain

To characterize the contemporary strain and to evaluate the partitioning of strain among faults in the YM region, crustal deformation of the YM region is being investigated using a satellite-based Global Position System survey. The survey is a collaborative program funded by the NRC that includes the California Institute of Technology and the Smithsonian Institute. The survey was established in 1991 to help assess the seismotectonic performance of the potential HLW at YM.

Preliminary results indicate significant accumulation of crustal strains along major fault zones within 50 to 100 km of YM. However, motions along these faults are only beginning to be measurable in this survey. Future occupation of the existing network over the next 3 yr should reduce uncertainties of these measurements by a factor of 3. Motions recorded by the survey to date include: (i) measurable offset related to the Little Skull Mountain Earthquake and (ii) uplift of the northern end of BM relative to YM. In addition, it appears that strain is accumulating across the Hunter Mountain right-lateral strike-slip fault. The Hunter Mountain Fault appears to be locked, raising the potential for future seismic activity there. Surprisingly, a clear pattern of right-lateral strike-slip strain has not yet emerged across the DVFC fault system. However, Death Valley appears to be subsiding with respect to stations in the surrounding highlands.

Fault-Slip Tendency

The fault-slip potential of known faults in the YM region relative to the current crustal stress field is being investigated using a new numerical slip-tendency analysis technique (part of 3DSTRESS) developed at the Center for Nuclear Waste Regulatory Analyses (Ferrill et al ., 1994; Morris et al., 1994; Ferrill et al., 1995). The technique provides an interactive means for assessing the relative risk of earthquakes and fault slip based on the orientation of faults, orientation and magnitudes of the principal stresses in the regional stress field, and frictional characteristics of the faults.

Slip tendency analysis indicates that the key uncertainty in estimating the relative potential for fault slip in the YM region is the orientation of the least principal stress (σ_3) with respect to the faults. Using current estimates of the regional stress field (e.g., Stock et al., 1985; Zoback, 1992; Zoback et al., 1992), faults that strike between N 0° E and N 30° E with steep dips between 60 and 90°, present the

greatest risk of both strike-slip and normal dip-slip motion. If σ_3 is oriented more east-west, then virtually all mapped faults at YM would be in nearly optimal orientations for slip, given the appropriate stress magnitudes. In addition to better constraints on the orientation and magnitude of the principal stresses, realistic estimates of the coefficient of friction for faults are needed to refine the predictive resolution of the slip-tendency analysis.

ACKNOWLEDGMENTS

This report was prepared to document work performed by the Center for Nuclear Waste Regulatory Analyses (CNWRA) for the Nuclear Regulatory Commission (NRC) under Contract No. NRC-02-93-005. The activities reported here were performed on behalf of the NRC Office of Nuclear Regulatory Research, Division of Regulatory Applications. The report is an independent product of the CNWRA and does not necessarily reflect the views or regulatory position of the NRC. Ronald H. Martin, Raymond A. Donelick, Sidney M. Jones, Bret Rahe, Kent Polk, Steven R. Young, Charles B. Connor, George Birchard, and Edward O'Donnell are thanked for technical contributions to the work presented here. We thank Cathy Garcia and Esther Cantu for preparation and James Pryor for editorial review. Thorough reviews by H. Lawrence McKague, Renner B. Hofmann, and Wesley C. Patrick were greatly appreciated and significantly improved this report.

QUALITY OF DATA, ANALYSES, AND CODE DEVELOPMENT

DATA: CNWRA-generated original data contained in this report meet quality assurance requirements described in the CNWRA Quality Assurance Manual. Sources for other data should be consulted for determining the level of quality for those data.

ANALYSES AND CODES: The geographic information system computer code ARC/INFO and the cross-section construction and balancing program GeoSec were used for some of the analyses contained in this report. These codes, which are commercially available, are not being modified by the CNWRA, and it has not been determined whether they will be used in the license application review processes. Therefore, they are not controlled under the CNWRA Software Configuration Procedure (TOP-018: Development and Control of Scientific and Engineering Software). This report describes analyses performed using the newly developed computer code 3DSTRESS; however, the code has not been sufficiently developed to be placed under the CNWRA Configuration Management system. Calculations were made using newly developed computer codes PDEFILTER, DEG2UTM, and EP_GRID. These codes have not been sufficiently developed to be placed under the CNWRA Configuration Management system.

1 INTRODUCTION

Yucca Mountain (YM), Nevada is located in the Central Basin and Range Province, which is characterized by complex extensional and strike-slip faulting throughout the Cenozoic (last 65 Ma). YM itself has been proposed as the site of a high-level radioactive waste (HLW) repository.

The Nuclear Regulatory Commission (NRC) is required to review a license application from the U.S. Department of Energy (DOE) to construct and operate a proposed repository for HLW at YM, Nevada. YM is located in a tectonically active area and contains numerous geologic faults. Key issues for compliance evaluation include whether a mined geologic repository at that location will provide effective long-term waste isolation from the accessible environment and whether short-term safety and retrievability objectives will be met as specified in 10 CFR Part 60. Because of risks to long-term performance associated with structural deformation and seismicity, potentially adverse conditions related to structural deformation and seismicity have been included in 10 CFR Part 60: (i) structural deformation, such as uplift, subsidence, folding, and faulting, that may adversely affect the regional groundwater flow system [60.122(c)(4)]; (ii) structural deformation, such as uplift, subsidence, folding, and faulting that may have occurred during the Quaternary Period (i.e., within the last approximately 2 million yr) [60.122(c)(11)]; (iii) earthquakes that have occurred historically that, if they were to be repeated, could affect the site significantly [60.122(c)(12)]; (iv) indications, based on correlations of earthquakes with tectonic processes and features, that may increase either the frequency of occurrence or the magnitude of earthquakes [60.122(c)(13)]; and (v) more frequent occurrence of earthquakes or earthquakes of higher magnitude than are typical of the area in which the geologic setting is located [60.122(c)(14)]. Additionally, design criteria must be met to provide protection against natural phenomena as specified in 10 CFR Part 60: the structures, systems, and components important to safety must be designed so that natural phenomena and environmental conditions anticipated at the geologic repository operations area will not interfere with the necessary safety functions [60.131(b)(1)]. Because of these regulatory concerns regarding structural deformation and seismicity, it is critical that the geologic structure of YM as well as the potential for displacement and seismicity on faults in the YM area be well understood.

Information concerning estimates of seismic risk, fault displacement, and structural deformation related to faulting will be necessary to assess compliance with specific regulatory requirements as documented in the License Application Review Plan (LARP) (Nuclear Regulatory Commission, 1994) Sections 3.2.1.5 through 3.2.1.9 and 3.2.2.8. Key Technical Uncertainties (KTUs) relevant to these fault-related processes include:

- Uncertainty in determining three-dimensional structure and tectonic setting of Yucca Mountain (see LARP Section 3.2.1.5)
- Uncertainty in determining spatial and temporal patterns of seismicity (see LARP Sections 3.2.1.7 and 3.2.1.8)
- Uncertainty in determining the slip history of faults (see LARP Sections 3.2.1.5, 3.2.1.7, and 3.2.1.8)
- Uncertainty in determining effects of structural deformation and tectonic processes on the flow and transport of groundwater (see LARP Section 3.2.2.8)

- Uncertainty in determining magnitude of fault slip and associated seismic shaking at the surface and shallow subsurface locations (see LARP Section 3.2.1.7)

- Uncertainty in determining effects of structural deformation and tectonic processes on rock mass properties (see LARP Section 3.2.1.5)

This report focuses on specific and critical uncertainties in understanding the tectonic setting of the proposed site for a HLW repository at YM. In this report, we evaluate faulting, seismicity, contemporary strain and fault-slip potential in the YM region with regard to the aforementioned KTUs. Techniques used in this evaluation include the following:

- Apatite fission-track thermochronometry

- Analyses of alluvial fan sedimentation

- Three-dimensional (3D) evaluation of earthquake hypocenters

- Analyses of spatial and temporal clustering of seismicity

- Measurement of contemporary crustal strain

- Numerical analyses of fault-slip tendency within the contemporary stress field

Continued development of new techniques, applications of existing techniques and acquisition of tectonic data are critical to the NRC and Center for Nuclear Waste Regulatory Analyses (CNWRA) ability to provide prelicensing and license application review of the proposed HLW repository site at YM.

2 FAULTING

YM is located in an active tectonic setting characterized by active faulting and seismicity in which measurable tectonic strain accumulates over periods as short as several years. Numerous normal and strike-slip faults that have documented Quaternary displacement are present in the vicinity of YM. Active faulting presents several important potential hazards for a HLW repository at YM. First, fault rupture within the repository area could cause direct damage to waste packages, which could potentially cause immediate canister failure or could cause damage to canisters that would enhance corrosion. Second, fault rupture and the associated brecciation of fault rock or fracturing of fault blocks could potentially produce new or enhanced barriers or pathways for groundwater flow. Alternatively, fault slip could increase the potential for groundwater perching, for example, by juxtaposing a relatively permeable layer against an impermeable layer in a groundwater-trapping configuration. Third, ground motion from slip on active faults could potentially damage surface and subsurface facilities and tunnels and waste canisters. Because of these potential hazards to the proposed HLW repository at YM, active faults have been the subject of intensive investigation by the DOE. The DOE investigations of faulting primarily involve surface mapping and trenching activities with the primary goal of assessing slip rate and fault-slip history to constrain paleoseismicity and fault displacement hazards. Investigations of paleoseismicity are necessary for seismic hazard predictions due to the long period of regulatory concern (10,000 yr) compared with the extreme brevity of the historic seismic record (<200 yr) for the YM region. Investigations of paleoseismicity and faulting help to address uncertainties in determining: (i) 3-D structure and tectonic setting of YM, (ii) spatial and temporal patterns of seismicity, (iii) the slip history of faults, and (iv) magnitude of fault slip and associated seismic shaking at the surface and shallow subsurface locations. In this chapter, sources of uncertainty in fault-trenching studies are discussed. One of the key structures in the YM tectonic setting is the Bare Mountain Fault (BMF). This chapter discusses the BMF in detail because it (i) illustrates the various sources of uncertainty associated with the determination of fault-slip, and (ii) may control slip on other faults in the YM region including those faults within YM itself.

2.1 QUATERNARY SLIP HISTORIES OF FAULTS IN THE YUCCA MOUNTAIN REGION

The DOE has undertaken a major program to determine the style of deformation, rate of activity, and length of Quaternary faults to identify and characterize potentially relevant sources of seismic activity in the YM area. The DOE fault characterization activities have focused on 88 faults within 100 km of YM as reported by Pezzopane (1995). Fault characteristics that are useful for seismic hazard analyses are tabulated by Pezzopane (1995) and include: faulting style, documented Quaternary displacement, maximum fault lengths, expected maximum moment magnitudes, expected average and maximum displacements, minimum source-to-site distances, and average Quaternary slip rates and recurrence intervals. Other characteristics that are also being compiled include fault dips, cumulative and single-event displacements, age of displaced deposits, and number of paleoseismic events. Faults located 100 to 300 km from YM that are capable of very large earthquakes are also included for ground motion assessments. Within 100 km of YM, Quaternary displacement is documented on 32 faults. An additional 34 faults are suspected of having experienced Quaternary displacement. The most active fault within 100 km of YM is the Death Valley-Furnace Creek (DVFC) Fault. Average Quaternary slip rate on the DVFC fault is estimated between 2.3 to 12.0 mm/yr (Pezzopane, 1995). The most active fault nearer to YM is the BMF. Quaternary slip rate on the BMF are estimated between 0.015 and 0.19 mm/yr (Pezzopane, 1995).

2.2 SOURCES OF UNCERTAINTY

Fault-trenching studies provide the principal source of data to constrain paleoseismicity. In trenching studies, sites are typically chosen at locations at which faults cut datable sedimentary units. Trench locations are commonly based on surficial mapping and/or low-sun-angle areal photography. In most cases, what is most easily measured is the vertical component, the fault throw. As discussed below, fault throw provides a minimum estimate of fault displacement.

Numerous potential sources of uncertainty are associated with interpretation of fault slip history from trenching studies. The proper design of a trench (e.g., location, orientation, length, and depth) is imperative in order to adequately capture the measurable surface effects of faulting. Other important sources of uncertainty relate to: (i) distributed faulting, (ii) blind earthquakes, (iii) fault orientation, (iv) fault slip direction, (v) noncorrelation across the fault, (vi) fault block deformation, and (vii) dating techniques.

Distributed faulting refers to fault zones that are diffuse or have multiple splays (Figure 2-1). To fully characterize the accumulated slip history of the fault, it is necessary to characterize the slip history of each splay or the slip history of the entire width of the fault zone. Consideration of only a portion of the fault zone could result in an underestimation of fault activity (e.g., slip rate or recurrence frequency).

Blind earthquakes produce no surface rupture (Figure 2-1). Some large earthquakes, including the recent 1992 Big Bear and 1994 Northridge earthquakes, caused significant damage without producing surface rupture. Obviously, trenching at the ground surface cannot identify a seismic event or fault slip that does not produce surface deformation.

Fault slip (or fault-slip rate) is the vector sum of the horizontal and vertical components of fault slip, the heave and throw, respectively (Figure 2-1). To calculate an actual slip magnitude or rate from one component (e.g., the throw), it is necessary to know the orientation of the fault slip vector. In the case of a dip-slip fault, this vector is the angle of dip of the fault. Because the throw (measured from vertical trench walls) is the most common component of displacement in trenching studies, it is critical to know the orientation of the slip vector in order to make realistic estimates of slip or slip rate from fault throw. The rate of throw only equals the slip rate in cases where dip slip occurs on a vertical fault. In all other cases, the throw underestimates the slip rate. Surface and shallow subsurface deformation associated with fault slip could complicate measurements of throw, heave, and slip.

An inability to correlate young datable units across a fault severely limits paleoseismic investigations (Figure 2-1). In the case of the BMF, along most of the length of the fault, Quaternary alluvial units are juxtaposed directly against Paleozoic and Precambrian strata of Bare Mountain (BM). Interpretations of number and frequency of ground-rupturing events can be inferred from deformation of alluvial units on the downthrown side of the fault. However, alternative techniques must be used to interpret slip rate.

Fault block deformation is capable of accommodating fault slip-related strain, which results in an underestimation of fault activity. For example, displacement along a normal fault may die out upward by strain in the hangingwall or footwall of the fault. Alternatively, seismic shaking may cause compaction of young sedimentary units (Figure 2-1). For example, alluvial units on the downthrown side of a normal

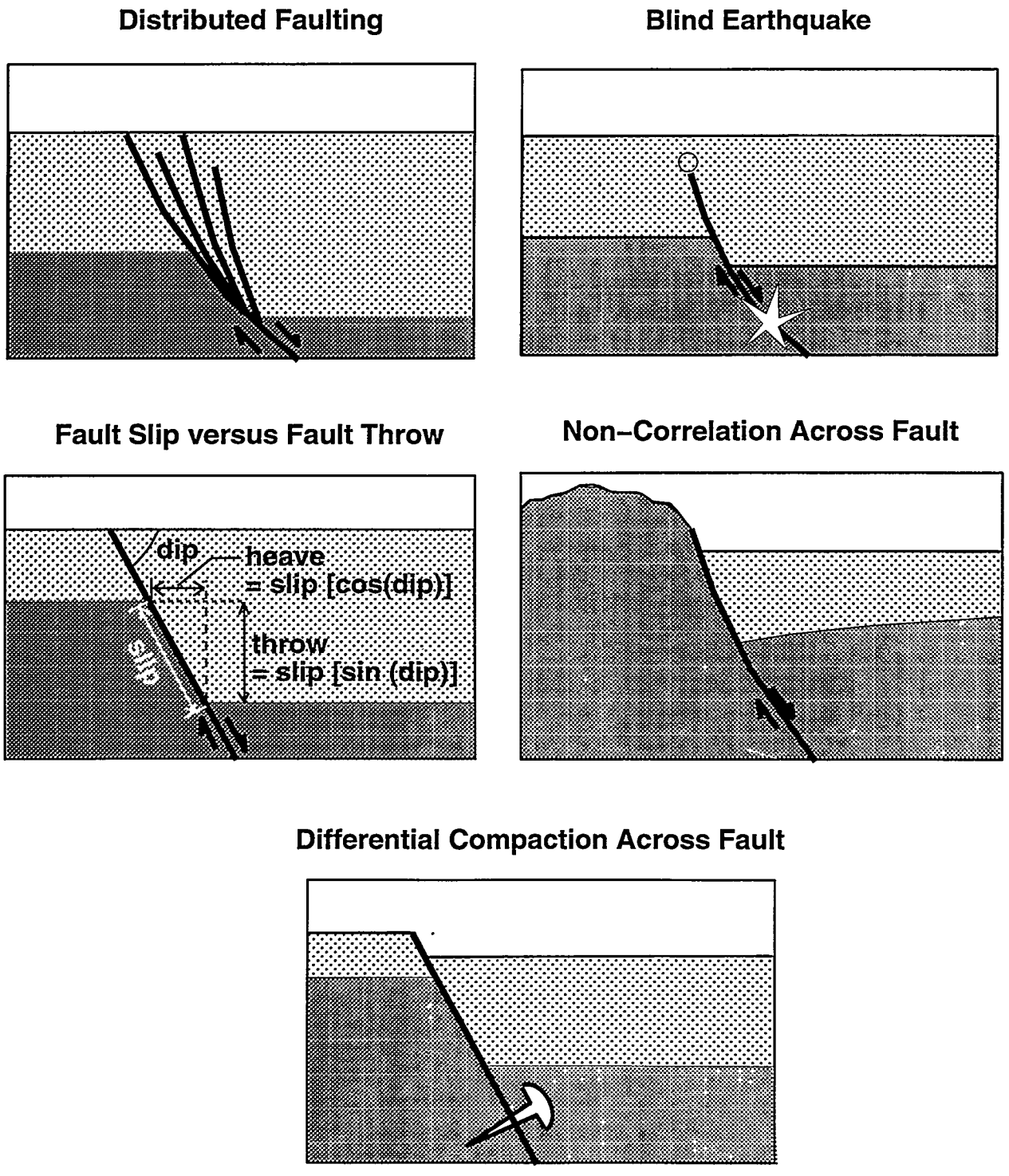

Figure 2-1. Potential sources of uncertainty in fault-trenching analyses of paleoseismicity. Relationships between heave, throw, and slip are illustrated for a dip-slip fault.

fault are commonly thicker than the equivalent sequence of layers on the upthrown side of the fault. Seismic shaking may cause a small percentage of compaction on either side of the fault. This compaction, due to the greater thickness on the downthrown side of the fault, could produce surface displacement along the trace of the fault. This surface displacement is not related to slip on the host fault at depth. In this case, this source of uncertainty could cause an overestimation of fault activity.

Interpretations of fault-slip history from trenching studies are limited by the resolution of dating techniques used to constrain the ages of deformation events characterized in trenches. Within trenches dug across fault traces, datable stratigraphic horizons are correlated along the trench walls, deformation events are interpreted, and cumulative offsets of dated horizons are measured. Estimates of ages of stratigraphic units and horizons that are either offset by or overlie a fault without displacement provide maximum or minimum ages for faulting, respectively. Dating of sedimentary wedges related to fault scarps is used to date fault slip events. Also, dating of undeformed secondary minerals within fault zones can potentially give the minimum age of the last fault-displacement event. Age determination methods that are appropriate for Quaternary events include ^{14}C, uranium series, thermoluminescence, and electron spin resonance. These methods are summarized by Young and Stirewalt (1993) and Hill et al. (1993).

2.3 BARE MOUNTAIN FAULT SLIP HISTORY

2.3.1 Tectonic Setting and Significance of Bare Mountain

BM, Nevada, is approximately 16.5 km west of the proposed site of the HLW repository at YM (Figure 2-2). BM consists of a folded, faulted, tilted, and uplifted sequence of rocks that range in age from late Proterozoic to (?)Mississippian with few gaps. This block of Precambrian to Paleozoic rocks forms the footwall of the BMF, an east-directed (top to the east) normal fault with approximately 2 km of throw (Snyder and Carr, 1984; Swadley et al., 1984; Reheis, 1986). The BMF is the most active fault within 50 km of YM (Pezzopane, 1995). Its documented recent activity, proximity to the proposed HLW repository, and the lack of consensus as to its slip history make the BMF an ideal test case for critical review. Specifically, there are three concerns: (i) the potential seismic hazard of the BMF, (ii) the amount of slip (coseismic or aseismic) and consequent deformation on the west-directed normal faults of the YM area resulting from slip on the BMF (seismic or aseismic), and (iii) the role that steep faults play in providing conduits for magma ascent from deep crustal levels. To address these concerns, it is necessary to understand the genesis of the BMF, determine its slip history, and generate realistic models of the degree to which the BMF is linked with faults to the east.

2.3.2 Slip History

There is evidence for Late Quaternary to Holocene slip on splays of the BMF exposed in alluvium, but there is no consensus as to the amount or precise timing of this slip (Swadley et al., 1984; Reheis, 1986; 1988). The slip rate for the BMF is a significant source of uncertainty for probabilistic seismic hazard assessments (PSHA) of YM. Slip-rate estimates for the BMF range from hundredths of mm/yr to over 1 mm/yr. Estimates of the time of the last slip range from Holocene (<10 Ka) to >100 Ka. Slip rate for the BMF has been interpreted for the purposes of PSHA to be in the range of 0.015 to 0.19 mm/yr (Pezzopane, 1995; Reheis, 1988). Trenching studies in the Tarantula Canyon fan suggest a minimum displacement of 1.5 m during the last 100 Ka. In contrast, Klinger and Anderson (1994) conclude that there has been no displacement on the BMF in the last 100 Ka. Level-line surveys between Tonopah and Las Vegas, Nevada, in 1907, 1915, and 1984 show a drop of about 125 mm

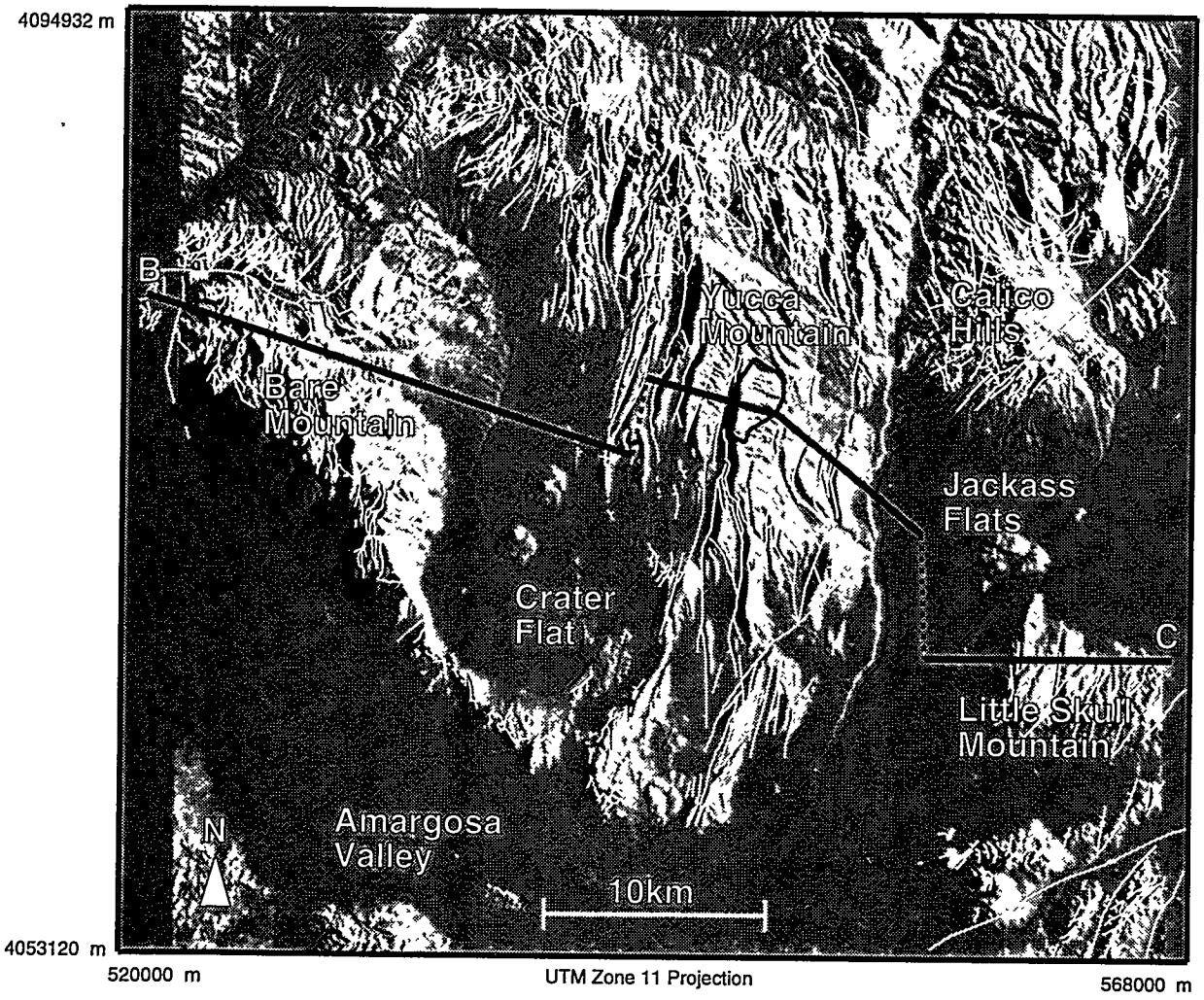

Figure 2-2. Digital elevation map of Bare Mountain, Nevada, and surrounding region. The line of the subregional cross section (Figure 2-3) is shown. Map projection is Universal Transverse Mercator Zone 11.

between 1907 and 1984 at the position that corresponds to the southward projection of the BMF, along US 95 south of Steve's Pass (Gilmore, 1992). This drop equates to a 1.6 mm/yr average subsidence between the two stations across the BMF.

We have initiated two approaches to better constrain the recent slip history of the BMF. The first approach is an apatite fission-track study, which provides information on the uplift history of the BM block over the last 45 m.y. The second is an analysis of the geometry of alluvial fans on the west and east flanks of BM, which provides information on patterns of uplift and faulting during the Quaternary.

2.3.3 Fault Linkage and Seismic Risk

Two end-member models of fault linkage between BM and YM can be formulated [Figures 2-3(a) and 2-3(b)]. The first model [Figure 2-3(a)], based on conceptual models of Scott (1990) and Hamilton (1988) and quantitative modeling of Young et al. (1993), assumes that the faults of YM developed as part of the Bullfrog Hills Detachment System (BHDS), a west-directed (top to the west) extensional detachment system that was active during the Miocene and accommodated as much as 275 percent extension. In this model, YM faults were subsequently isolated by the rise of the BM block (e.g., Scott, 1990). YM faults are considered to have formed during the Middle to Late Miocene as a little

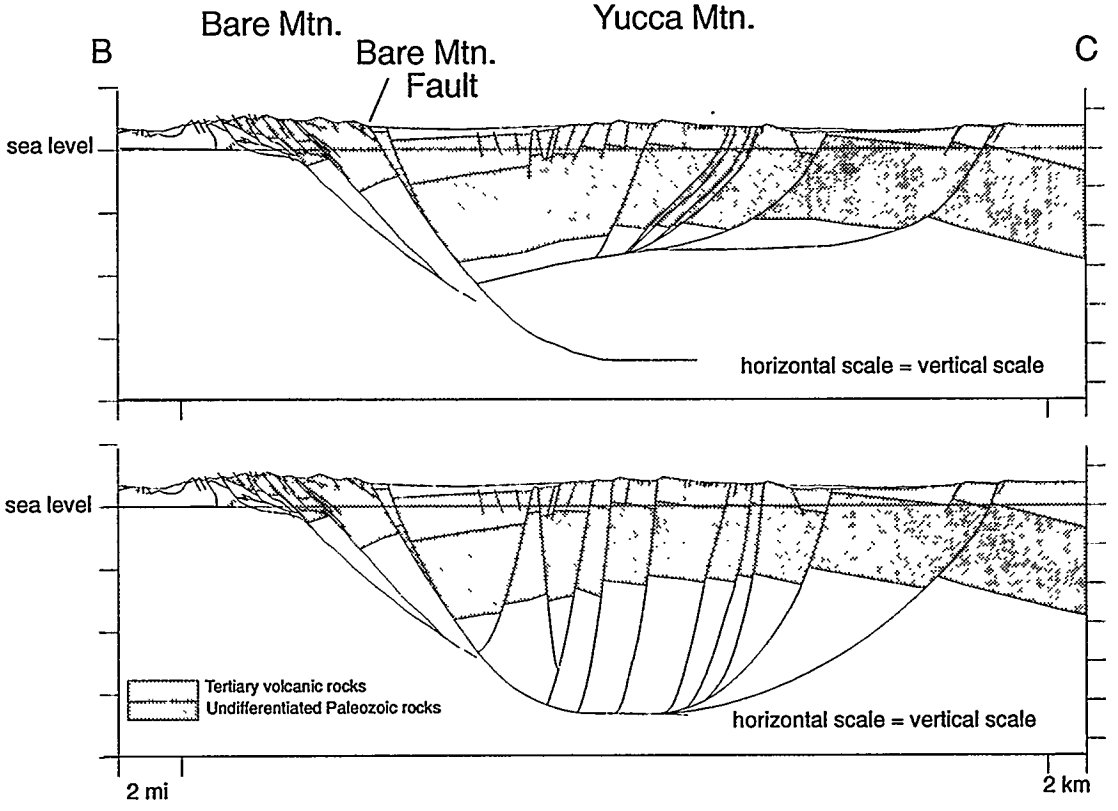

Figure 2-3. Semirestorable cross sections through Bare Mountain and Yucca Mountain from B to C (Figure 2-1) illustrating two alternative interpretations of the deep Bare Mountain Fault-Yucca Mountain fault system

extended (12 to 20 percent in YM compared with 275 percent in the Bullfrog Hills) "headwall" portion of the BHDS (Maldonado, 1990; Scott, 1990; Young et al., 1993a,b). Subsequent motion on the BMF, cutting to greater crustal depths, truncated the older west-directed detachment system. The depths to detachment are modeled using the regional geometry of the Paintbrush Tuff and assuming vertical shear as the hangingwall deformation mechanism (e.g., Young et al., 1993). The greater depth to detachment of the BMF compared with the YM faults is geometrically required by the rollover or hangingwall collapse (defined by westward drop in elevation of the Paintbrush Tuff) within the Crater Flat graben, which is constrained by geophysical and geological data (Snyder and Carr, 1984; Faulds et al., 1994). The second model [Figure 2-3(b)] is based upon conceptual interpretations of Carr and Monsen (1988) and Gilmore (1992) and assumes that the east-directed BMF system generated the YM faults as antithetic faults in its hangingwall. In this second model, YM faults are considered to have formed to accommodate hangingwall deformation required by movement on the BMF. YM faults can be modeled to these depths by increasing the dips of the near-surface segments of the faults from about 70° to 80–85°. This procedure can be justified on the grounds that few major faults are exposed in bedrock at the surface, and there is considerable uncertainty as to the dips of many of the YM faults. Hybrids of these two end members are also permissible. For example, YM faults may have originated as part of the BHDS, but may continue to accumulate slip because they are optimally oriented to accommodate antithetic shear in the hangingwall of the more recently active BMF. Knowledge of the precise nature of the linkage between the BMF and faults in its hangingwall is critical to assessing seismic and aseismic slip risks posed by the faults of YM. A combination of geometric and finite-element modeling has been undertaken to determine the viability of the range of potential models for the tectonic development of BM and YM (e.g., Ofoegbu and Ferrill, 1995).

The models in Figure 2-3 illustrate the BMF soling into a subhorizontal detachment at a depth of about 12 km. However, other alternative models can be developed. For example, the BMF may penetrate the entire thickness of the seismic crust to depths exceeding 15 km or it may sole into a subhorizontal detachment at shallower crustal levels (e.g. 7 km) (Gilmore, 1992; Scott, 1990). A model in which the BMF extends to great depth as a steeply dipping planar fault may have implications for more or larger earthquakes than a shallow listric-fault model, due to the general lack of seismicity on low-angle faults (e.g., Ofoegbu and Ferrill, 1995). In any case, if the BMF is still active, then it is likely to be a source of earthquake activity. Any slip on the BMF may be translated into dependent coseismic or aseismic slip on the faults in the YM area regardless of whether the YM faults originated as part of the BHDS or as later antithetic faults that accommodate deformation of the BMF hangingwall.

2.3.4 Bare Mountain Uplift History from Fission Track Thermochronometry

BM is a roughly triangular inlier of Late Proterozoic to Paleozoic rocks bounded on the west by Quaternary alluvial cover, on the east by the BMF and Quaternary alluvial cover, and on the north by the Fluorspar Canyon Fault, a west-directed (top to the west) Miocene extensional fault system that carried Miocene volcanic rocks westward with respect to the inlier. The Fluorspar Canyon Fault at the north end of BM carried mid-Miocene volcanic rocks over the pre-Tertiary sequence. Although the Fluorspar Canyon Fault cannot be mapped continuously to the Bullfrog Hills, it likely connects with the BHDS to the west (Hamilton, 1988; Maldonado, 1990; Scott, 1990). There is broad agreement on the Miocene age and top to the west-northwest sense of displacement of the BHDS. Most authors consider movement on the BHDS to have been the probable cause of the tectonic denudation of BM and the subsequent rise of the BM block (e.g., Hamilton, 1988; Scott, 1990).

Following the Miocene faulting, but with an unknown time of initiation, shallow, east-dipping normal faults displaced parts of the pre-Tertiary mountain core. One of these faults is also expressed in early Pleistocene and Pliocene alluvial fan material on the east side of BM (Monsen et al., 1992). The BMF, which marks the eastern edge of the mountain block, may have more than 2 km of vertical displacement (Snyder and Carr, 1984). Based on the occurrence of megabreccia of Paleozoic rock between the 12.7-Ma Tiva Canyon Member and the 11.6-Ma Rainier Mesa Member in Crater Flat, it has been inferred that the BMF was active prior to 11.6 Ma, which produced a source for the megabreccia (Carr and Parrish, 1985; Faulds et al., 1994). The BMF may be a buttress unconformity between younger tuffs deposited in Crater Flat and the pre-Tertiary rocks of BM. The most recent slip on the BMF is interpreted by Reheis (1986) to have been during the Holocene. However, Klinger and Anderson (1994) interpreted the most recent slip on the BMF to be older than 100 Ka, based on alluvial fan morphology.

The uplift history of BM was investigated using Fission Track Thermochronometry (FTT) to provide an independent constraint on the slip history of the BMF. In principle, the fission track method is similar to other absolute dating techniques based upon the natural decay of radioactive isotopes into nonradioactive daughter products. In FTT, the record of radioactive decay is the resulting fission tracks. Because these tracks anneal at temperature-dependent rates, FTT also provides information on the thermal history of the host rocks.

In apatite, fission tracks begin annealing at 100 ± 20 °C, depending on the apatite's exact mineral composition. Thus, apatite FTT is well-suited to constrain low-temperature thermal histories associated with recent thermal and tectonic events, regardless of the age of the host rock. At BM, apatite FTT reveals a detailed history of the mountains uplift history since the Early Miocene. Knowledge of this uplift history provides insight into the most recent tectonic development of the region and is critical to the evaluation of seismic risk at YM.

2.3.4.1 Fission Track Dating

FTT is based upon the binary fragmentation of heavy unstable nuclides (atomic numbers >90) into daughter nuclides of approximately equal size. Upon fission, these daughter nuclides are repelled in opposite directions at high speeds (Hahn and Strassmann, 1939). In mineral crystals or glass, fission of these nuclides result in linear zones of intensely damaged hosts tens of micrometers long and several nanometers wide (Yada et al., 1981; Bean et al., 1970). These tracks require chemical etching to enlarge them to micrometer diameters, large enough to be visible under an optical microscope.

Natural fission tracks are most commonly found in volcanic glass, apatite, mica, sphene, and zircon that contain trace amounts of ^{238}U. Fission tracks are metastable and begin to anneal immediately after they form. Annealing rate is temperature dependent. For each natural system, an effective retention or "closure" temperature has been determined experimentally (see Wagner and Van Den Haute, 1992, table 4.1, p. 119). Below the closure temperature, tracks accumulate in the host mineral and continue to do so as long as the ambient temperature remains below the closure temperature. However, because partial annealing continues below the closure temperature, the degree of partial annealing (resulting in shorter but still detectable track lengths) provides a sensitive record of the host rock's temperature-time history.

In apatites, FTT makes use of both total number of tracks and the distribution of track lengths to develop cooling ages and uplift histories for the host rocks. Ages are determined from the proportion

of naturally occurring fission tracks to the total concentration of ^{238}U, using the 8.2×10^{15} yr half-life of ^{238}U spontaneous fission (Holden, 1989). Temperature-time histories are determined from an analysis of the distribution of fission track lengths. Exhumation or uplift histories can then be determined from the cooling histories based upon knowledge of the regional geothermal gradient.

2.3.4.2 Sampling and Methodology

Samples for apatite FTT were collected from 25 sites in the BM block [Figure 2-4(a)] from a variety of exposed clastic and igneous rocks, including the Wood Canyon and Eleana formations, Stirling, Zabriskie, and Eureka quartzites, Cretaceous granite, and Miocene quartz-latite dikes. Sample locations were chosen to provide complete spatial and topographic coverage.

Apatite mineral separates, ranging between 70 and 300 μm, were obtained from crushed samples using conventional gravimetric and magnetic heavy mineral separation techniques. Grains were mounted in an epoxide resin on petrographic slides, polished, and etched for 20 sec in 5.5 M HNO_3 at 21 °C. Each apatite grain mount was then covered by an external, fission product detector consisting of a sheet of low-uranium muscovite mica, a chip of CN-1 glass (which served as a neutron dosimeter), and a second mica sheet. The package was irradiated at the Texas A&M Nuclear Science Center reactor in position A-2 for 60 min at 1-MW power, giving a total thermal neutron fluence of approximately 1×10^{16} neutrons/cm^2. Following irradiation, the micas and glass dosimeters from the sample mounts were etched for 13 min in 48 percent hydrofluoric acid at 24 °C in order to reveal induced fission tracks. Dosimeters were calibrated against the Durango standard and ages adjusted according to the zeta calibration method (e.g., Naeser and Naeser, 1988). Natural and induced fission track densities were measured optically (1562.5× magnification) under transmitted and reflected light, respectively.

Horizontal confined fission track lengths were used for track length measurements in the temperature-time analyses (e.g., Laslett et al., 1987). Length and crystallographic orientation of each track were determined using a digitizing tablet calibrated for length measurement using a 100-lines/mm microscope micrometer. To enhance fission track densities in low-spontaneous track density apatites, one apatite grain mount for each sample was irradiated at the Renssalaer Polytechnic Institute with 252-Cf (californium) fission fragments for 17 hr at a distance of 8 cm, giving a Cf-derived fission track density of approximately 1.0 to 2.0×10^6 tracks/cm^2. The induced tracks from the 252-Cf irradiation intersect previously unaltered, confined tracks, and thus, open new pathways for etching solvents. Re-etching the apatite grain mounts enhances the number of natural, horizontal confined tracks available for length measurements. Temperature-time records are constructed from forward kinetic-based modeling of the distribution of track lengths and their ages (Ravenhurst et al., 1994). The underlying assumption is that the rocks have only cooled since they last passed through the closure temperature.

2.3.4.3 Results

Apatite fission track results have been obtained from 25 samples (Table 2-1). There is large variability in the number of apatite grains extracted for analysis and in ^{238}U concentrations. Low ^{238}U concentrations are found in the Stirling Quartzite, quartzites in the Wood Canyon Formation, and Cretaceous and Mesozoic intrusive rocks, whereas higher concentrations are found in the pelitic rocks of the Wood Canyon Formation, the Zabriskie and Eureka quartzites, and the Eleana Formation. All apatites appear to be end-member fluorapatite, based upon the diameter of track apertures parallel to the *c* crystallographic axis (Donelick, 1993), with a closure temperature of 110 °C.

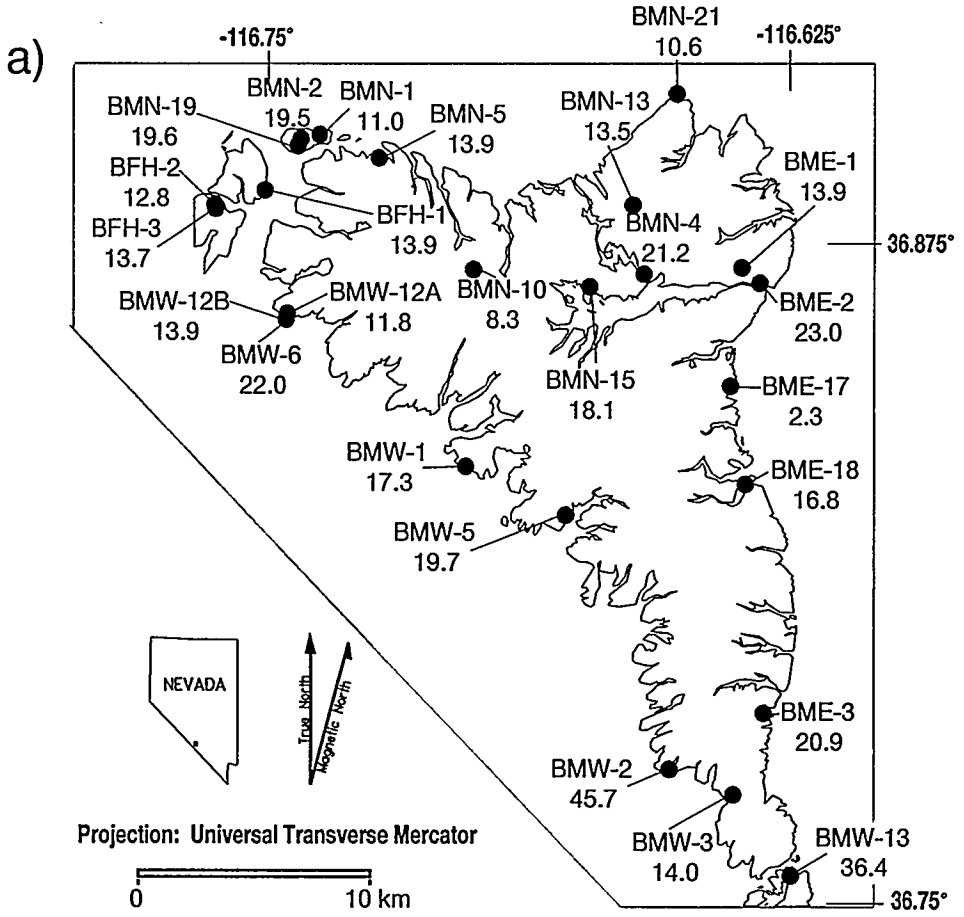

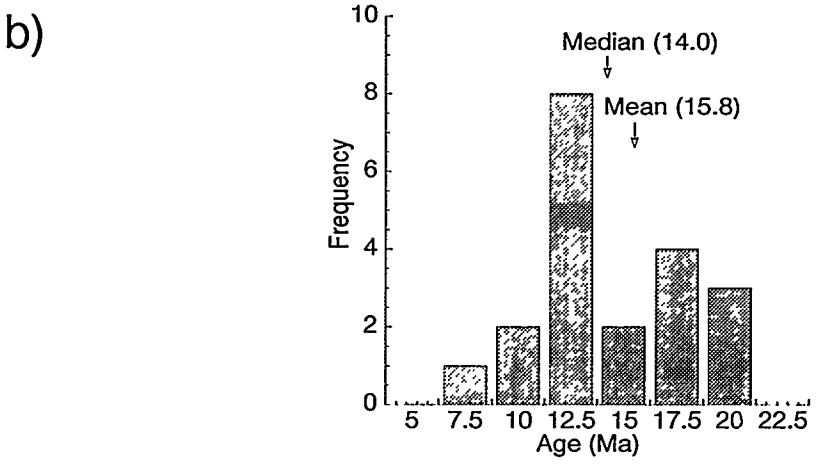

Figure 2-4. (a) Map showing the distribution of samples collected for apatite Fission Track Thermochronometry. Sample names begin with a three-letter prefix, indicating location within Bare Mountain. Sample ages are also shown. (b) Histogram showing the distribution of apatite fission track ages.

Table 2-1. Fission track results from Bare Mountain, Nevada

Sample	Rock Type	Elevation (m)	ρs	N_S	N_I	N_T	N_G	Age (Ma)	Length (μm)	U_C (ppm)
BFH-1	CZw (schist)	988	0.168	157	3,386	75	40	13.9±1.2	14.3±0.2	45
BFH-2	CZw (schist)	1,073	0.170	159	3,739	101	34	12.8±1.1	14.1±0.2	59
BFH-3	Zs(quartzite D member)	1,091	0.209	124	2,712	51	26	13.7±1.3	13.8±0.3	48
BMN-1	Kg (granite)	1,110	0.033	17	374	26	34	11.0±2.8	13.9±0.2	8
BMN-2	Td (diorite)	1,061	0.148	13	201	20	11	19.5±5.6	13.8±0.5	15
BMN-4	Cz (quartzite)	1,360	0.227	82	1,163	30	23	21.2±2.5	ND	48
BMN-5	Cz (quartzite)	1,232	0.149	75	1,624	14	22	13.9±1.7	13.4±0.5	29
BMN-10	Cz (quartzite)	1,677	0.152	22	799	5	14	8.3±1.8	12.4±2.6	66
BMN-13	Oe (quartzite)	1,787	0.148	46	1,033	12	12	13.4±2.1	13.4±0.9	49
BMN-15	Cz (quartzite)	1,610	0.313	45	749	4	11	18.1±2.9	ND	56
BMN-19	Cz (quartzite)	1,055	0.103	28	431	33	24	19.6±3.9	13.4±0.4	15
BMN-20*	Oe (quartzite)	1,445	0.142	4	32	12	4	29.3±15.6	14.5±1.3	17
BME-1	MDe (conglomerate)	1,317	0.183	42	906	12	20	13.9±2.2	13.9±0.5	49
BME-2*	Tl (latite)	1,226	0.062	35	458	18	33	23.0±4.1	12.5±0.8	8
BME-3	CZw (schist)	1,024	0.072	12	173	2	15	20.9±6.3	ND	9
BME-17*	Oe (quartzite)	1,207	0.008	1	128	0	13	2.3±2.3	ND	10
BME-18	Zs (quartzite E member)	1,189	0.232	87	1,546	30	32	16.8±1.9	13.7±0.4	46

Table 2-1. Fission track results from Bare Mountain, Nevada (Cont'd)

Sample	Rock Type	Elevation (m)	ρs	N_S	N_I	N_T	N_G	Age (Ma)	Length (μm)	U_C (ppm)
BMW-1	Zs (schist C member)	1,128	0.168	93	309	8	28	17.3±4.3	12.1±1.0	7
BMW-2*	Zs (quartzite D member)	976	0.063	28	150	23	29	45.7±9.5	12.5±0.7	4
BMW-3	Zs (quartzite D member)	997	0.115	89	1,569	26	33	14.0±1.6	13.0±0.4	28
BMW-5	Cz (quartzite)	1,220	0.128	28	352	7	21	19.7±3.9	12.6±0.7	18
BMW-6	Zs (quartzite D member)	1,049	0.137	30	413	51	18	22.0±4.2	13.2±0.3	20
BMW-12A	Zs (quartzite D member)	1,098	0.074	10	256	23	14	11.8±3.8	13.2±0.7	18
BMW-12B	Td (diroite)	1,098	0.123	12	261	0	7	13.9±4.1	ND	29
BMW-13*	Zs (quartzite A member)	939	0.155	28	234	5	9	36.4±7.4	13.8±1.2	17

Sample numbers are the same as in Figure 2-4. *designates samples not used in the calculation of the mean age or distribution of ages in Figure 2-5a (see text). Rock type is the sampled formation; Zs—Precambrian Stirling Quartzite, CZw—Precambrian-Cambrian Wood Canyon Schist, Cz—Cambrian Zabriskie Quartzite, Oe—Ordovician Eureka Quartzite, MDe—Mississippian-Devonian Eleana Formation, Kg—Cretaceous granite sill, Td—Oligocene diorite dike, Tl—Miocene quartz-latite dike. Elevation is the sampling site at BM in meters. ρs is the track density ($\times 10^6$ tracks/cm^2). N_S and N_I are the number of natural and induced tracks. N_T is the number of track-lengths counted for temperature-time modeling. N_G is the number of apatite grains from the sample. Age is the mean age in Ma, reported with the pooled standard deviation. Length is the mean etched track length (μm), reported with the pooled standard deviation (ND indicates that a mean track length was not determined for the sample). U_C is the concentration of ^{238}U in parts per million (ppm).

Fission Track Ages

Reliable ages were obtained from 22 of the 25 samples (Table 2-1). Samples BMN-20 and BME-3 contained less than five apatite grains, too few for adequate statistical control. BME-2 yielded a fission track age significantly older than the reported 13.9-Ma potassium-argon age for the host rock (Carr, 1984). Therefore, the apatite fission track age for BME-2 is considered unreliable. Of the remaining samples, all but two yield Miocene ages. The two anomalous samples, BMW-2 and BMW-13, yield lower Tertiary ages. Both samples are from the south tip of BM [Figure 2-4(a)] and suggest that this region may have experienced a different cooling history than the rest of the mountain. These older ages indicate that the southern tip of BM remained below apatite annealing temperatures since at least the Eocene, and suggest an earlier uplift of BM in the Late Cretaceous or Early Tertiary. Although geologically interesting, these results are not relevent to the most recent uplift of BM. Therefore, these two samples have also been excluded from the calculations of FTT age means and the temperature-time analysis.

The mean age of the remaining 20 samples is 15.8 ± 1.7 Ma (two standard errors about the mean). The ages are slightly skewed toward a younger age, with a median age of 14.0 Ma [Figure 2-4(b)]. Examination of the geographic distribution of fission-track ages does not reveal any statistically distinguishable age-trends, either across or along the spine of BM, or in relation to elevation.

Cooling Histories

Induced, unannealed, etched fission tracks in the BM apatites average 16.2 μm in length. Mean confined track lengths of natural fission tracks range between 13.0 to 14.3 μm. The majority of samples have mean track lengths of natural fission tracks of greater than 13.5 μm with standard deviations less than 1.5 μm. These relatively long track lengths, with minimal variation, suggest rapid cooling after the samples passed through closure temperature. Tracks are slightly longer in the northwest (average of 14.1 μm) than in the northeast (average of 13.8 μm), indicating that samples in the northeast remained at slightly elevated temperatures (but below closure temperature) longer and may have been more recently exposed than samples in the northwest.

Temperature-time models from western BM were derived for 16 samples [Figure 2-5(a)]. An average cooling curve was also constructed from the mean of the individual model temperatures at 750,000-yr intervals [Figure 2-5(b)]. The error bars are two standard errors around the 750,000-yr averages. The temperature-time models indicate a three-phase cooling history for BM since the Miocene: (i) 11.8 °C/Ma cooling for the period between 15 and 10 Ma, (ii) 3.7 °C/Ma cooling for the period between 10 and 4.0 Ma, and (iii) 7.2 °C/Ma for the period between 4 Ma and the present.

Explanation of these cooling rates encompasses two end-member models dependent on assumptions of the geothermal gradient. In the first model, the changes in cooling rate represent changes in uplift rates for BM, in which the Southern Nevada geothermal gradient remained near an average continental value of 30 °C/km since the Miocene. In the second model, the changes in cooling rate represent changes in the geothermal gradient through time with constant uplift of BM since the Miocene.

Assuming a constant geothermal gradient of 30 °C/km and a mean annual surface temperature of 15 °C, these cooling rates suggest that BM rose at a rate of (i) 0.39 mm/yr between 14 and 10 Ma, (ii) 0.12 mm/yr between 10 and 4 Ma, and (iii) 0.24 mm/yr between 4 Ma and the present. One interpretation of this uplift history would be rapid uplift in the middle Miocene (14–10 Ma) followed by a second period of uplift (4 Ma to present) related to activity of the BMF.

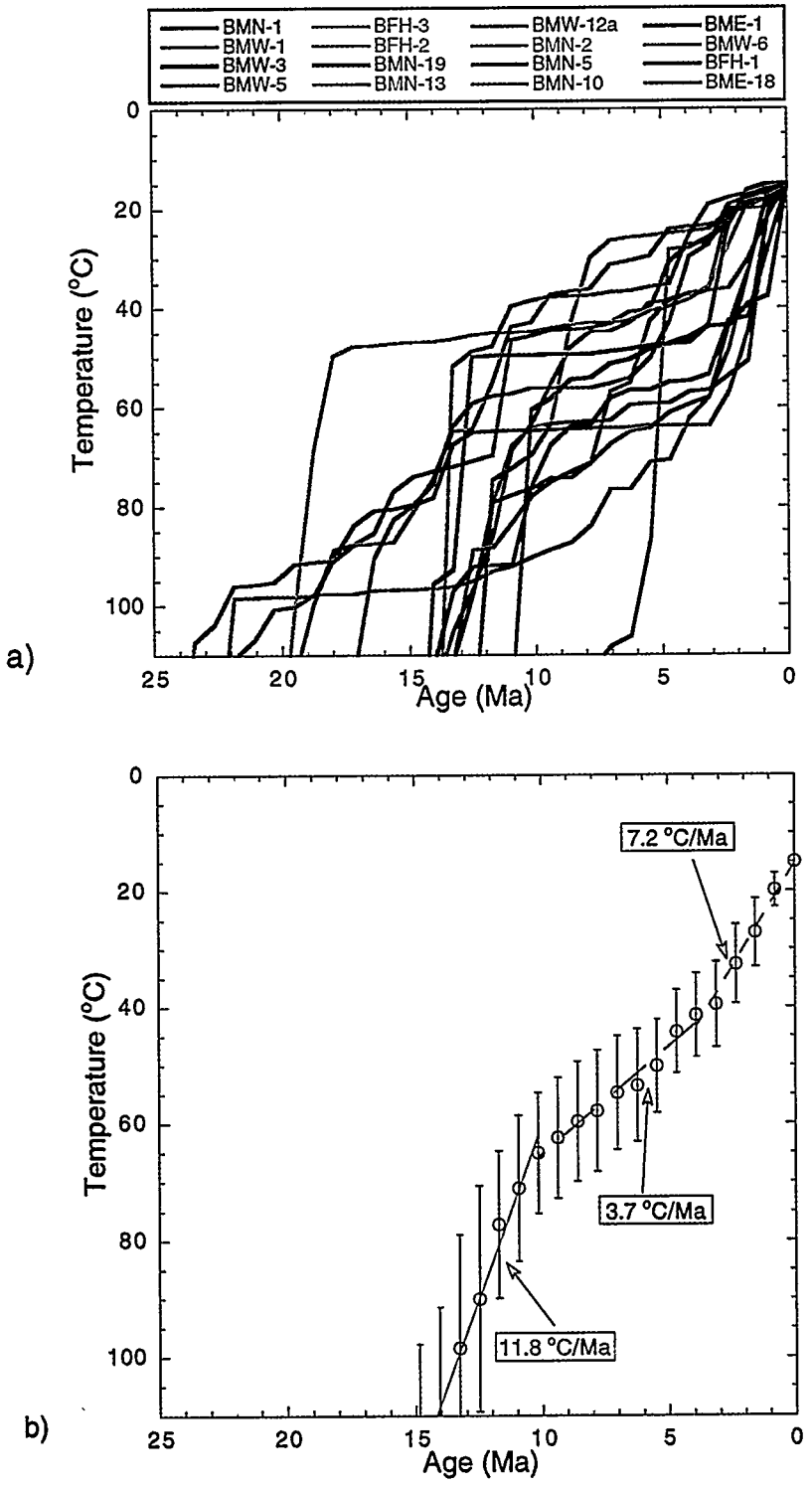

Figure 2-5. (a) Modeled temperature-time diagrams from the distribution of confined fission track lengths. (b) An average temperature-time curve derived from the curves in (a). The error bars are two standard errors about the mean model temperatures calculated at 750,000-yr increments.

Alternatively, the more rapid cooling between 10 and 4 Ma may represent a higher geothermal gradient associated with extensive Early and Middle Miocene volcanic activity in southwestern Nevada (Sawyer et al., 1994). For example, doubling the geothermal gradient to 60 °C/km during this period would result in an uplift rate of 0.20 mm/yr, consistent with the average uplift rate for the Late Miocene to the present.

2.3.4.4 Tectonic Implications

In concert with other geological and geo-chronological data, we conclude from the apatite FTT results that the BMF was continuously involved in BM tectonism since the Middle Miocene. Four lines of reasoning support our conclusion.

- Fission track ages indicate cooling of BM through 110 °C between 14 and 15 Ma, probably as the result of tectonic denudation of BM as the BHDS developed. Maldonado (1990) concluded that the upper plate of the BHDS was active between 10 and 8 Ma. Yet radiometric ages of metamorphism of the lower plate range between 16.3 and 10.5 Ma, suggesting that the BHDS may have been active since at least 16 Ma (McKee, 1983; Maldonado, 1990). Our fission track results support this earlier BHDS motion.

- The occurrence of megabreccia of Paleozoic rock in Crater Flat between the 12.7-Ma Tiva Canyon Member and the 11.6-Ma Rainer Mesa Member indicate that the BMF was active prior to 11.6 Ma (Carr and Parrish, 1985). Therefore, the early (15 to 10 Ma) uplift history for BM is not solely attributable to the BHDS.

- The temperature-time diagrams [Figures 2-5(a) and 2-5(b)] show continued uplift of BM from 15 Ma to the present, with a possible increase in uplift rates to 0.24 mm/yr since 4 Ma. In addition, 4 Ma to present motion on the BMF may have more recently exposed those samples collected in the northeast corner of BM compared with those collected in the northwest corner of BM, as indicated by the different mean track lengths from the two regions.

- The fission track results indicate that the total uplift of BM since 15 Ma is between 2 and 3 km, depending on the specific assumptions of the regional geothermal gradient. This amount is consistent with the estimated vertical displacement of the BMF (> 2 km; Snyder and Carr, 1984).

2.3.5 Bare Mountain Alluvial Fan Sedimentation Patterns

2.3.5.1 Introduction to Bare Mountain Alluvial Fans

Pleistocene and Holocene alluvial fans on the east side of BM juxtaposed directly against the BMF are noticeably smaller than alluvial fans on the west side of BM. On topographic maps and on a slope map of BM (Figure 2-6), alluvial fans on the eastern side of the mountain appear as isolated fan lobes, defined topographically by contours that are convex basinward. In contrast, the fans on the west side of the mountain have coalesced to form a bahada. Alluvial fan sedimentation patterns can be used to constrain the activity of the BMF during the last 2 Ma (Pleistocene and Holocene Epochs).

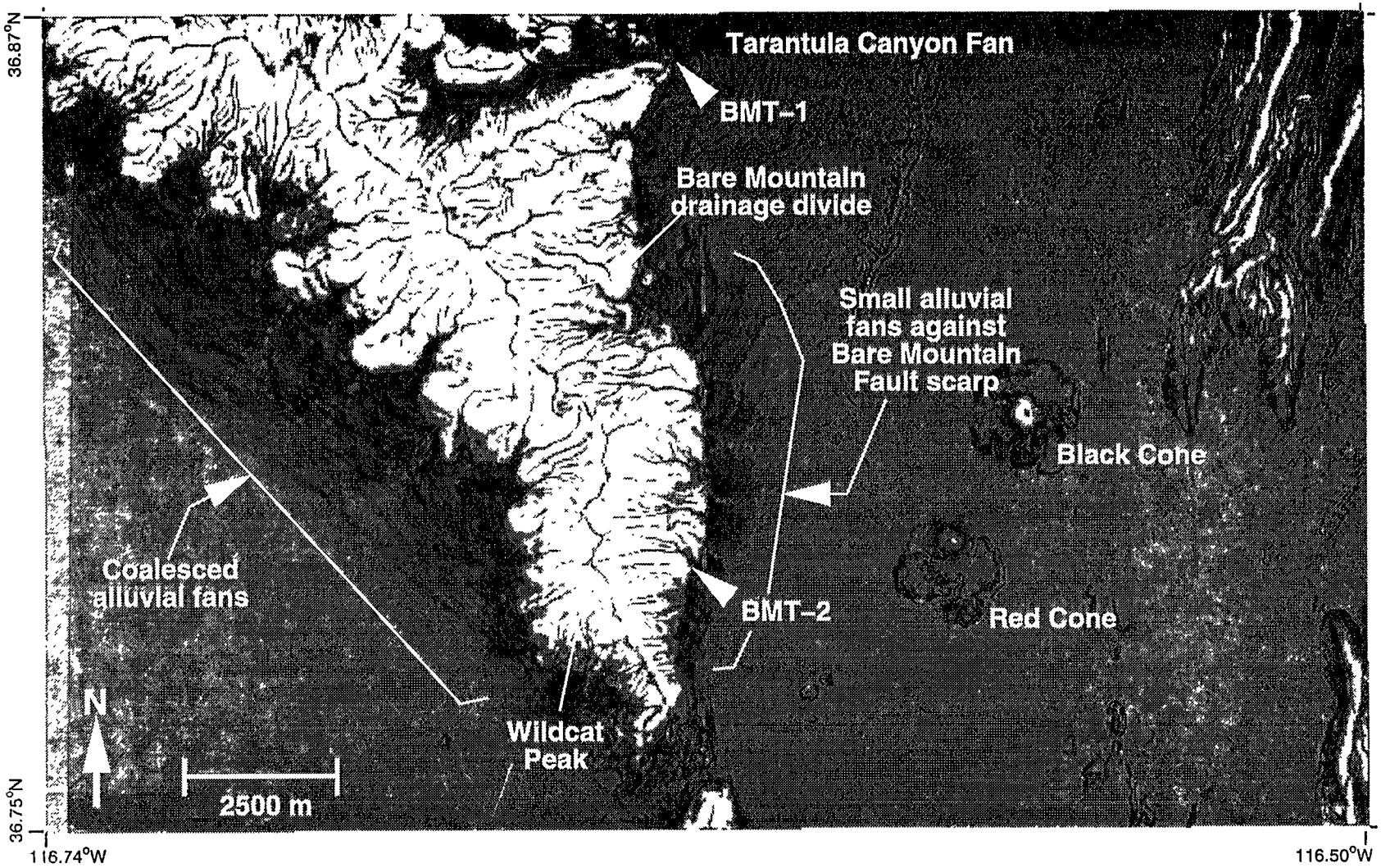

Figure 2-6. Slope map for Bare Mountain, Nevada, illustrating relatively small alluvial fans on the eastern side of BM in comparison to the larger alluvial fans on the western side of the Mountain. Arrows labelled BMT-1 and BMT-2 indicate approximate positions of Bare Mountain fault trenches which are the principal sources of interpretations of Bare Mountain Fault slip history (Reheis, 1988; Pezzopane, 1995)

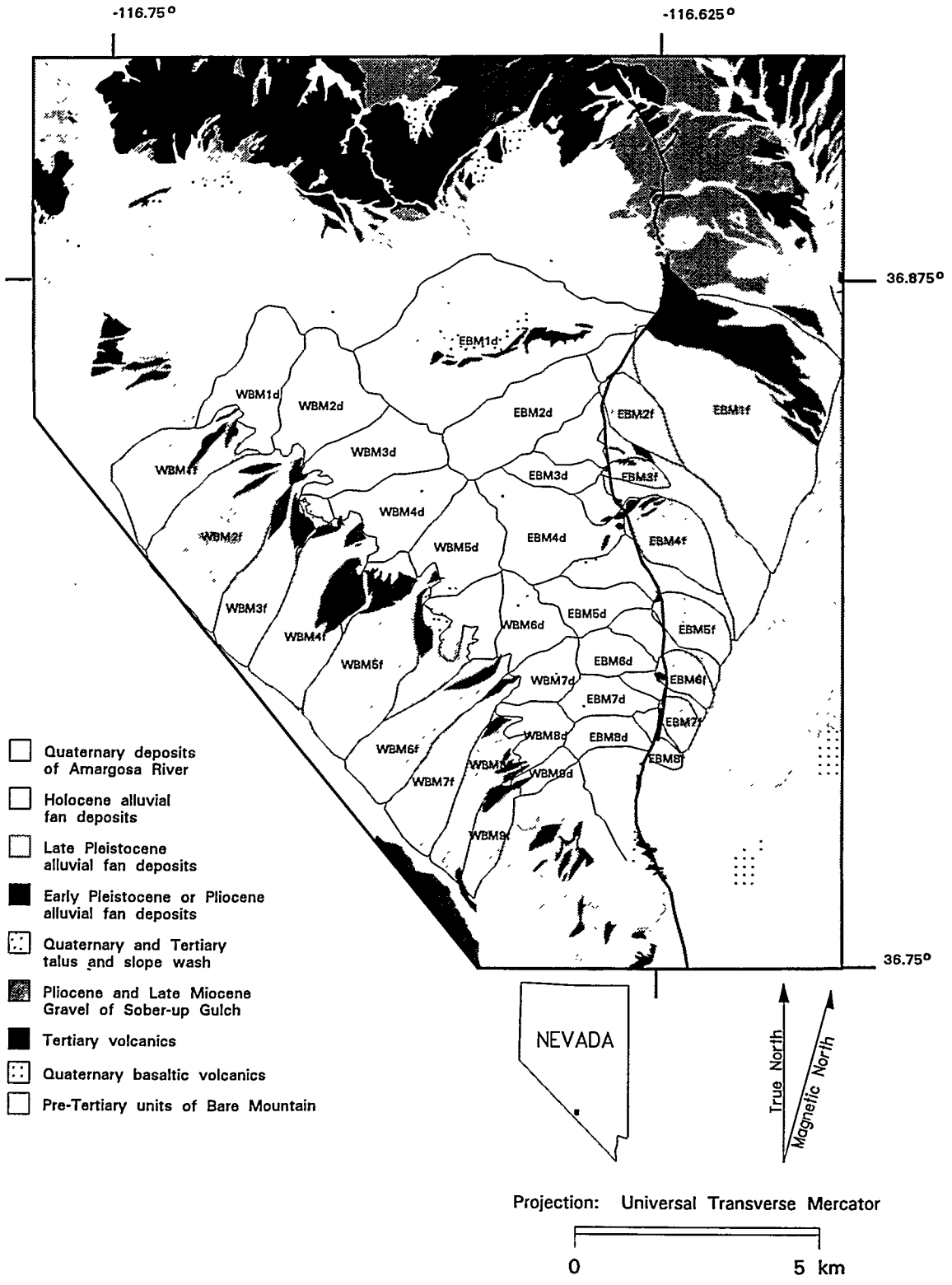

Figure 2-7. Map showing the outlines of measured alluvial fans and corresponding drainage basins, and distribution of alluvial fan sediments of different ages. Map compiled from Monsen et al., 1992 and Swadley and Parrish, 1988.

Analyses of the fans and their source areas indicate that differences in morphology of BM alluvial fans cannot be explained by differences in the size of drainage basins or rock type exposed in drainage basins (Figure 2-7). Drainage basins are of similar size for fans on the east and west sides of BM. Exposed strata vary from basin to basin but are generally the same units on either side of the mountain. There is no evidence to suggest that weather patterns on the east and west sides of the mountain would have been sufficiently different during the Pleistocene and Holocene to cause a significant difference in the rate of alluvial sediment production. Therefore, differences between fans on the east and west sides of BM appear to be tectonically controlled, either by (i) displacement on the BMF causing vertical aggradation of alluvial fans on the east side of the mountain (versus lateral progradation on the west side of the mountain), or (ii) uplift and tilting of BM, concomitant with displacement on the BMF, causing tilting of the western fans to steeper dips and a basinward shift in the position of sedimentation on western fans, causing the fans to enlarge. An investigation was undertaken to evaluate these two working hypotheses and, in particular, to study the potential role of slip on the BMF on alluvial fan sedimentation on the east side of BM.

2.3.5.2 Controls on Alluvial Fan Size

Alluvial fans are accumulations of clastic sediment that commonly occur at mountain fronts where streams empty into an adjacent basin (Reading, 1978; Leeder, 1982). Alluvial fans in semiarid to arid climates tend to have length/width ratios of approximately 1 to 5 and typically have channels that are entrenched at the upstream end and that deposit downstream of the intersection point (intersection of fan surface and channel profile; Hooke, 1967; Heward, 1978). Alluvial fan size is controlled by the sediment production rate and the rate of development of accommodation space (Heward, 1978; Nilsen, 1982). Sediment production rate is a function of drainage basin area, exposed rock type(s), and climate. Accommodation space (vertical space available for sediment accumulation) development is primarily a function of basin subsidence and source area uplift, which are tectonically controlled. An empirical relationship to describe controls on alluvial fan area (A_f) exists, based on regression on a log-log plot of fan area versus drainage area (A_d) (Bull, 1964; 1968; Denny, 1965; 1967; Hooke, 1968).

$$A_f = c(A_d)^n \tag{2-1}$$

where n is the slope of the regressed line, and c is a constant that is dependent on source area lithology, climate, and tectonic activity. In a tectonically inactive setting, the rate of vertical accommodation space development is low. Alluvial fans at inactive mountain fronts tend to prograde laterally, which causes a progressive increase in fan area with respect to drainage area. At tectonically active mountain fronts, where the mountains are rising with respect to the adjacent basin, alluvial fans tend to aggrade vertically (filling vertical accommodation space), resulting in fans of relatively small area with respect to drainage area. In the case in which an alluvial fan has been tilted to a steeper slope angle, the upstream end of the fan may be entrenched and dissected and the active deposition shifted to the most distal portion.

2.3.5.3 The Example of Death Valley Alluvial Fans

Central Death Valley contains classic examples of the effects of active tectonics on alluvial fan sedimentation (Denny, 1965; Hooke, 1972) and can be used to frame the discussion of the BM fans. The extensive system of coalesced alluvial fans that has been shed eastward from the Panamint Mountains into western Death Valley is significantly dissected at the upstream (proximal) ends of the fans. Deposition in the western Death Valley alluvial fan system has shifted basinward and is concentrated at the toes of

the alluvial fans (Hooke, 1972). The ratio of fan area to drainage area (A_f/A_d) for eight alluvial fans on the west side of central Death Valley is 0.35 ± 0.13 (based on measurements of Denny, 1965) (Figure 2-8). In contrast, alluvial fans shed from the Black Mountains (on the east side of Death Valley) into eastern Death Valley are dramatically smaller than those on the western side of Death Valley, generally appearing as individual fans that are not in contact with each other. Eleven eastern Death Valley fans have A_f/A_d ratios that average to 0.1 ± 0.04 (based on measurements of Denny, 1965). Sedimentation on the eastern Death Valley fans tends to be on the fans, and concentrated in the upper fan against the mountain range (Hooke, 1972).

The differences between alluvial fan sedimentation on the eastern and western sides of central Death Valley are thought to be directly related to displacement on the central Death Valley Fault, which bounds central Death Valley on the east side. Displacement on the Death Valley Fault continues to lower eastern Death Valley fans with respect to the source mountain range. Therefore, fans do not prograde significantly. On the western side of central Death Valley, there is no major active fault at the surface to steadily drop the valley floor. In this case, alluvial fans remain relatively stable and tend to prograde basinward. Tilting of the eastern flank of the Panamint Range, probably due to displacement on the Death Valley Fault (along the eastern side of Central Death Valley), has caused steepening of the fans such that hydraulic energy is relatively high on the alluvial fan surface, and sediment is transported basinward to the toe of the alluvial fans, where deposition occurs.

2.3.5.4 Bare Mountain Alluvial Fans

Alluvial fan sediments mapped on the east and west sides of BM are interpreted, based upon correlation with dated sediments, to be Holocene to early Pleistocene or Pliocene in age (Reheis, 1986; Monsen et al., 1992). The BM alluvial fan sediments are subdivided into three units: (i) younger alluvial fan deposits (Holocene), (ii) intermediate alluvial fan deposits (late Pleistocene), and (iii) older alluvial fan deposits (early Pleistocene and/or Pliocene) (Figure 2-7). Fans on the west side of BM contain relatively large amounts of exposed intermediate and older alluvial fan sediments. The bulk of younger alluvial fan deposits on the west side of the mountain are in mid-fan and distal positions. In contrast, Holocene alluvial fan sedimentation on the eastern side of BM (south of Tarantula Canyon) has occurred at the heads of the alluvial fans, producing young fan lobes immediately against the BMF (Reheis, 1986; 1988).

To address quantitatively the relationships between fan and drainage areas for fans on either side of BM, alluvial fans and drainage basins were delineated on 7.5-min topographic maps and digitized (Figure 2-7). Areas for BM fans were calculated using ArcInfo(TM) (Table 2-2) and graphed with previously measured fans in Death Valley (Figure 2-8). Although drainage areas are of similar size on the eastern and western sides of BM, fans on the eastern side of BM are distinctly smaller in area than those on the western side of the mountain (Figure 2-9). The average ratio A_f/A_d of fan area to drainage area for fans on the western side of the mountain is 1.76, whereas the average A_f/A_d for eastern fans is 0.65. If the Tarantula Canyon (EBM1) fan is excluded from the population of eastern BM fans, the average A_f/A_d ratio for eastern fans is 0.57. Area calculations for discrete alluvial fans and drainage basins do not include the entire alluvial fan and source areas on both sides of BM. The total source area for the fan system on the western side of BM encompasses a map area of 22.5 km^2, and the western fan system covers a 35.1 km^2 area. The total source area for the fans on the eastern side of BM cover a 29.8 km^2 area, and the eastern fan system covers an area of 26.8 km^2. The ratio of alluvial fan (bahada) area to source area for western BM is 1.56, compared with 0.90 for the eastern BM fans and drainage

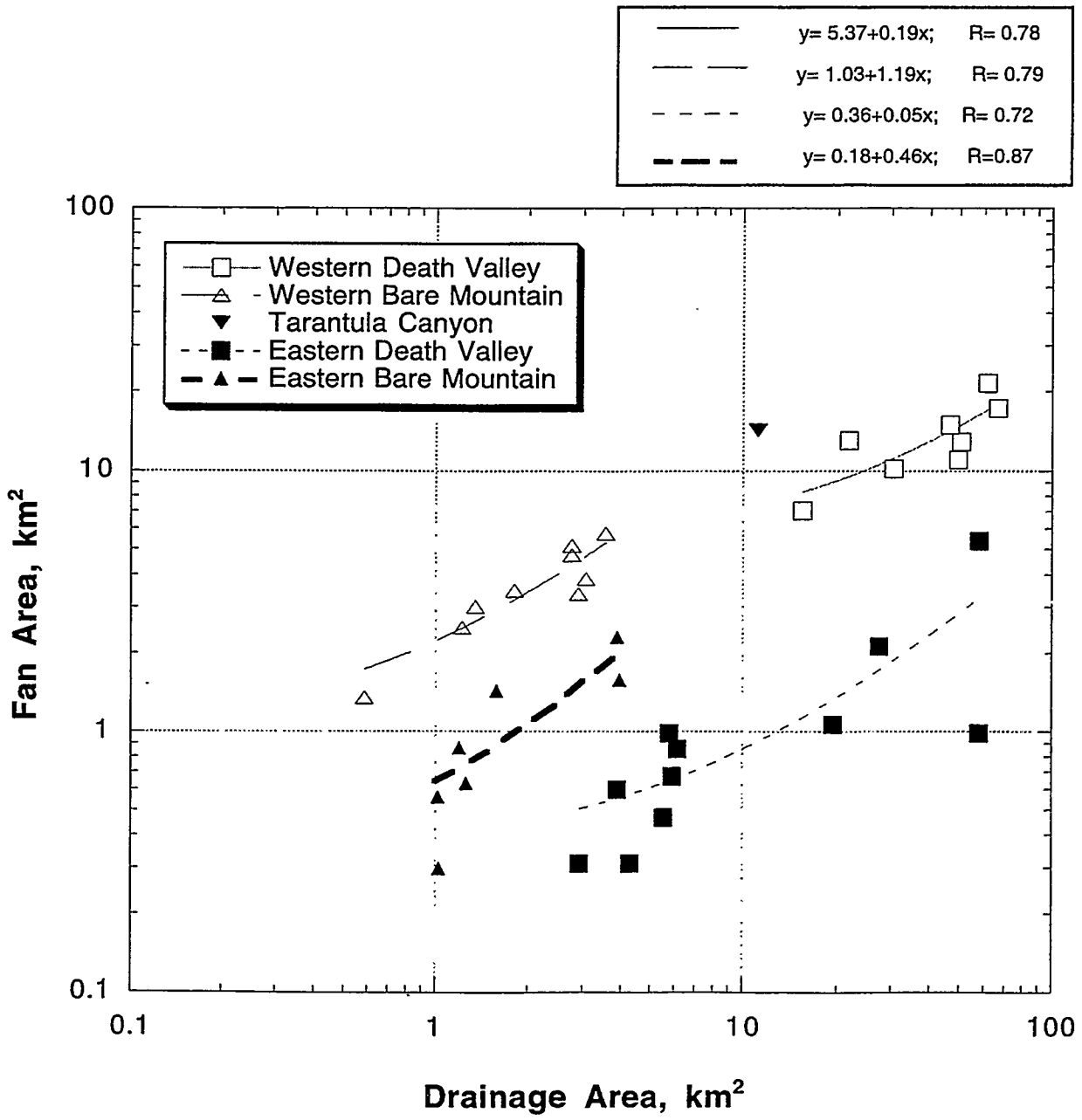

Figure 2-8. Log-log plot of alluvial fan area versus drainage area for alluvial fans on the east and west sides of central Death Valley, and the east and west sides of Bare Mountain. Eastern Death Valley is bounded by the active Death Valley Fault, and eastern Bare Mountain is bounded by the Bare Mountain Fault.

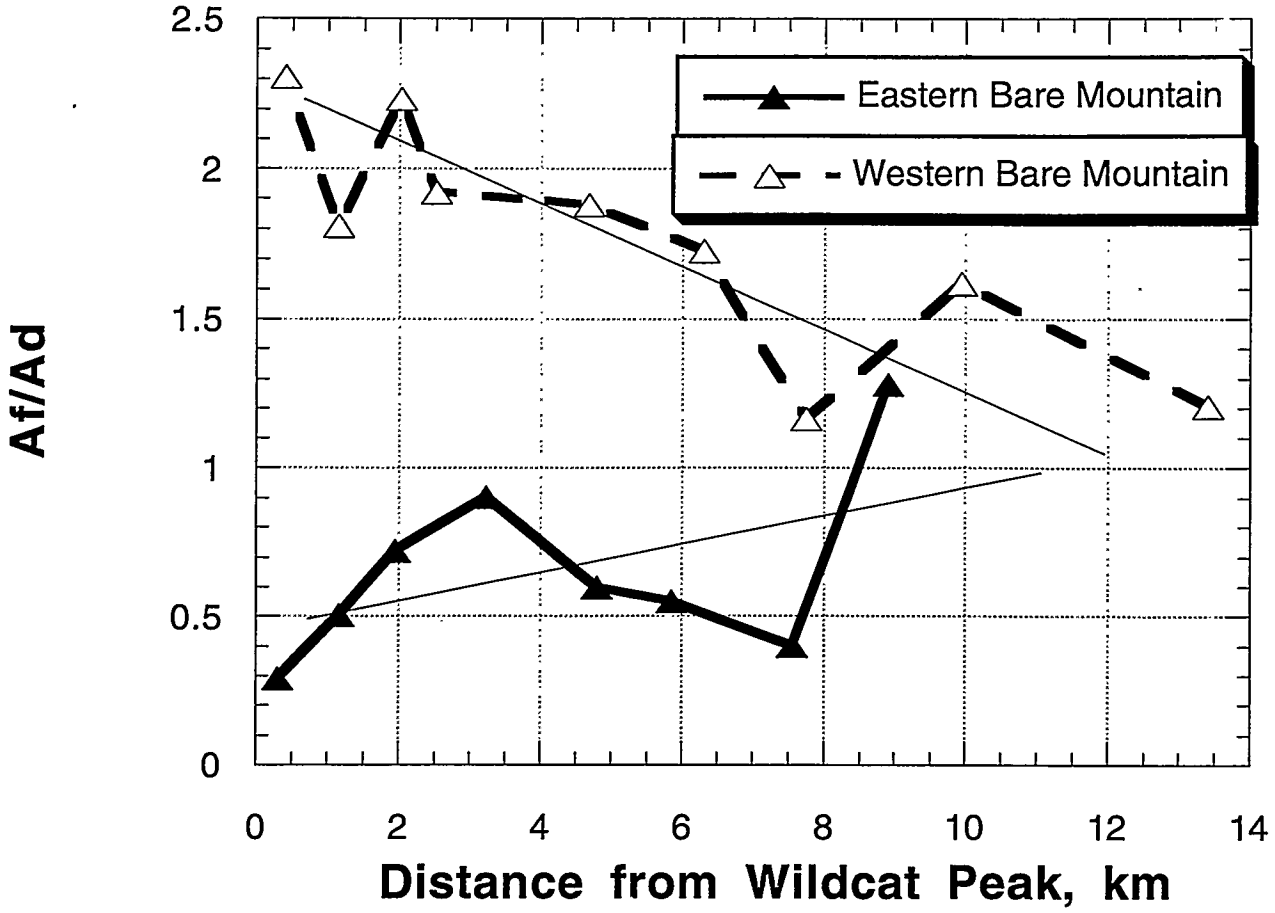

Figure 2-9. Plot of the ratio of alluvial fan area (A_f) to drainage area (A_d) for Bare Mountain alluvial fans versus distance from Wildcat Peak in southern BM. Fans on the western side of Bare Mountain generally decrease in A_f/A_d ratio from a maximum near the southern end of BM. A_f/A_d ratio for fans on the eastern side of Bare Mountain generally increases from south to north, which, along with the trend on the west side of the mountain, may correspond to a general south to north decrease in Pleistocene and Holocene displacement on the Bare Mountain Fault. Fluctuations in the overall south to north decline in A_f/A_d ratio along the Bare Mountain Fault may be due to differences in the rate of throw caused by variations in fault dip. See text for further discussion.

Table 2-2. Paired alluvial fan area and drainage area measurements from alluvial fans on the east and west sides of Bare Mountain, Nevada. Distance of eastern (western) Bare Mountain fans from Wildcat Peak is measured in km by projecting the mouth of the drainage basin onto a north-south (northwest-southeast) transect. Units I, II, and III, refer to the normalized percentages of map-view exposure areas of lower clastic, carbonate, and upper clastic source units for each drainage area.

	Drainage Area (A_d)	Fan Area (A_f)	Distance from Wildcat Peak	A_f/A_d	Unit I	Unit II	Unit III
Eastern Bare Mountain							
EBM1	11.17	14.28	8.9	1.28	11.1	63.7	25.2
EBM2	3.96	1.58	7.56	0.40	1.1	98.9	0.0
EBM3	1.02	0.56	5.85	0.55	0.0	100.0	0.0
EBM4	3.88	2.31	4.8	0.60	18.8	81.2	0.0
EBM5	1.58	1.43	3.22	0.90	49.4	50.6	0.0
EBM6	1.20	0.86	1.94	0.72	0.0	100.0	0.0
EBM7	1.26	0.63	1.16	0.50	0.0	100.0	0.0
EBM8	1.03	0.30	0.30	0.29	28.3	71.7	0.0
Average	3.14	2.74	4.22	0.65	13.6	83.3	3.1
Western Bare Mountain							
WBM1	3.14	3.78	13.42	1.21	100.0	0.0	0.0
WBM2	3.55	5.75	9.95	1.62	77.8	22.2	0.0
WBM3	2.90	3.37	7.75	1.16	25.3	74.7	0.0
WBM4	2.76	4.76	6.31	1.73	45.3	54.7	0.0
WBM5	2.75	5.17	4.68	1.88	26.8	73.2	0.0
WBM6	1.81	3.48	2.52	1.92	91.0	9.0	0.0
WBM7	1.35	3.01	2.02	2.23	69.9	30.1	0.0
WBM8	1.33	2.40	1.14	1.81	56.3	43.7	0.0
WBM9	0.58	1.35	0.41	2.31	100.0	0.0	0.0
Average	2.24	3.67	5.36	1.76	65.8	34.2	0.0

system. These total source and total fan areas include the discrete basins and fans noted in Table 2-2 and the areas between discrete basins and fans. The smaller fan-to-source ratio on the east side of BM indicates that vertical accumulation of sediment has occurred on the east side.

The relatively small A_f/A_d ratios for eastern fans and fan deposition directly against the BMF both suggest activity of the BMF during Pleistocene and Holocene time. Moreover, uplift and tilting of BM may have tilted alluvial fans on the west side of BM, causing a basinward shift in the position of alluvial fan sedimentation toward the toes of the alluvial fans similar to sedimentation on the west side of central Death Valley (Hooke, 1972). Variation in exposed stratigraphic units in drainage basins could also potentially affect fan size because of differences in mechanical and chemical weathering.

Stratigraphic units exposed in drainage basins on the eastern and western sides of BM consist almost entirely of late Proterozoic and Paleozoic clastic and carbonate sedimentary rocks (Figures 2-10 and 2-11). The stratigraphic sequence exposed in BM is subdivided into three units based on the overall erosional tendencies of the host units. The erosional behavior is likely to be controlled by lithology and the extent of metamorphism. Metamorphism in BM generally increases from northeast to southwest (Monsen, 1983; Monsen et al., 1992). The upper clastic unit (unit III) is exposed in BM only at the northeastern corner. Due to the low metamorphic grade, these clastic rocks in northeastern BM may be more susceptible to weathering and erosion than clastic rocks of unit I. The carbonate sequence is more susceptible to chemical weathering than units I and III, and therefore may produce less clastic sediment per original unit volume of bedrock than the clastic units (I and III). Although the current climate at BM is arid, precipitation rates were considerably higher during the Pleistocene, which may have enhanced chemical weathering.

Drainage basins on the western side of BM generally expose a greater proportion of unit I than unit II (Figure 2-12), whereas drainage basins on the eastern side of BM generally expose a greater proportion of unit II than unit I (Figure 2-13). There are, however, notable exceptions in this pattern of stratigraphic exposure that suggest that the exposed strata do not exert the dominant control on alluvial fan size. Three fans on the western side of BM correspond to drainage basins in which greater than half of the drainage area exposes unit II carbonate strata. These three fans have A_f/A_d ratios that are indistinguishable from fans for which 50 to 100 percent of the drainage area is in unit I clastics. On the eastern side of BM, the drainage basin that exposes the greatest proportion of unit I clastics (50 percent; EBM5) corresponds to a fan that has a relatively large ratio (0.90) compared with the average for eastern fans of 0.65. This value is considerably smaller than the average A_f/A_d ratio for western fans of 1.76, or even the minimum value for a western fan (WBM3) of 1.16. Based on these observations, we interpret that the dominant cause of the differences in fan size relative to drainage basin size for fans on eastern BM and western BM is tectonically, not stratigraphically, controlled. The exception may be the Tarantula Canyon drainage basin (EBM1), which exposes unit III clastics over 25 percent of its area. The A_f/A_d ratio for the Tarantula Canyon drainage system is 1.27 and is the largest of any fan on the eastern side of BM. Significant alluvial fan area, southeast of EBM3f and EBM4f, is unassigned to specific fans that were defined based on geomorphology. Part of this area may represent sediment sourced from Tarantula Canyon, which would increase the A_f/A_d ratio for EBM1. In addition, EBM1 may capture sediment from EBM2, EBM3, and EBM4, which would partially explain the low A_f/A_d ratios in EBM2, EBM3, and EMB4. Another potential cause of the large A_f/A_d ratio for EBM1 is the significant exposure of the easily weathered unit I. Regardless of these second-order effects, the overall A_f/A_d ratio is smaller on the eastern side of BM compared to the western side. Moreover, on both sides of BM, there are first-order

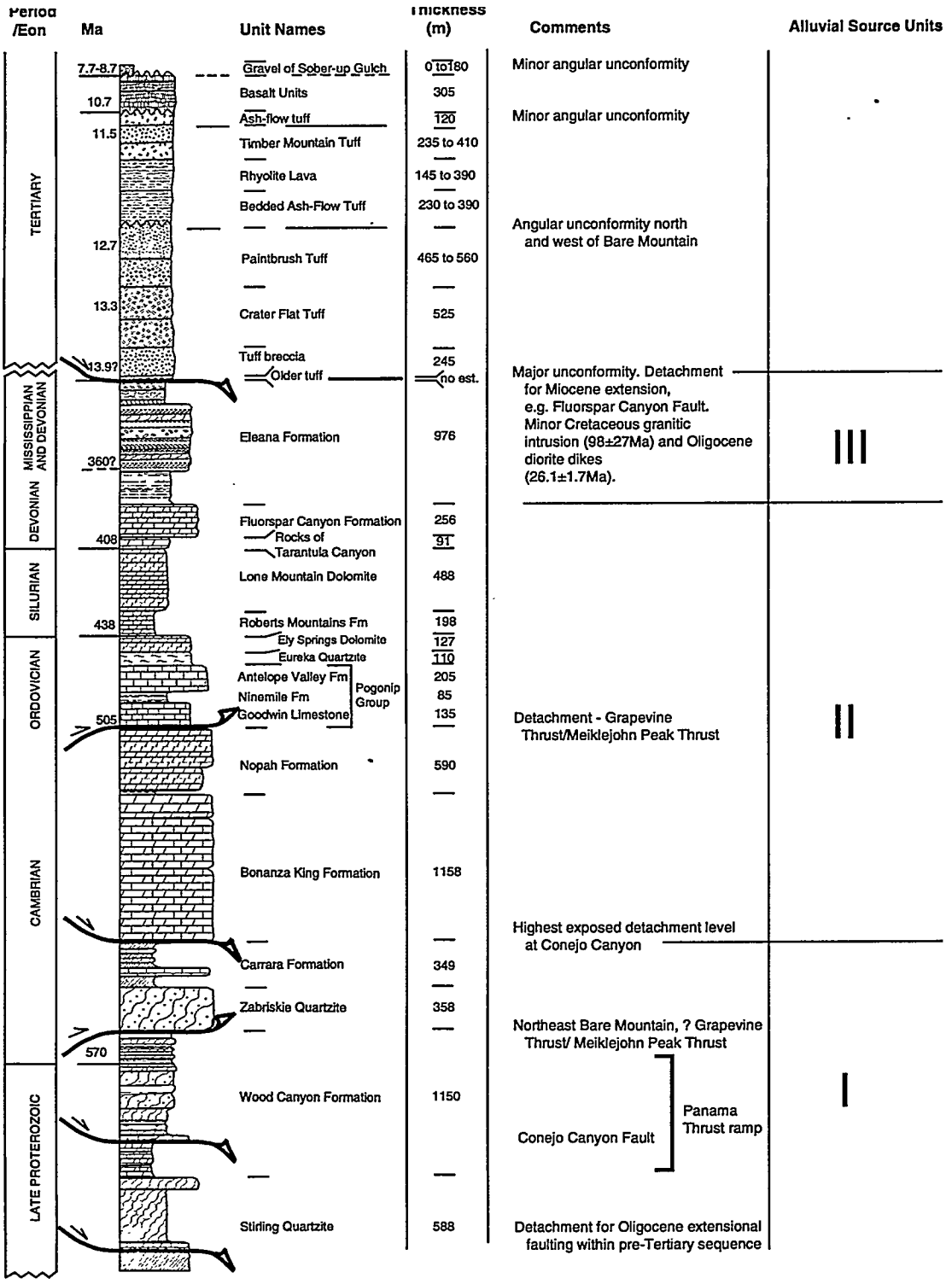

Figure 2-10. Stratigraphic section of Bare Mountain (after Monsen et al., 1992 and Sawyer et al., 1994) with interpretations of weathering profile pre-Tertiary strata are grouped into the alluvial source units: I=lower clastic, II=carbonate, and III=upper clastic

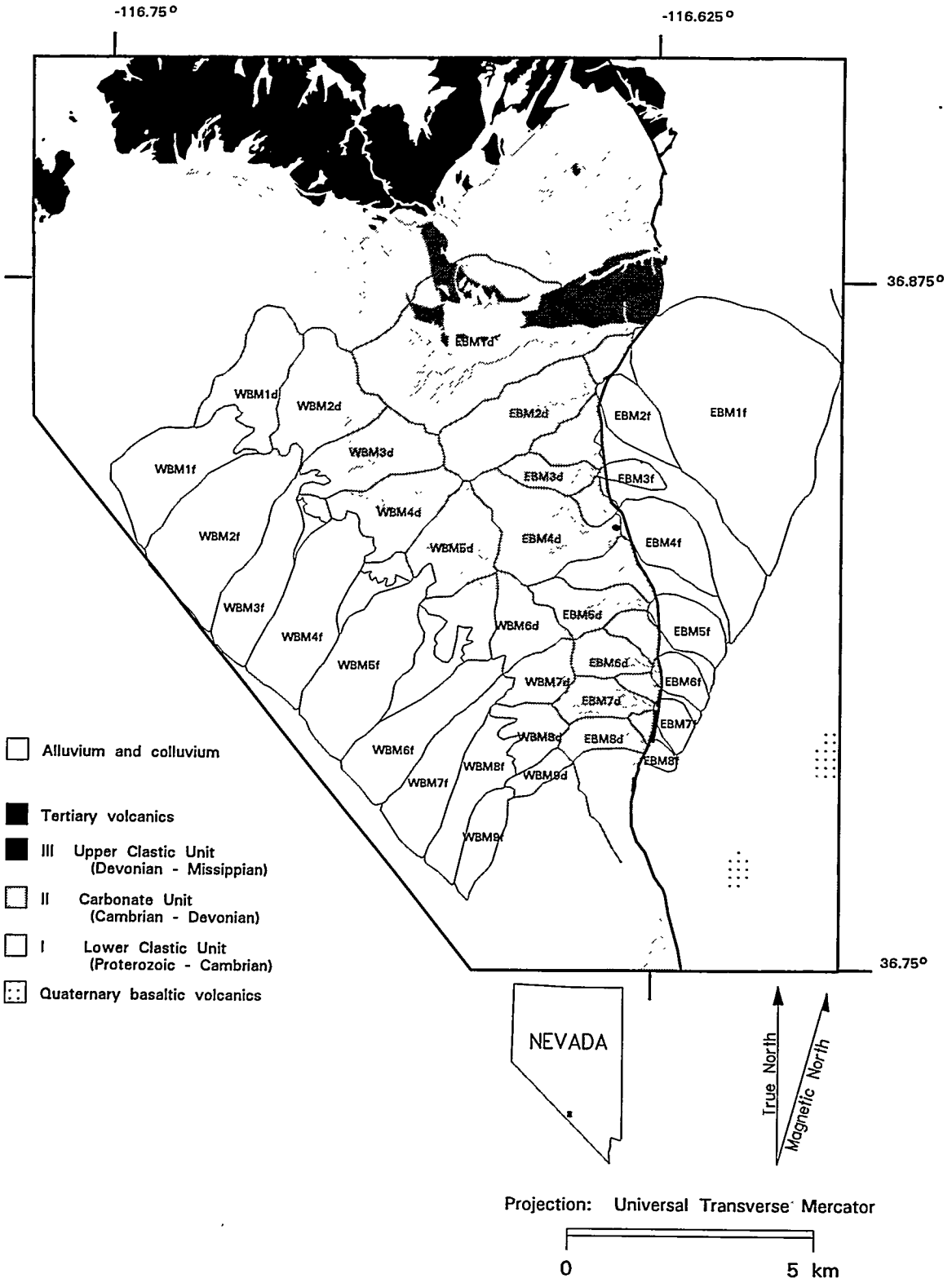

Figure 2-11. Map of Bare Mountain illustrating drainage basins subdivided according to exposed alluvial source units

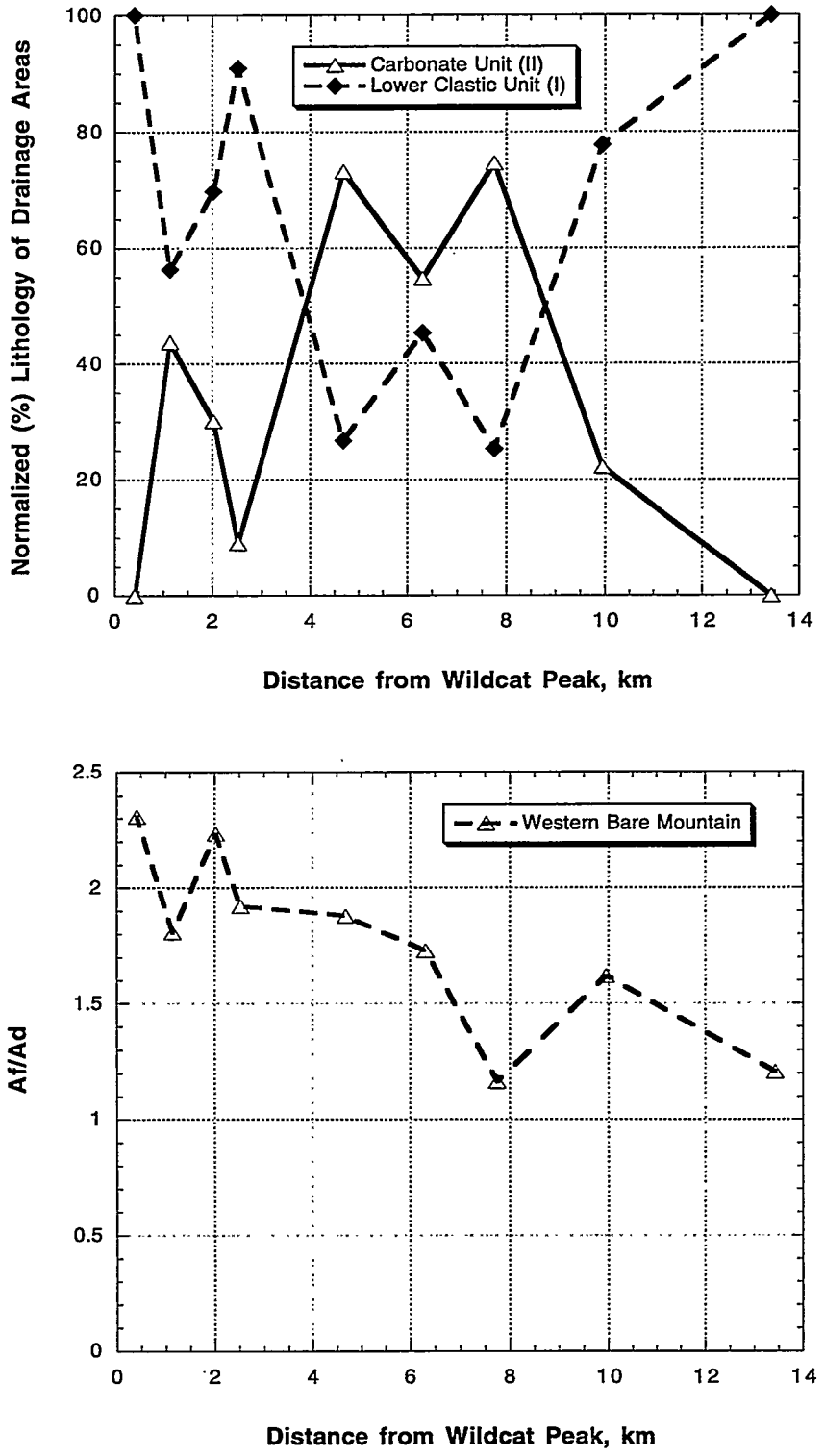

Figure 2-12. Graph of normalized percentages of alluvial source units versus distance plotted for comparison with A_f/A_d ratio for western Bare Mountain fans

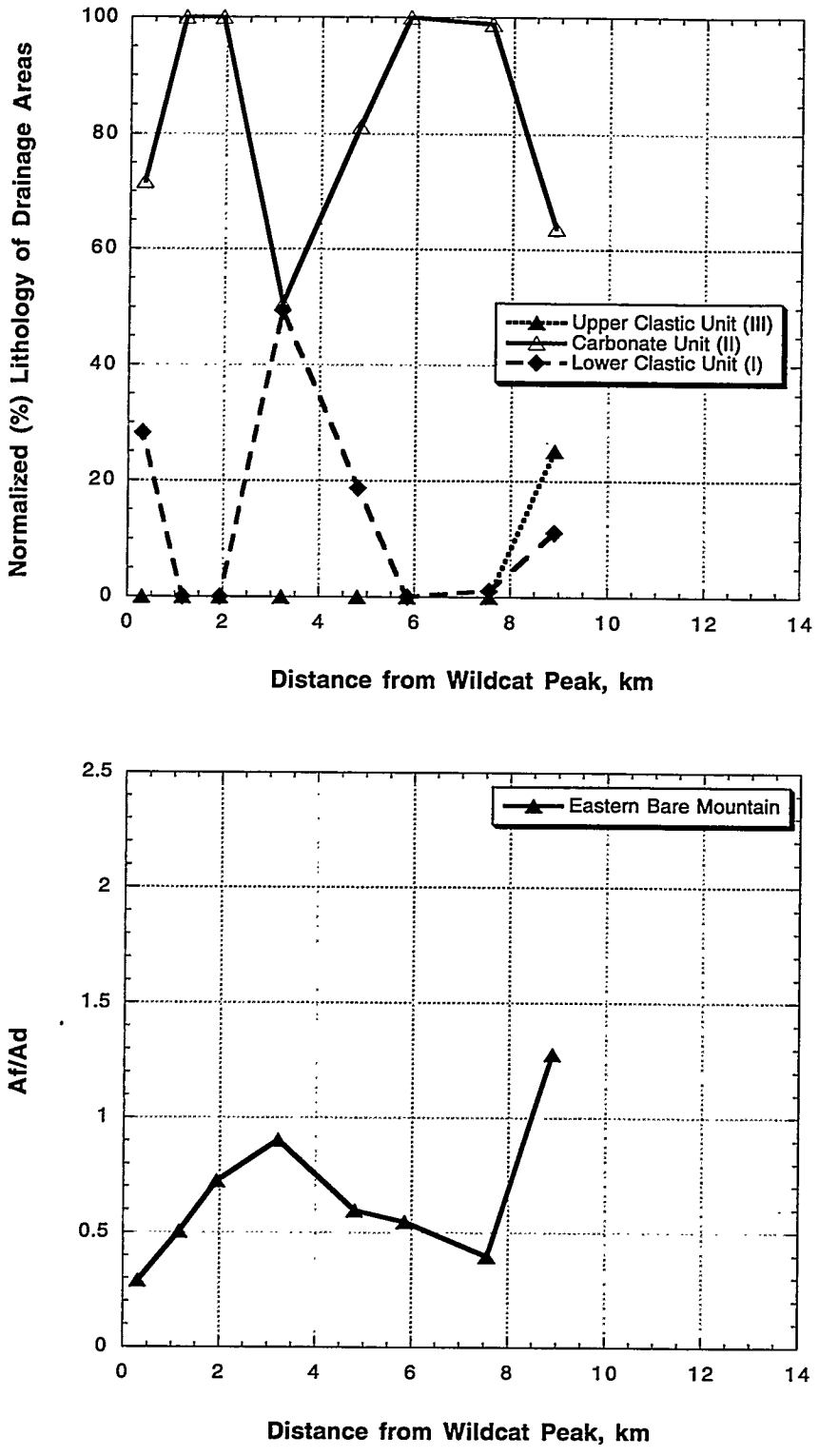

Figure 2-13. Graph of normalized percentages of alluvial source units plotted for comparison with A_f/A_d ratio for eastern Bare Mountain fans

changes in A_f/A_d ratio away from Wildcat Peak. These changes in A_f/A_d ratio are best explained in terms of the uplift of BM and, as such, indicate that the rate of throw on the BMF increases to the south. The details of the evolution of BM alluvial fans as a result of BMF motion are discussed in the following section.

2.3.5.5 Bare Mountain Fault Slip Rate and Alluvial Fans

On the west side of BM, comparison of A_f/A_d ratio with respect to distance (from Wildcat Peak) along a northwest-southeast transect indicates a general northwest-to-southeast increase in the A_f/A_d ratio (Figure 2-9). In contrast, there is a general north-to-south decrease in the A_f/A_d ratio along the east side of BM (Figure 2-9). The A_f/A_d ratio for the Tarantula Canyon fan is similar to values for fans on the western side of BM. One explanation for the general north-to-south trends in A_f/A_d ratios along the east and west sides of BM is that Pleistocene and Holocene slip on the BMF increases from north to south.

Variations in A_f/A_d on the eastern side of BM (Figure 2-9) may be directly related to the rate of fault throw. Fault displacement is the offset across a fault measured on the fault surface parallel to the slip direction. Throw is the vertical component of fault displacement, and heave is the horizontal component of fault displacement. The rate of fault throw is dependent on the rate of extension accommodated by the fault (equivalent to heave if extension is horizontal), or fault displacement, and the plunge of the fault slip direction (Figure 2-14). For an extensional fault, the plunge of the slip direction is dependent on the fault orientation and the direction of extension. In the case of a pure dip-slip, normal fault, for example, a 20° change in fault dip from 50 to 70° causes a 125-percent increase in the rate of throw (from 0.12 to 0.27 mm/yr, assuming a heave rate of 0.10 mm/yr; Figure 2-14). The BMF dips eastward at 45 to 55° near Tarantula Canyon, whereas south of Tarantula Canyon the dip of the fault is generally 60 to 70° eastward (Monsen et al., 1992). The minimum rate of throw estimated from a trench dug across a fault trace in Quaternary alluvium of the Tarantula Canyon fan is 0.015 mm/yr (Pezzopane, 1995 and references therein). If an average dip of 50° is assumed for the BMF in the vicinity of Tarantula Canyon, then the minimum rate of horizontal extension is calculated to be 0.013 mm/yr. Using this 0.013 mm/yr extension rate and the 70° fault dip measured approximately 4 km to the south, the calculated rate of throw would be 0.035 mm/yr. Obviously, the rate of fault throw for a normal fault is not only dependent on the rate of extension but is also strongly dependent on the dip of the fault.

These preliminary analyses of alluvial fan sedimentation patterns around BM indicate movement along the BMF during Pleistocene and Holocene time. There is a general correlation between A_f/A_d, the amount of Holocene alluvial fan sedimentation at the fan head, and the dip of the BMF. Area relationships and the depositional pattern of virtually no Holocene sedimentation at the fan head suggest that the Tarantula Canyon Fan (EBM1) is located at a position of relatively little Holocene throw along the BMF. The relatively low angle of dip (45 to 50°) in the vicinity of Tarantula Canyon also suggests that vertical offsets of trenched alluvium will tend to be smaller for a given increment of horizontal extension than along a more steeply dipping fault segment. These results suggest that fault slip rates derived from trenching studies in the Tarantula Canyon fan should be considered absolute minimum values and not representative of the BMF as a whole.

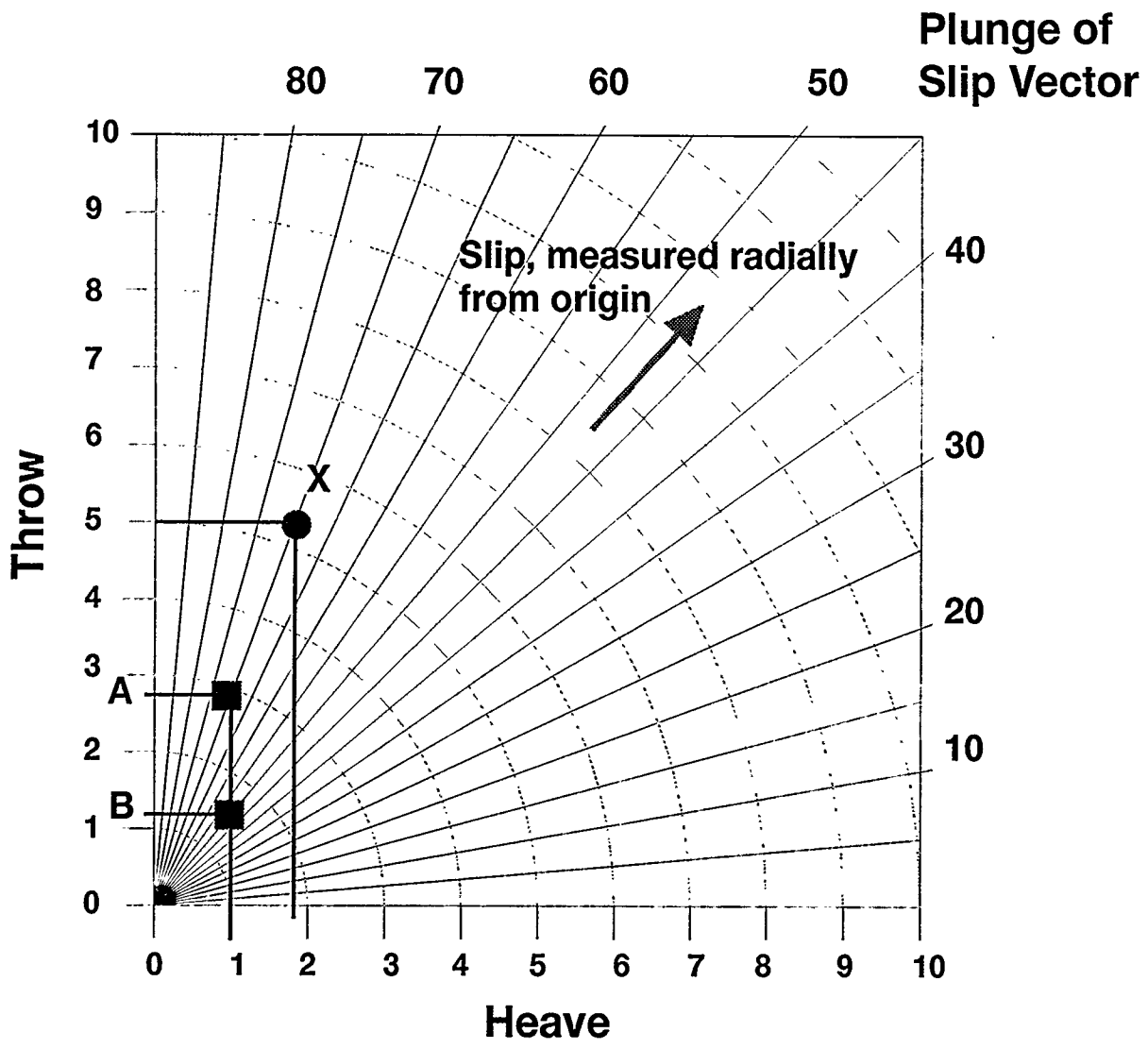

Figure 2-14. Two-dimensional plot to show the relationship between throw, heave, slip, and slip-vector plunge. The values of throw, heave, and slip are dimensionless, thus any units appropriate for these quantities can be substituted. For example, a dip-slip fault with a dip of 70° experiencing a throw of 5 units (mm, cm, m, km, etc.) would exhibit a heave of 1.8 units (measured along the abscissa axis) and a slip of 5.3 (measured radially from the origin, same units as throw and heave) as illustrated by point X on the figure. Alternatively, a dip-slip fault with dip varying from 50 to 70° along its strike but experiencing a constant rate of heave of 0.1 mm/yr would exhibit a throw rate of 0.12 mm/yr where it dips at 50° (point B on figure), and 0.27 mm/yr where it dips at 70° (point A on figure, see text).

2.4 DISCUSSION AND SUMMARY

Apatite FTT results presented in this report suggest a possible slip rate for the BMF during the Quaternary of approximately 0.28 mm/yr (using 0.24 mm/yr uplift and assuming an average fault dip of 60°). This rate is in obvious contrast with the estimate from the level-line survey and suggests that either the level-line survey records a strain rate anomaly that has not been sustained during the last few Ma, or that the level-line survey records nontectonic subsidence. Apatite FTT results suggest a much higher slip rate for the BMF than the 0.015 mm/yr rate determined by trenching of the Tarantula Canyon alluvial fan (Pezzopane, 1995). The rate determined from the fission track analysis is also greater than the 0.18 mm/yr maximum used by Pezzopane (1995). Alluvial fan sedimentation patterns discussed in the present report suggest that displacement has occurred on the BMF during the Pleistocene and Holocene, and that throw-rate increases southward from an approximate minimum at the Tarantula Canyon fan. This evidence is in contrast to interpretations from alluvial fan morphology of no slip in the last 100,000 yr, interpreted by Klinger and Anderson (1994). Results of these varied techniques used to estimate rate and timing of fault slip suggest that uncertainties associated with fault-trenching studies can be quite large and that multiple techniques should be used, when possible, to constrain fault-slip history.

3 SEISMICITY

Earthquake activity in the YM area represents a significant risk to the proposed HLW repository at YM because of potential adverse effects on long-term repository performance and preclosure safety. Realistic prediction and probability assessment of future seismicity is severely hampered by the extreme brevity of the historical seismic record (<200 yr) for the YM region compared with the 10,000 yr period of concern for licensing. KTUs related to future seismicity include uncertainties in determining: (i) spatial and temporal patterns of seismicity, (ii) slip history of faults, and (iii) magnitude of fault slip and seismic shaking at surface and shallow subsurface locations.

In this chapter, the historic seismic record is evaluated in order to: (i) assess the completeness of the historical seismic record, (ii) assess patterns of temporal and spatial clustering of earthquakes, (iii) characterize the position of YM with respect to belts of historic seismicity, (iv) evaluate the Landers Earthquake sequence as a potential analog for a major slip event on the DVFC fault system, and (v) assess potential for earthquake triggering in the YM area.

Historic earthquake data from the National Earthquake Information Center (NEIC) Preliminary Determination of Epicenters (PDE) database through February 11, 1994, have been studied to evaluate relationships between earthquakes and mapped faults, temporal and spatial clustering, and 3-D distribution of earthquake hypocenters through time with emphasis on the Landers earthquake sequence. The data set does not include all recorded earthquakes for the studied region in that it lacks most earthquakes smaller than M=3. The data set should, in general, include all recorded earthquakes of M=3 and larger for which epicenter locations have been determined. The data presented in Figure 3-1 include all earthquakes in the database and have not been filtered in any way. Therefore, earthquakes with manmade sources (i.e., nuclear weapons tests at the Nevada Test Site) have not been excluded. The hypocenters (3D positions of the earthquake foci) have considerably better accuracy for the map view position than the vertical positions. The horizontal positions are provided in the PDE database to the nearest 0.001 arc degree, which corresponds to a distance on the ground of about 100 m. This precision has improved from about 50 km for most epicenters in 1960 to 100-m precision today. The vertical positions (depths) are reported in whole kilometers. As indicated by the difference in reporting resolution between the horizontal and vertical positions, the vertical positions have about an order of magnitude lower reported resolution than the horizontal positions. Inaccuracy in earthquake hypocenter depths and epicenter location is significantly greater for earthquakes recorded prior to the mid 1960's.

The earthquake record for the western Great Basin extends for significantly less than 200 yr. Networks of seismographs have existed in the region for less than 100 yr. Figure 3-2 presents histograms of historic seismicity (for the region covered by Figure 3-3) for magnitude ranges from M=3 to greater than M=8. These histograms illustrate increases in abundance of recorded earthquakes that correspond to the establishment of networks of seismographs. Very large earthquakes (M>7) do not show a very distinct change in frequency, whereas smaller earthquakes (particularly M3 to M5) show pronounced increases since 1930, due to the establishment of seismic networks in the region. The historic earthquake record is too brief to assess accurately the earthquake risk based on the historic record alone. As an example, the Death Valley-Furnace Creek fault system appears from the earthquake data to be relatively quiet seismically (Figure 3-1). In contrast, Reheis (1994) has, based on trenching studies and ^{14}C dating in the northern Furnace Creek-Fish Lake Valley fault system, interpreted a minimum of seven ground-rupturing events over the past 5,000 yr, a recurrence interval of 500 to 1,000 yr, and an average right lateral displacement rate of 4 to 12 mm/yr. The time interval since the last ground-rupturing earthquake in the

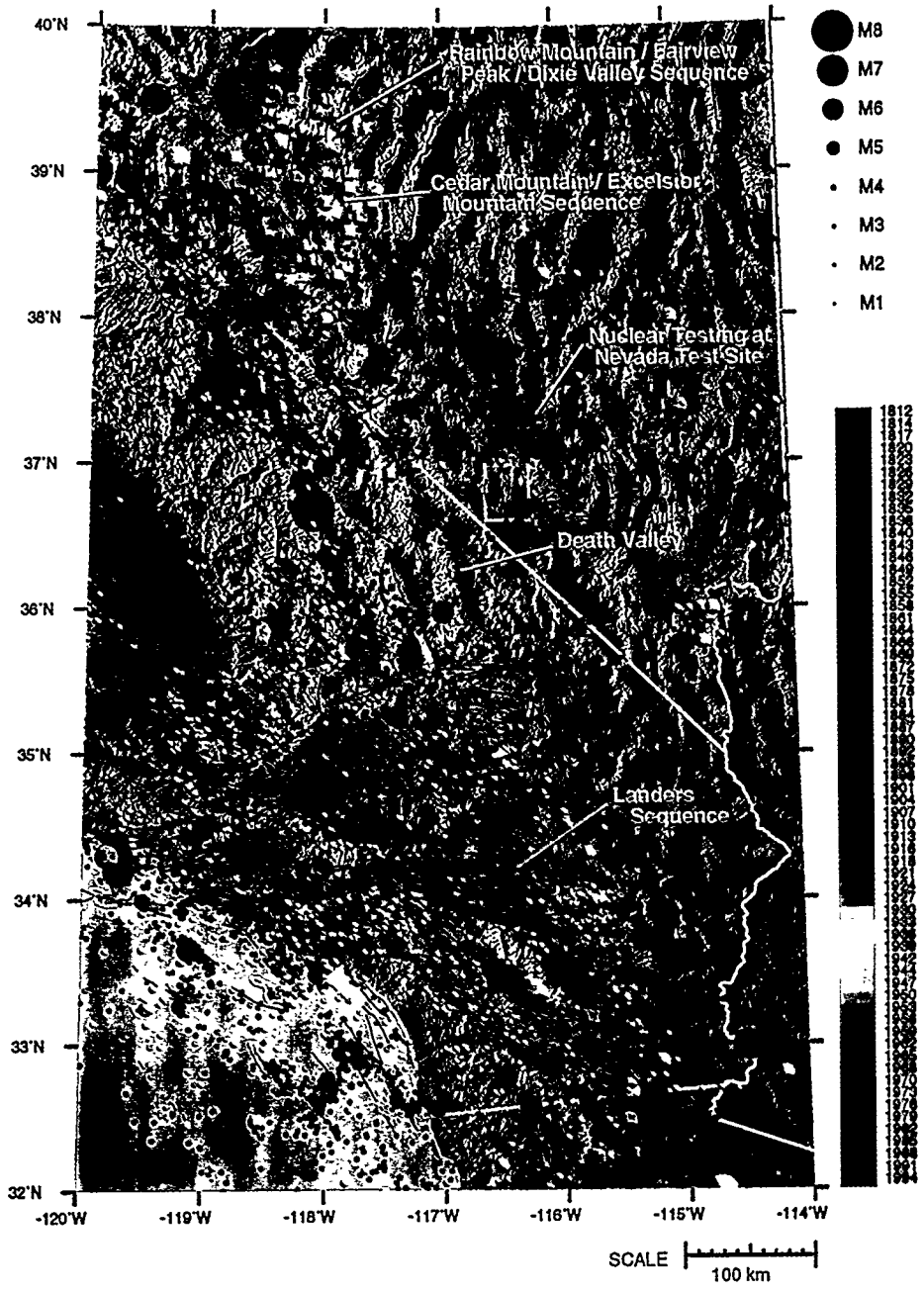

Figure 3-1. Earthquake hypocenters (1812 through 11 February 1994) in southern California, southern Nevada, and western Arizona are colored by date, sized by magnitude, and stacked by depth. Earthquake data are from PDE Catalog/National Earthquake Information Center. Magnitudes are assigned a value from one of the following fields in order of preference: Ms (average surface-wave magnitude), mb (average body-wave magnitude), contributed magnitude 1, or contributed magnitude 2. Fault traces are from Jennings (1992) in California; Dohrenwend (1982), Dohrenwend et al., (1991a-f, 1992a, b), and Nakata et al. (1982) in Nevada. The white rectangle indicates the boundary of the nine 7.5-minute U.S. Geological Survey topographic quadrangles that comprise the Yucca Mountain area.

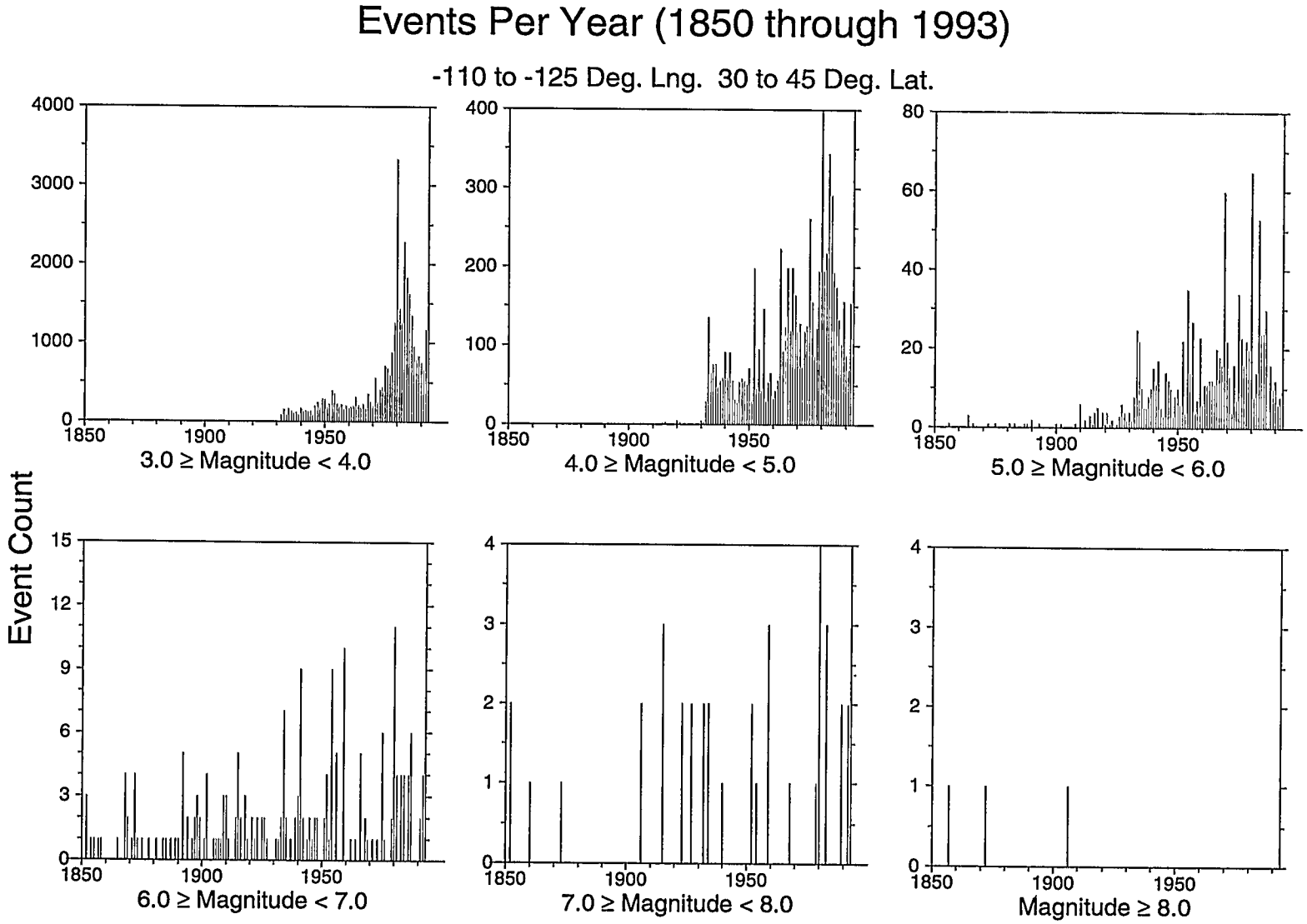

Figure 3-2. Histograms illustrating annual number of recorded earthquakes by magnitude range. See Figure 3-3 for area of analysis. The histograms illustrate a drastic increase in number of recorded earthquakes within approximately the last 50 yr.

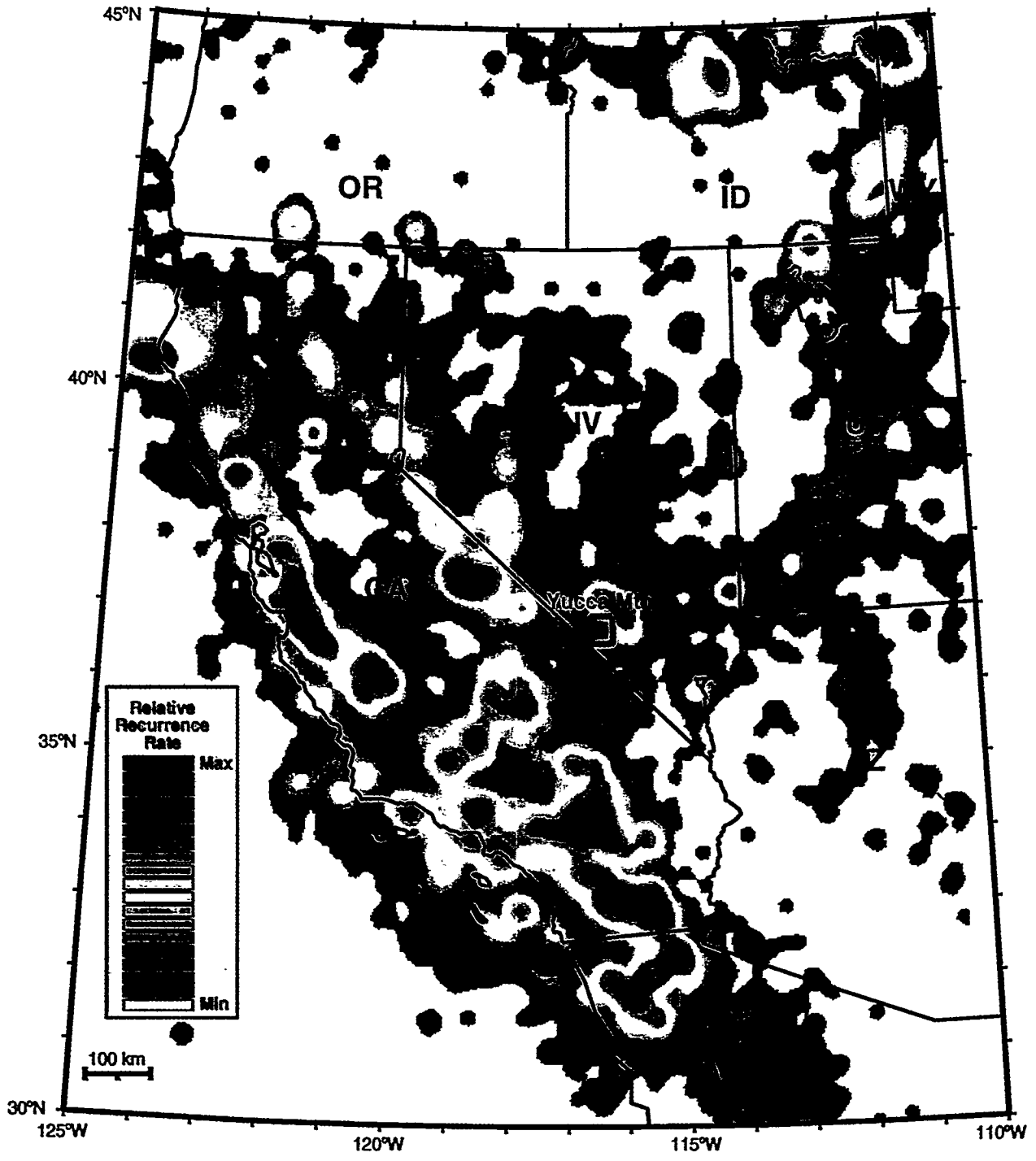

Figure 3-3. Analysis of earthquake clustering using a filter with a radius of 25 km. Bands of hotter colors (yellow to red) define belts of seismicity.

northern Furnace Creek fault system is thought to equal or exceed the recurrence interval (Reheis, 1994). Based on the temporal and spatial clustering of earthquakes observed regionally, and geological interpretations of slip along the Death Valley-Furnace Creek fault system, modern aseismicity is not an indication that the system is incapable of supporting large earthquakes. Rather, the Death Valley/Furnace Creek/Fish Lake Valley fault system is arguably the most active fault system in the western Great Basin (Reheis, 1994). As such, it may be capable of supporting very large ($M>7.5$) earthquakes (Reheis, 1994).

3.1 SPATIAL AND TEMPORAL CLUSTERING OF EARTHQUAKES

The distribution of earthquake hypocenters in southern Nevada and southern California illustrates a pronounced increase over the last 50 yr (Figure 3-1) and clustering of earthquakes along the San Andreas fault system, western Mojave Desert, southern Sierra Nevada Range, Owens Valley, Long Valley Caldera, Walker Lane Seismic Belt, Central Nevada Seismic Belt, and the Intermountain Seismic Belt (Figures 3-1, 3-3, and 3-4; Rogers et al., 1991; Smith and Arabasz, 1991; Oldow, 1992). Most of these seismically active areas show abundant recent activity as indicated by the red spheres, which represent earthquakes that occurred from the 1960's through February 1994 (Figure 3-1). The northwestern corner of the map contains a concentration of large yellow and orange spheres indicating two clusters of earthquakes; one that occurred in the early 1930's (yellow spheres) and the other in the mid 1950's (orange spheres). The concentration of earthquakes in the 1930's includes the 1932 Cedar Mountain earthquakes (M7.2 and M6.2) and the 1934 Excelsior Mountain earthquake (M6.3) that produced significant normal-displacement surface rupture (Rogers et al., 1991). The cluster of earthquakes in the 1950's includes the 1954 earthquakes at Rainbow Mountain (M6.8 and M6.8), Fairview Peak (M7.3), and Dixie Valley (M6.9), each of which caused normal-displacement surface rupture (Slemmons, 1957; Doser, 1986; Zhang et al., 1991; Rogers et al., 1991). No similar sequences of earthquakes had been recorded in those areas prior to the relatively intense activity in the 1930's and 1950's, nor have major earthquakes been recorded in that area since that time (Figure 3-1).

Spatial cluster analysis is here used to define belts of seismicity in order to assess the position of YM with respect to regions of historic seismicity. In these analyses, each recorded seismic event is counted as a single event, regardless of magnitude. A filter of a specified radius is moved from point to point through a rectilinear grid with a specified point spacing. The procedure used here is nearly identical to the kernel estimate (method 2) of Connor and Hill (1995), who used spatio-temporal modeling to assess probability of future basaltic volcanism in the YM region. The approach used here differs only from method 2 of Connor and Hill (1995) in that the temporal term is unused due to the brevity and lack of consistency of historical earthquake measurements. The filter weights earthquake events proportionally to their distance from the counting point. Small filter radii tend to emphasize events close to the counting point. Larger filter radii tend to smooth and de-emphasize local anomalies. Figures 3-3 and 3-4 illustrate cluster analyses of historic seismicity for the southwestern United States using a 25-km radius filter and a grid spacing of 5 km. A 25-km filter radius was selected in order to deemphasize local anomalies (see Figure 3-1) to emphasize regional belts of seismicity. Belts of seismicity are clearly associated with the San Andreas fault system, the southern Mojave Desert, Owens Valley, and the southern end of the Sierra Nevada Range, north of the Garlock Fault. The Central Nevada Seismic Belt, although clearly marked by large earthquakes in Figure 3-1, is de-emphasized in Figures 3-3 and 3-4 because the seismic networks in place at the time of major activity were unable to record small earthquakes. The Intermountain Seismic Belt projects into the Walker Lane Seismic Belt in the general vicinity of YM. This westward projection

of the Intermountain Seismic Belt has also been referred to as the Las Vegas Shear Zone or the East-West Seismic Belt. Although there has been no period of major seismic activity recorded in the YM area, the tendency for clustered activity to occur in a previously quiet area (such as the clustered activity in the Central Nevada Seismic Belt) is a cause for concern for the proposed repository site. One such cluster of seismic activity, the Landers earthquake sequence, occurred in the Mojave Desert in 1992.

3.2 THE LANDERS EARTHQUAKE SEQUENCE

The Ms7.6 Landers earthquake that occurred on June 28, 1992 near Landers, California, and the sequence of aftershocks, is important for several reasons: (i) the mainshock was large magnitude, (ii) a major surface rupture was created, (iii) other earthquakes, including the Little Skull Mountain earthquake, were triggered remotely, and (iv) it caused surface rupture on several mapped faults and a previously unmapped linking fault. Based on these reasons, the Landers earthquake provides a natural analog for the pattern of slip and distribution of aftershocks associated with a large strike-slip mainshock.

The Landers earthquake sequence is particularly important for understanding the seismic risk at YM because the Landers sequence is similar to the type and magnitude of large earthquake that would potentially occur along the DVFC fault system. Similarities between the Landers rupture and the DVFC fault system are that both are steeply dipping right-lateral strike-slip faults, and the Landers surface rupture and aftershock sequence has a bend at its northern end that is similar to the bend of about 20° at the point along the DVFC fault system nearest YM (Figure 3-6). The DVFC fault system is, at its closest, 50 km southwest of YM and could be the most active fault in the western Great Basin (Reheis, 1994). As such, the DVFC fault system is considered to be the most proximal potential source (with respect to YM) of a large magnitude mainshock (e.g. $M>7$), and, perhaps more importantly, could produce local aftershocks and more distant remotely triggered earthquakes that could significantly impact YM.

The Landers earthquake sequence (Figures 3-6 and 3-7), as it will be referred to here, started with the April 22, 1992, Joshua Tree (Ms 6.3) earthquake, located between the Pinto Mountain Fault and the Mission Creek Fault (segment of the San Andreas fault system). The Landers mainshock occurred about 2 mo later, on June 28, 1992, approximately 30 km north-northwest of the Joshua Tree epicenter, and about 7 km north of the Pinto Mountain Fault. The Landers mainshock was followed 3 hr later by the Ms 6.7 Big Bear Lake earthquake, 35 km to the west. The following day (June 29, 1992) an earthquake ($M=5.4$) occurred in Nevada near Little Skull Mountain about 15 km southeast of YM. The Landers earthquake sequence ended a period of relative seismic quiescence in the southern Mojave Desert that had lasted for several years or more (Wiemer and Wyss, 1994).

Surface rupture associated with the Landers earthquake extends from a few km south of the Landers epicenter to about 70 km north of the epicenter and is characterized by right-lateral strike-slip or right-lateral dominated oblique-slip (Kanamori et al., 1992; Sieh et al., 1993; Hudnut et al., 1994). Nearly continuous surface rupture associated with the Landers earthquake occurred along portions of several previously mapped faults (from south to north, the Johnson Valley Fault, Homestead Valley Fault, Emerson Fault, and Camp Rock faults) and the previously unmapped Kickapoo Fault, linking the Johnson Valley and Homestead Valley faults (Hart et al., 1993; Sieh et al., 1993; Sowers et al., 1994). Measured slip varies along the trace of the rupture. Based on mapped displacements, slip maxima occur along two distinct segments: one located about 15 km north of the Landers mainshock epicenter and the other 40 km north of the Landers epicenter (Kanamori et al., 1992; Hudnut et al., 1994). The total-slip maximum of

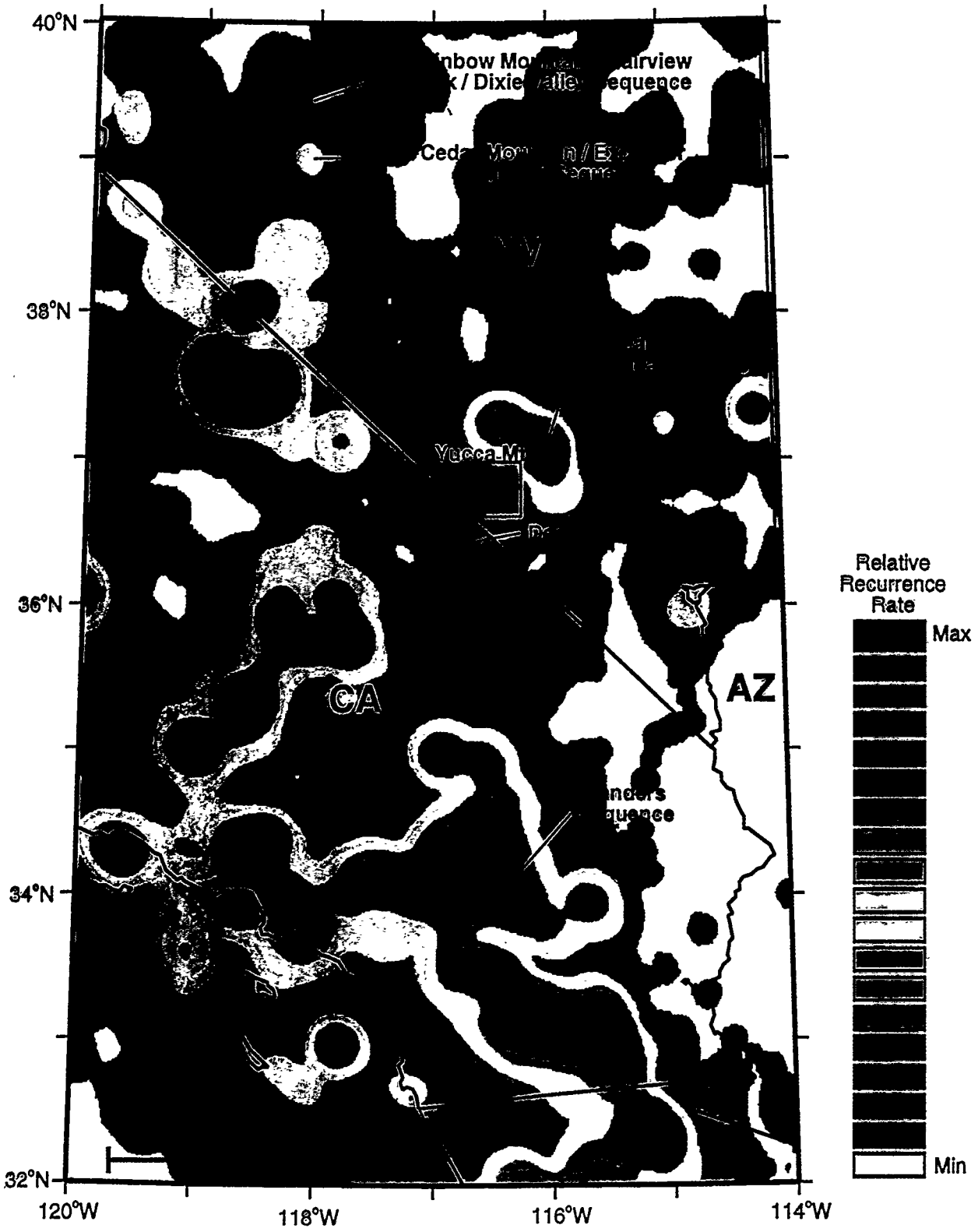

Figure 3-4. Earthquake cluster analysis for area of Figure 3-1 using a filter with 25-km radius and a grid spacing of 5 km. The map illustrates the close proximity of YM to other belts of seismicity.

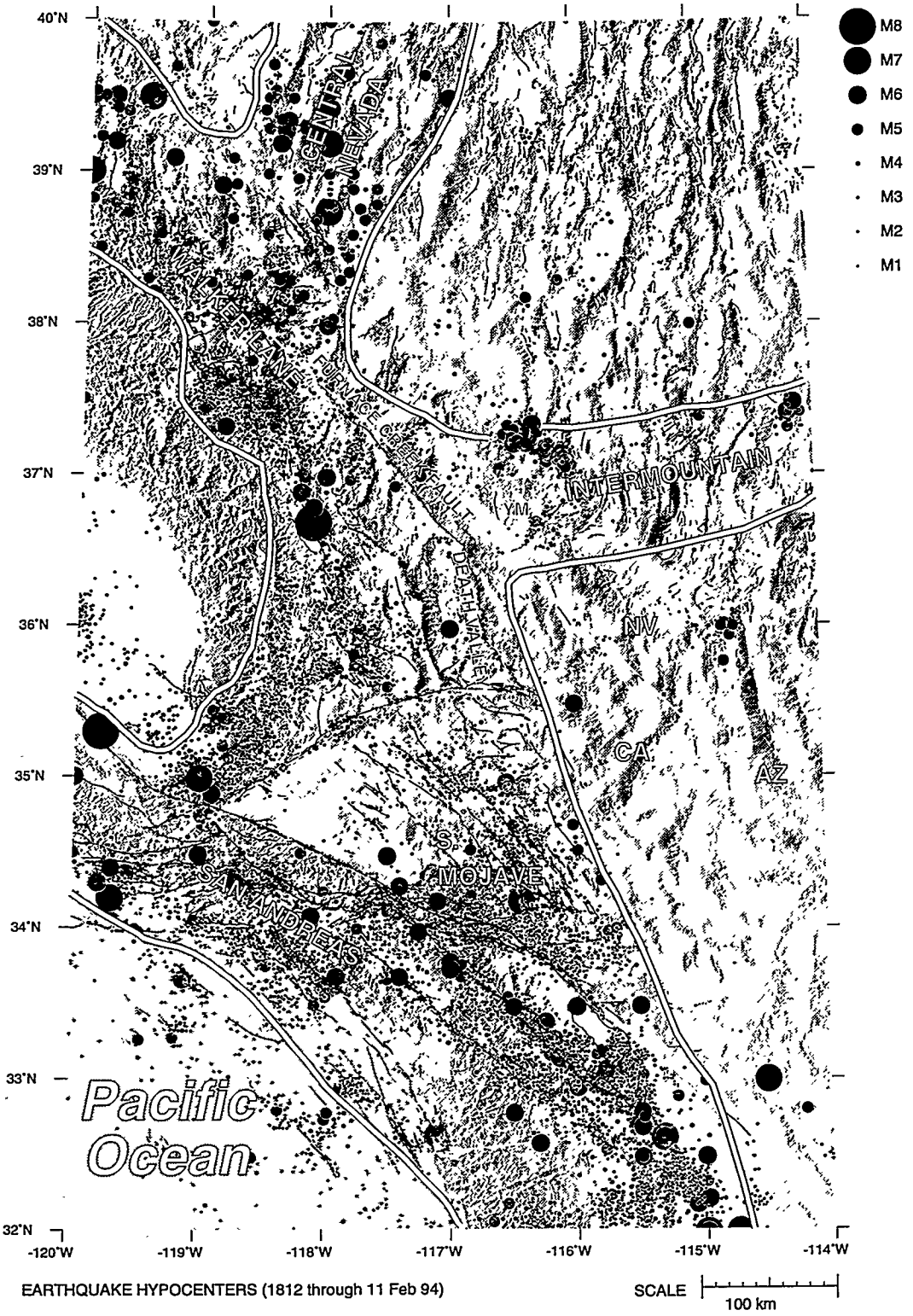

Figure 3-5. Earthquake activity belts of southern California and southern Nevada

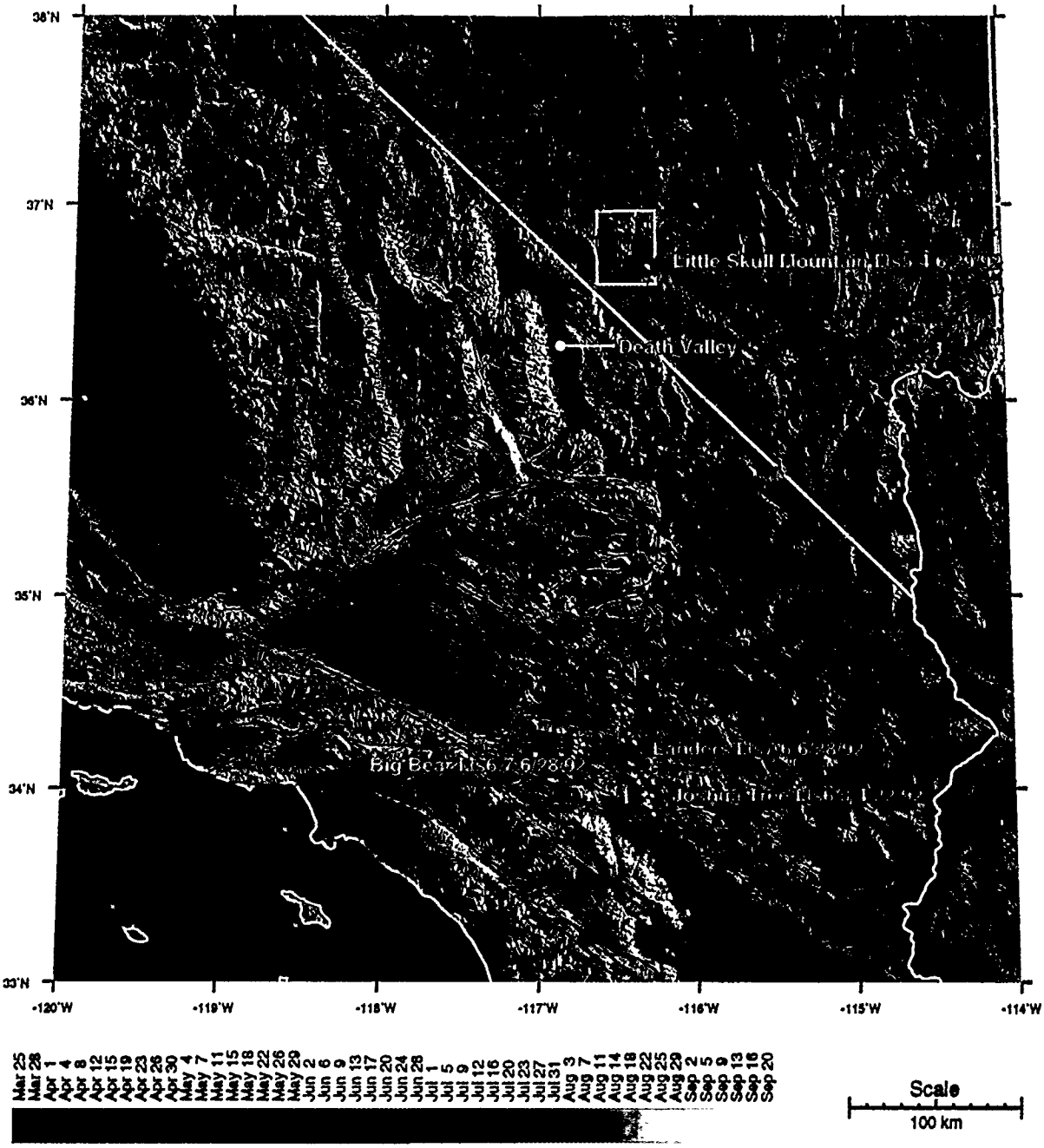

Figure 3-6. Landers earthquake sequence (earthquake hypocenters from 25 March through 28 September 1992) in plan view. Earthquake hypocenters are colored by date, sized by magnitude, and stacked by depth. Earthquake data are from PDE Catalog/National Earthquake Information Center. Magnitudes are assigned a value from one of the following fields in order of preference: Ms (average surface-wave magnitude), mb (average body-wave magnitude), contributed magnitude 1, or contributed magnitude 2. Fault traces are from Jennings (1992) in California; and Dohrenwend (1982), Dohrenwend and Moring (1991a,b,c), Dohrenwend et al. (1991a–f, 1992a,b), and Nakata et al. (1982) in Nevada. The white rectangle indicates the boundary of the nine 7.5-minute U.S. Geological Survey topographic quadrangles that comprise the YM area.

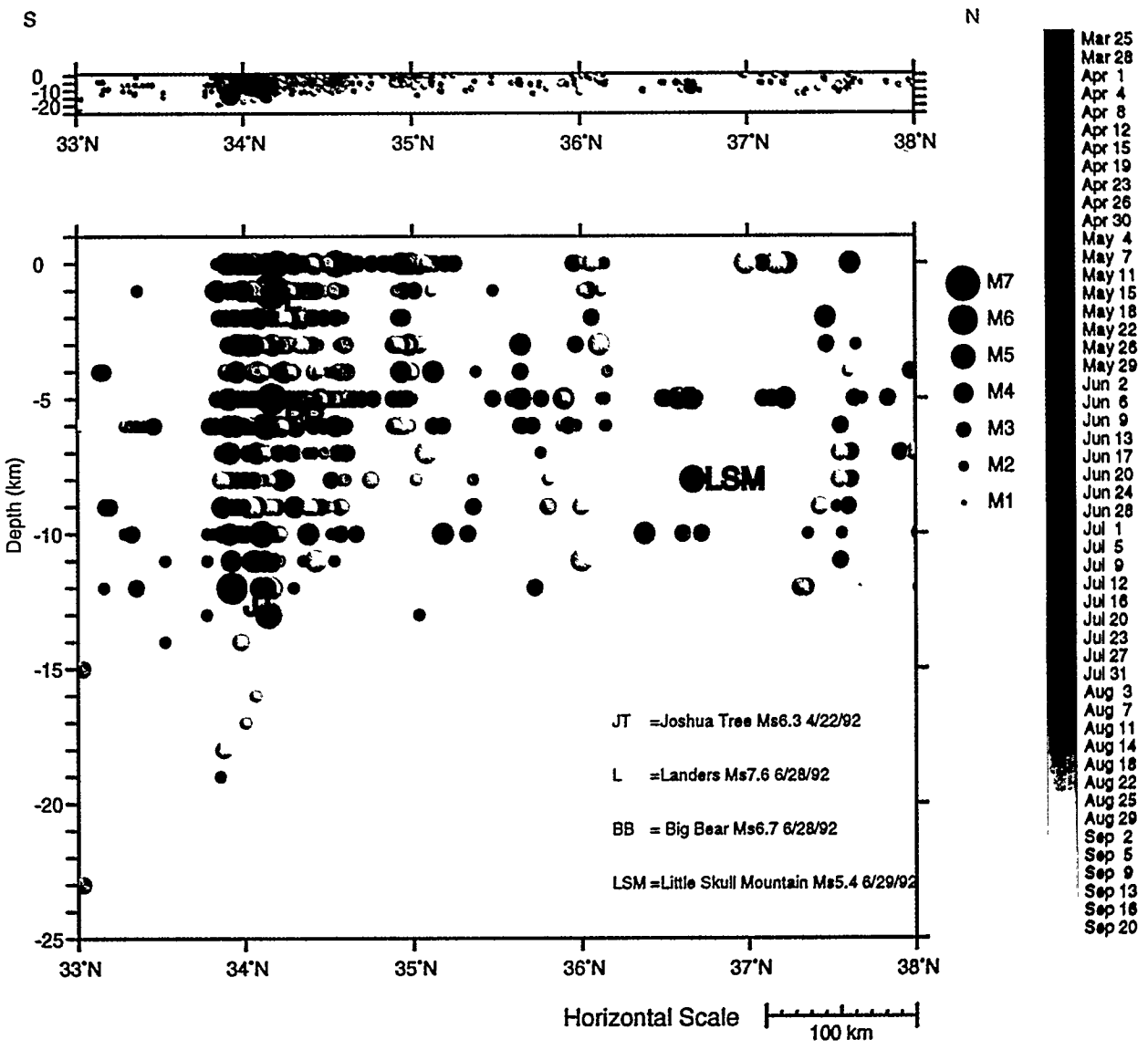

Figure 3-7. Landers sequence in profile viewed from east to west. Earthquake hypocenters are shaded by date and size by magnitude. Earthquake data are from PE Catalog/National Earthquake Information Center. Magnitudes are assigned a value from one of the following fields in order of preference: Ms (average surface-wave magnitude), mb (average body-wave magnitude), contributed magnitude 1, or contributed magnitude 2. Rows of hypocenters with 1-km spacing reflect roundoff of depth estimates to nearest 1 km because of limited accuracy.

7 m occurred on the segment 40 km north of the mainshock epicenter along the Emerson Fault (Galway Lake Road site; Irvine and Hill, 1993; Hart et al., 1993; Reynolds, 1993; Arrowsmith and Rhodes, 1994) (Figure 3-8). The two peaks in the slip profile along the fault are interpreted to suggest that the Landers rupture event was composed of two subevents marked by the surface slip maxima along the trace of the surface rupture (Kanamori et al., 1992; Toppozada, 1993; Dreger, 1994; Hudnut et al., 1994).

The aftershock pattern for the Landers sequence follows an arcuate, vertical surface, extending for 95 km and that has a strike of N 10° W in the south and curves into a trend of N 30° W in the north (Figure 3-6; Sieh et al., 1993). Viewing the earthquake sequence in 3D illustrates some important points regarding the aftershock patterns with respect to the mainshock (Figures 3-1 and 3-7). The hypocenter for the Joshua Tree mainshock is reported at a depth of 12 km. Hypocenters for the subsequent aftershocks of the Joshua Tree earthquake were virtually all shallower (Figure 3-7). The pattern for the Landers earthquake and aftershocks is dramatically different. The hypocenter for the Landers mainshock is reported to be at a depth of 1 km. The preponderance of aftershock hypocenters occurred deeper and to the north of the Landers mainshock (Figure 3-7).

3.3 EARTHQUAKE TRIGGERING

The Landers earthquake, based on cumulative numbers of earthquakes, cumulative seismic moment, and statistical analyses, triggered a dramatic increase in earthquake activity throughout much of the western United States (Hill et al., 1993). Some noteworthy characteristics of the triggered earthquake activity are that: (i) all the recognized triggered earthquake activity occurred north of the Landers mainshock, (ii) much of the triggered activity occurred in areas of geothermal or relatively recent volcanic activity, (iii) triggered activity occurred up to 1,250 km away from the Landers main-shock, and (iv) all sites of triggered activity show strike-slip to normal displacements, suggesting that regionally σ_3, the least principal stress, is horizontal (Hill et al., 1993). Remotely triggered earthquakes associated with the Landers mainshock have been interpreted for the following sites; distances from Landers mainshock are shown in parentheses: Coso-Indian Wells, California (165 to 205 km), Little Skull Mountain, Nevada (280 km), White Mountains, California (380 to 420 km), Long Valley, California (415 km), Mono Basin (450 km), Cedar City, Utah (490 km), Walker Lane Belt, western Nevada (450 to 650 km), Lassen, California (840 km), Burney, California (900 km), Cascade, Idaho (1,100 km), and Yellowstone, Wyoming (1,250 km; Hill et al., 1993; Anderson et al., 1994; Bodin and Gomberg, 1994; Gomberg and Bodin, 1994; Roquemore and Simila, 1994).

Two processes are discussed by Hill et al. (1993) as possible mechanisms for remotely triggering slip. Both triggering mechanisms involve brittle slip on favorably oriented faults either due to stress changes sufficient to surpass the frictional strength, or a decrease in the frictional strength. One mechanism involves static stress changes produced by dislocation along the Landers rupture, and the other mechanism involves dynamic stresses associated with propagating seismic waves generated by abrupt slip along the rupture surface. Modeling of static-elastic dislocation in homogeneous media suggests that a static stress mechanism may be responsible for aftershocks within one to two rupture lengths of a fault. Hill et al. (1993) state that "the temporal form and spatial distribution of the remote triggering point...to a class of explanations involving critically loaded faults in a heterogeneous crust, static strain amplification within weak boundaries (fault zones) between crustal blocks, and nonlinear interactions between dynamic stresses in seismic waves and crustal fluids." Bodin and Gomberg (1994) used numerical modeling to test the viability of static stress change as a mechanism for remote triggering of earthquakes. The results of these models suggest that regional fault connectivity can increase the static

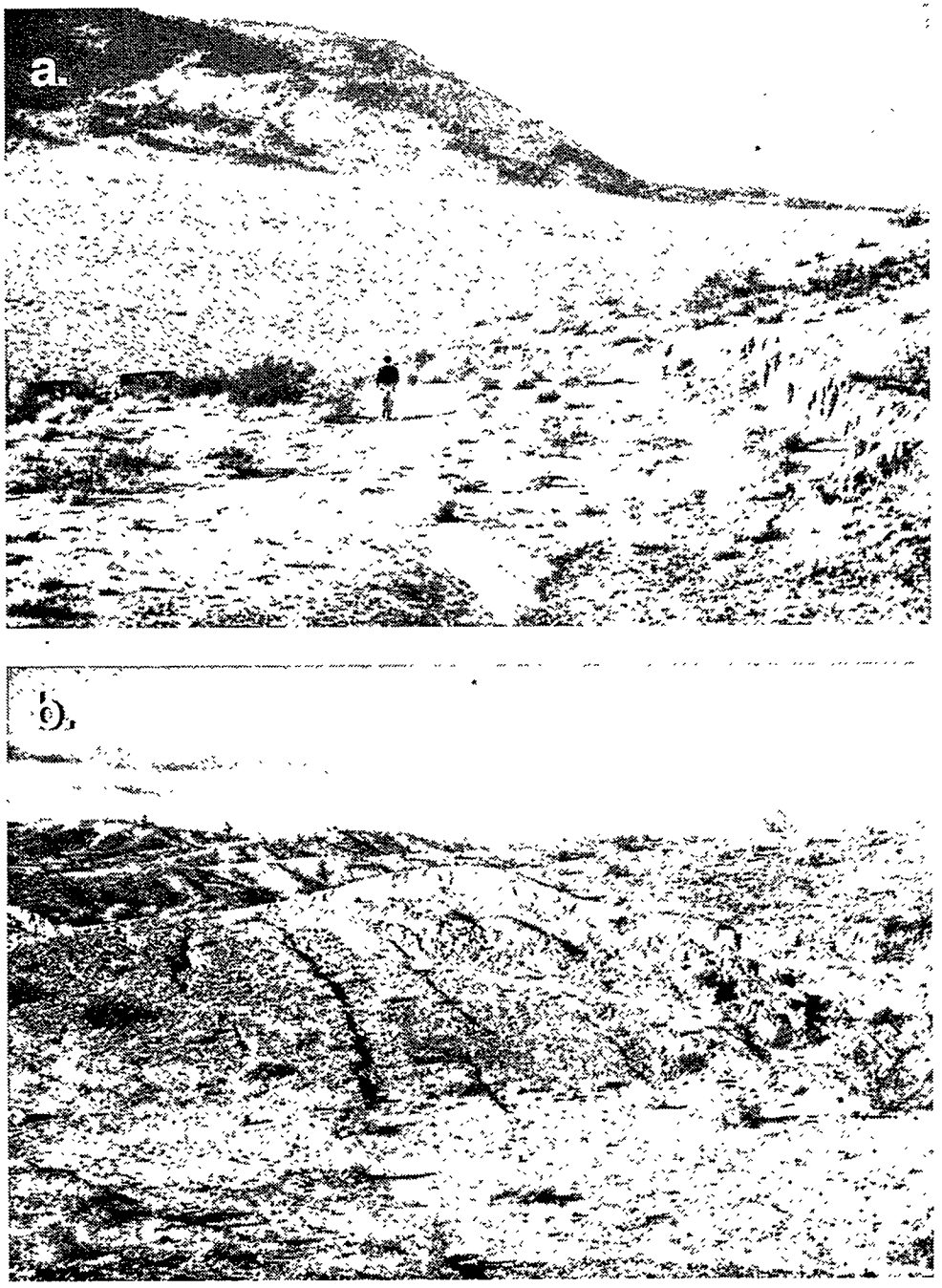

Figure 3-8. Field photographs of Emerson Fault rupture at the Galway Lake Road site. Right-lateral-dominated oblique slip of 7 m was measured at this site. (a) View toward NW displays fault scarp in foreground (1.5 to 2 m high) and trace of rupture crossing desert toward eastern end of distant ridge. (b) View toward NE shows main scarp (1.5 to 2 m high) dipping southwestward and subsidiary normal faults that form horsts and grabens in hangingwall of main fault. Photographs taken on 24 March 1994.

change by about an order of magnitude at distances of at least 280 km, which would include the distance between the Landers mainshock and Little Skull Mountain. Dynamic strain may also be channeled by structure and the direction of rupture propagation, which would in the case of the Landers sequence, focus generally toward the north and Little Skull Mountain (Figure 3-6; Bodin and Gomberg, 1994).

Remote triggering like that following the Landers mainshock may serve to release strain in the regions between the most active faults, and may thereby inhibit large strain buildup that could support large earthquakes. The Landers surface rupture includes slip along numerous faults, rather than being restricted to a single major fault or a part of a fault. Though the strain released by the Landers earthquake is attributable to the San Andreas Fault, the earthquake sequence did not occur on the San Andreas Fault. The fact that the earthquake sequence extended from near the San Andreas Fault northward into the Mojave Desert was a surprise and led A. Nur and coworkers (as discussed by Monastersky, 1993) to suggest that the main locus of seismicity that is now associated with the San Andreas fault system may be shifting to a new position, extending along the Landers earthquake sequence and northward along Owens Valley on the eastern side of the Sierra Nevada.

3.4 DISCUSSION AND SUMMARY

The brevity of the historic record of seismicity (less than 200 yr) severely limits the utility of historic seismicity for attempting to estimate seismic activity for the next 10,000 yr. Within the historic record, seismic activity has not been uniformly distributed through the region surrounding YM, but it has instead been concentrated in belts of seismicity. The specific location of YM is within an area of relatively low natural seismicity over the last 100 yr. However, YM is located approximately at the intersection of two seismic belts; the Intermountain Seismic Belt and the Walker Lane Seismic Belt.

Spatially clustered seismicity is fairly common within the historic record. YM is located approximately 50 km east of the DVFC fault system, one of the most active faults in the western Basin and Range Province. Although the DVFC fault system has not experienced major seismic activity within the period of historic observations, the fault system may be prone to clustered seismic activity.

King et al. (1994) modeled stress changes associated with the Landers earthquake sequence and found that the pattern of aftershocks correlated with the pattern of Coulomb stress increases of greater than one-half bar (0.05 MPa) on optimally oriented faults. Aftershocks were found to be sparse in areas corresponding to stress decreases on the order of 0.5 bar. Areas of 0.5 bar Coulomb stress increases associated with the Landers earthquake are modeled to have extended approximately 50 km away from the Landers rupture and may have triggered the Big Bear shock (King et al., 1994). Based on this model, a slip event similar to the 1992 Landers earthquake on the DVFC fault system could potentially alter the stress field sufficiently to directly trigger earthquake activity at distances of up to 50 km (e.g., YM and BM).

4 CONTEMPORARY STRAIN ANALYSIS WITH GLOBAL POSITIONING SYSTEM

Characterization of the contemporary tectonic setting of YM and assessment of the potential for future tectonic events are important aspects of the scientific investigations being conducted during the prelicensing phase for the candidate HLW repository site at YM. To characterize contemporary strain history and consider partitioning of strain along faults in the YM region, it is necessary to assess distribution and rates of contemporary slip along faults and fault zones in the region. Satellite-based Global Positioning System (GPS) surveying is the primary method for conducting crustal deformation investigations, acquiring information on contemporary strain, and assessing distribution and rates of contemporary displacement along faults for characterizing the present-day tectonic setting and analyzing the potential for future tectonism.

The primary KTU that will directly apply information on contemporary strain acquired by GPS surveying is related to consideration of the uncertainty in determining 3D structure and tectonic setting of YM. This KTU is a Type 5, which indicates that independent NRC research efforts may be required for its evaluation. In addition to KTU evaluation, independent research may also be needed to provide the basis for analyzing the plans that the DOE has for addressing the determination of 3D structure and tectonic setting and the potential consequences of tectonic activity on repository performance. Additionally, GPS data will help to address (i) uncertainty in determining the slip history of faults, and (ii) uncertainty in determining magnitude of fault slip and associated seismic shaking at surface and subsurface locations. The contemporary strain pattern provides the important link for comparing past historical events with present-day slip information to establish the tectonic framework in which the potential for future displacements can be analyzed. The contemporary strain information provides important descriptions of faulting and tectonic activity, which may bear a relationship to seismic activity. The NRC/California Institute of Technology/Smithsonian (NRC/CalTech) GPS survey was established in 1991 to acquire information for use in assessing performance of the potential HLW repository at YM relative to seismotectonic issues.

4.1 HISTORY AND COMPONENTS OF THE GLOBAL POSITIONING SYSTEM

The NAVSTAR (NAVigation Satellite Timing and Ranging) GPS is a satellite-based positioning system under development by the U.S. Department of Defense (DOD), work on which was begun about 1973 (Wells et al., 1987). The surveying capabilities of the GPS were well-documented by the mid-1980's (e.g., Bock et al., 1985; Ruland and Leick, 1985; Goad, 1986). In the late 1980's and early 1990's, concepts specifically related to application of GPS surveying to studies of crustal deformation were evolving and were discussed in a variety of papers (e.g., Davis et al., 1989; Dong and Bock, 1989; Prescott et al., 1989; Larson and Agnew, 1991; Larson et al., 1991). More recent papers present results from the growing application of GPS surveying techniques to analysis of tectonic deformation of the crust (e.g., Donnellan et al., 1993; Feigl et al., 1993; Larson, 1993; Shen and Jackson, 1993; Savage et al., 1994; Darby and Meertens, 1995). Information presented in the referenced sources illustrates the relatively rapid development and evolution of GPS surveying techniques for use in crustal deformation studies.

The three major components of the GPS are the space segment (satellites), the control segment (monitor stations), and the user segment (receivers). The satellites of the existing constellation provide

essentially global coverage with about four to eight observable satellites above a 15° elevation mask (Hofmann-Wellenhof et al., 1993). Elevation masks are necessary because tropospheric effects on signal propagation are particularly unpredictable for altitudes in the masked region (Leick, 1990). The total control system consists of the master station, worldwide monitor stations, and ground control stations. In general, operational tasks of the control segment are, (i) tracking of satellites for orbit and clock determinations and prediction modeling, (ii) time synchronization of the satellites, and (iii) upload of data to the satellites. The user segment comprises both military and civilian users, with civilian use years ahead of the schedule originally envisaged by those who planned the system. Static relative positioning, or static surveying, with GPS involves receivers that remain stationary until observations are completed, and is the general approach applied for analysis of crustal deformation. A GPS survey of the type being conducted in the NRC/CalTech network (cf Section 4.3) has been specifically referred to as a "quasi-static" application by Wells et al. (1987). The quasi-static application concept is meant to address surveys in regions where, while there may be perceptible relative motion between the points being surveyed, it is generally so slow that it can be detected only between campaigns that are months to decades apart.

4.2 PRECISION AND ACCURACY OF GLOBAL POSITIONING SYSTEM

Accuracy is defined as closeness of the observations to the true value (Bevington, 1969; Leick, 1990; Larson and Agnew, 1991), the measurement of which is done by determining agreement between GPS and some other technique [e.g., Very Long Baseline Interferometry (VLBI)]. Precision is the closeness of repeated observations to the sample mean (Leick, 1990), and, hence, a measure of how exact the estimate is (Bevington, 1969) based on scatter of results about a mean value (Larson and Agnew, 1991).

4.2.1 Factors Affecting Precision and Accuracy

Errors that affect precision and accuracy of GPS measurements are either systematic or random. Hofmann-Wellenhof et al. (1993) have classified systematic errors into three source groups: satellite source (orbital errors and clock bias); signal propagation source (tropospheric and ionospheric refraction in the atmospheric propagation medium); and receiver source (antenna phase center variation and clock bias). Random noise includes multipath reflections, which can be lessened by pre-survey planning for careful site selection, measurement noise (Hofmann-Wellenhof et al., 1993), and bench mark stability (Davis et al., 1989). Davis et al. (1989) point out that such errors may be highly correlated over short experiments and would not affect estimates of precision based on observations spanning a week or two. However, if the errors were not constant over long time periods, precision from experiments spanning months to years may be different (Davis et al., 1989). Systematic effects can be largely eliminated by considering appropriate combinations of the observables: differencing between receivers removes satellite-specific biases; differencing between satellites takes care of receiver-specific biases; ionospheric refraction can be virtually eliminated by proper combination of dual frequency data (Hofmann-Wellenhof et al., 1993).

4.2.2 Currently Attainable Resolution

By mid 1984, 1–2 parts per million (ppm) GPS surveying results had been demonstrated for static relative positioning, with 1 ppm accomplished in less than 15 min; 0.1 ppm routinely obtained by researchers; and 0.01 ppm considered the possible limit of GPS static relative positioning surveying (Leick, 1990). Hofmann-Wellenhof et al. (1993) indicate accuracies in static surveys of 0.1 to 0.01 ppm

for dual (P-code) frequency receivers with baseline lengths of 100 and 500 km, using five satellites, in 60- and 120-min sessions, respectively. These accuracies are equivalent to millimeter accuracy for baselines of the lengths shown in static relative positioning surveys. The GPS results from regional investigations in which data were collected for more than 2 yr are found in papers by Larson and Agnew (1991) and Davis et al. (1989). Prior to the paper of Davis et al. (1989), in which they discussed long-term precision and accuracy based on over 2 yr of measurements for baselines of 240 m to 223 km, GPS results had been derived mainly from experiments spanning only a few days or weeks at most.

In a 1993 GPS survey at YM (Savage et al., 1994), overall accuracy in positioning for the interstation distances (about 20 km in their network) was described by a standard deviation of approximately 3.6 mm in the north-south component and 5.8 mm in the east-west component. Larson and Agnew (1991) have pointed out that a standard deviation derived from short-term (i.e., a few days) reproducibility is about half that from long-term (a few years) reproducibility. In light of this fact, Savage et al. (1994) speculated that the variations noted in standard deviation suggested a systematic bias in each survey–perhaps related to the multiday satellite orbit used, the prevailing weather system or ionospheric state, or possibly monument stability.

Deformation of the network was calculated by Savage et al. (1994) using Geodolite measurements taken in 1983, 1984, and 1993 plus the 1993 GPS observations. Geodolite measurement of 14 lines in 1993 revealed values that averaged 5.7 ± 1.2 mm longer than the GPS measurements taken in the same survey. However, Savage et al. (1994) noted this difference between the two types of measurements fell within the range of previously recognized systematic errors in the measurements. They considered the deformation rate to be low (i.e., 2 mm/yr across the 50-km breadth of the network), and the coseismic deformation associated with the Little Skull Mountain earthquake of June 29, 1992 to account for deformation observed in the network. Deformation related to this M5.6 earthquake, which occurred as a triggered event related to the Landers, California, earthquake of June 28, 1992 (Anderson et al., 1992; Gomberg et al., 1992; Reasenberg et al., 1992), was deemed significant only at Station Rock, located 3 km east of the epicenter (Savage et al., 1994). Deformation associated with the 1992 Little Skull Mountain earthquake was also measured by the NRC/CalTech GPS survey, which is discussed in Section 4.3.

4.2.3 Global Positioning System Survey Design

Because precision and accuracy of GPS survey results are a function of the number of satellites, the baseline length, and session duration (Hofmann-Wellenhof et al., 1993), pre-survey planning of campaigns designed to analyze crustal deformation is essential. To illustrate the importance of pre-survey planning, consider the determination of two important aspects of a survey, optimum observation windows and optimum session times. Selection of the optimum observation window, determined as the period at which the maximum number of satellites can be observed simultaneously, is accomplished by pre-survey inspection of satellite azimuth-elevation charts. These periods are then divided into sessions (i.e., the best time for observation within the periods), determined by the time within the periods at which receivers can track the satellites simultaneously, such that the sessions are long enough to achieve the required accuracy. Additional considerations for design of a GPS survey, discussed in Chapter 14 of Wells et al. (1987) and Chapter 7 of Hofmann-Wellenhof et al. (1993), address the concept of designing a survey to achieve the highest accuracy.

4.3 THE NUCLEAR REGULATORY COMMISSION/CALTECH/ SMITHSONIAN GLOBAL POSITIONING SYSTEM SURVEY

4.3.1 Importance of the Survey

The NRC/CalTech GPS survey network was established in 1991 to provide information for aiding assessment of performance of the proposed HLW repository at YM relative to seismotectonic issues. These issues include consideration of how tectonically active the region containing YM may be; whether the repository area could experience surface or subsurface rupture from future tectonic events in the next 10,000 yr; and what maximum ground accelerations could occur at the repository due to future earthquakes. Fundamental data for evaluating these issues are provided by measurement of contemporary strains accumulating across the YM region, including measurement of strains accumulating on fault zones close enough to YM that accelerations from the maximum credible earthquake generated on those zones would be significant at YM.

Many Quaternary faults, at least some of which exhibit Holocene displacement, have been identified in the vicinity of YM (Nakata et al., 1982), suggesting that significant strains may be accumulating in that region. If the rate of strain accumulation is high enough, coseismic surface or subsurface rupture may occur at or near the potential repository site. Two major fault systems located within 100 km of the site, the Northern Death Valley-Furnace Creek and the Panamint Valley-Hunter Mountain-Saline Valley fault zones, are 150 and 300 km long, respectively. Therefore, these fault zones have the potential for generating earthquakes in the 8.0 to 8.5 range on the moment magnitude scale (Kanamori, 1977). The rate of strain accumulation across the fault zones may provide an indication of the number and size of very large earthquakes expected in the next 10,000 yr. Consequently, geodetic monitoring of these features using GPS surveying provides *prima facie* evidence for assessing their potential impact on repository performance.

4.3.2 Design of the Survey Network

The network was established and first occupied in the fall of 1991. It presently consists of 15 survey sites comprising three subnetworks—the YM (5 sites), Hunter Mountain (4 sites), and Death Valley (4 sites) subnets—plus two additional sites, Dante and Aguereberry, spanning central Death Valley (Figures 4-1 through 4-4). The two additional survey sites were located to provide control for determining strains across the Death Valley-Furnace Creek (i.e., site Dante) and Hunter Mountain-Panamint Valley (i.e., Augereberry site) fault zones at positions south of the Hunter Mountain and Death Valley subnets. Each survey site is delineated by three standard brass or aluminum marker disks set in concrete and attached to bedrock. The main marker is usually occupied, but the two nearby reference marks may be used if the main mark has been vandalized or destroyed.

4.3.2.1 The Yucca Mountain Subnet

The YM subnet, including sites Claim, Black, Mile (at the crest of YM and, hence, essentially the repository site), 67TJS, and Wahomie (Figure 4-2), was established to measure strain across the BMF, Crater Flat, YM proper, and Jackass Flat. The sites of this subnet were located so as to be aligned approximately parallel to the direction of at least principal stress in the YM area, or west-northwest (Stock et al., 1985; 1986), to optimize determination of maximum principal strain across the area.

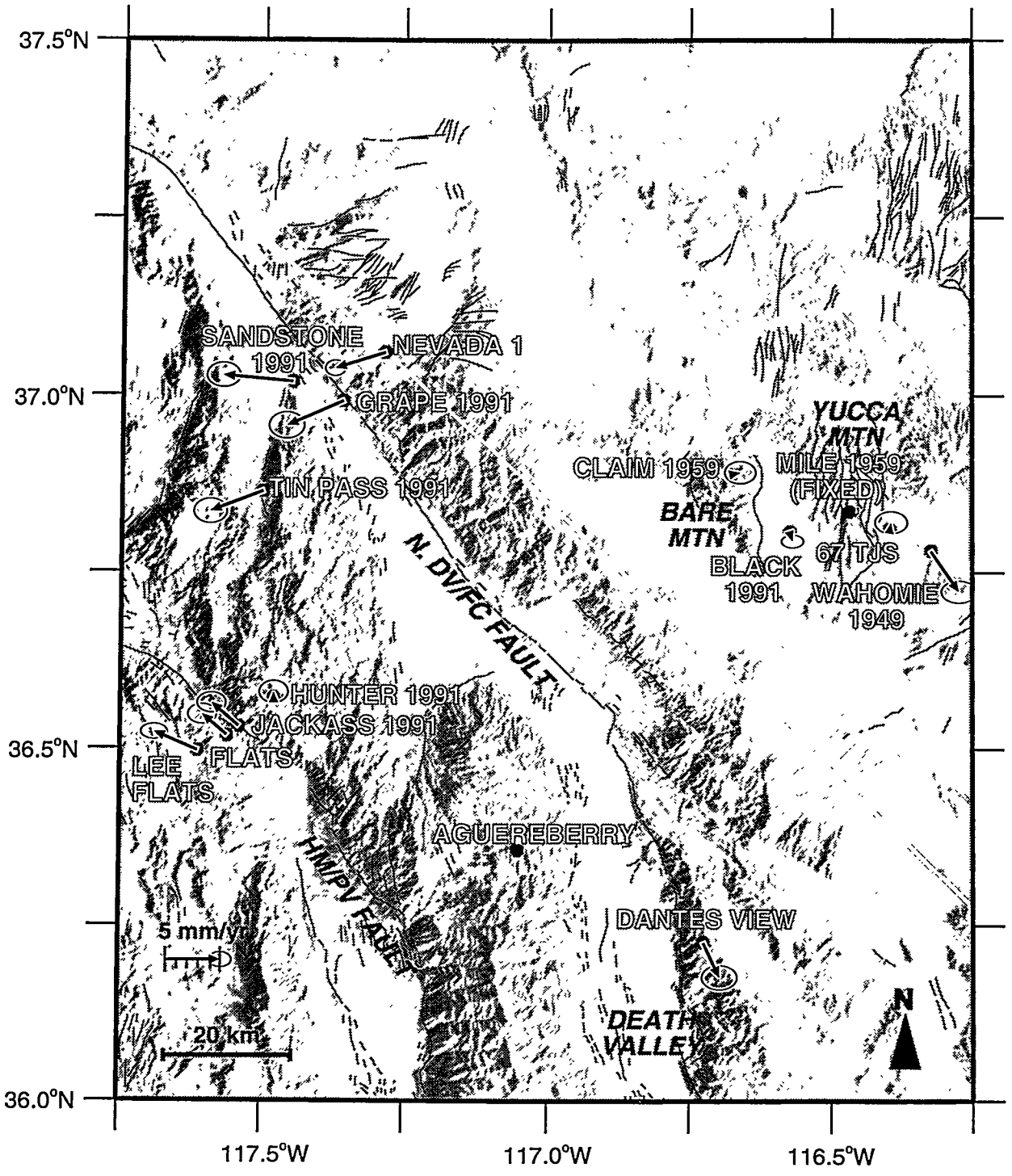

Figure 4-1. Map showing location of network sites and relative motions based on 1991, 1993, and 1994 Global Positioning System surveys, relative to site Mile. Ellipses show estimated 1σ errors.

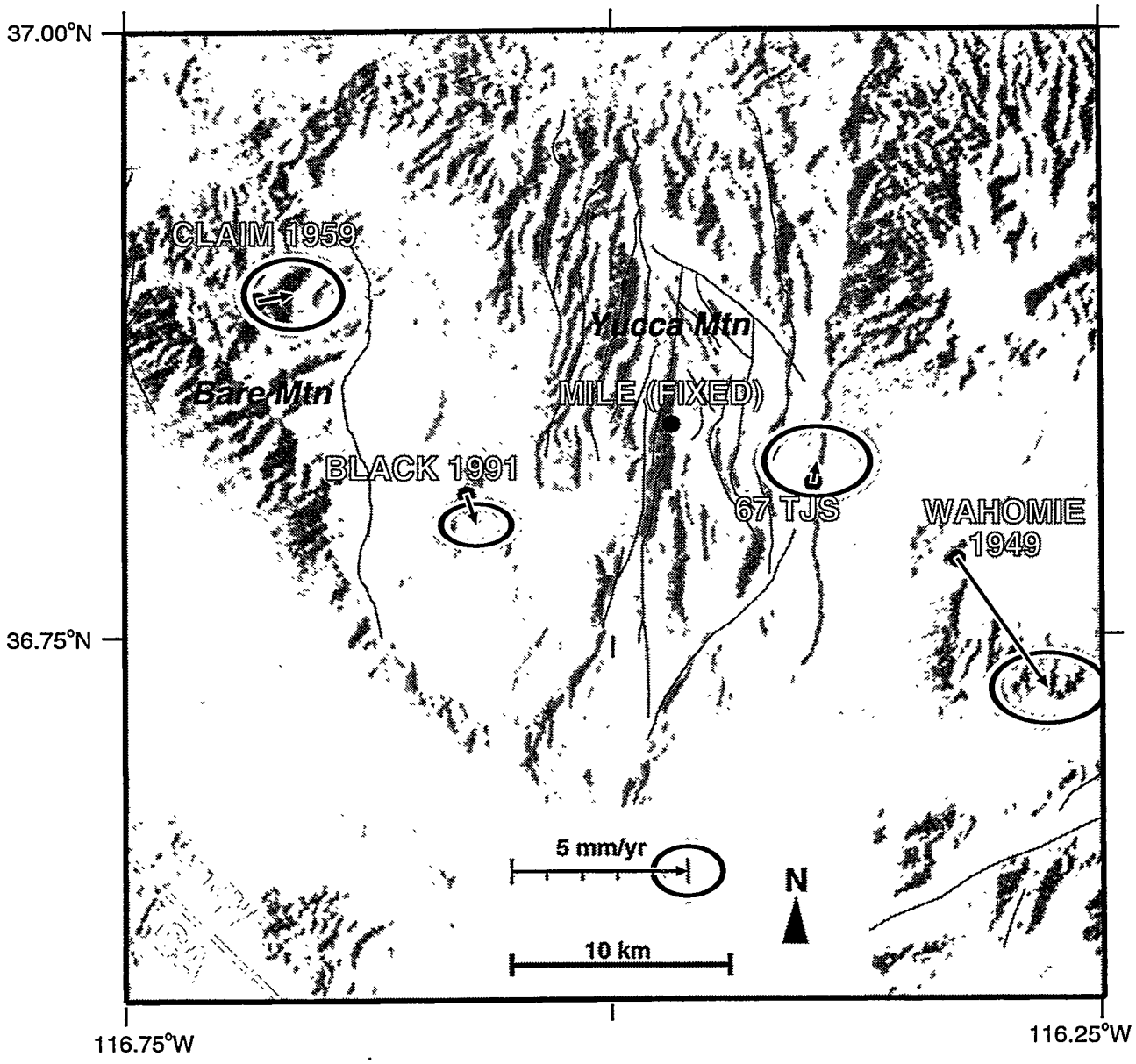

Figure 4-2. Map showing relative motions based on the 1991, 1993, and 1994 Global Positioning System surveys within the Yucca Mountain subnet. Ellipses show estimated 1σ errors.

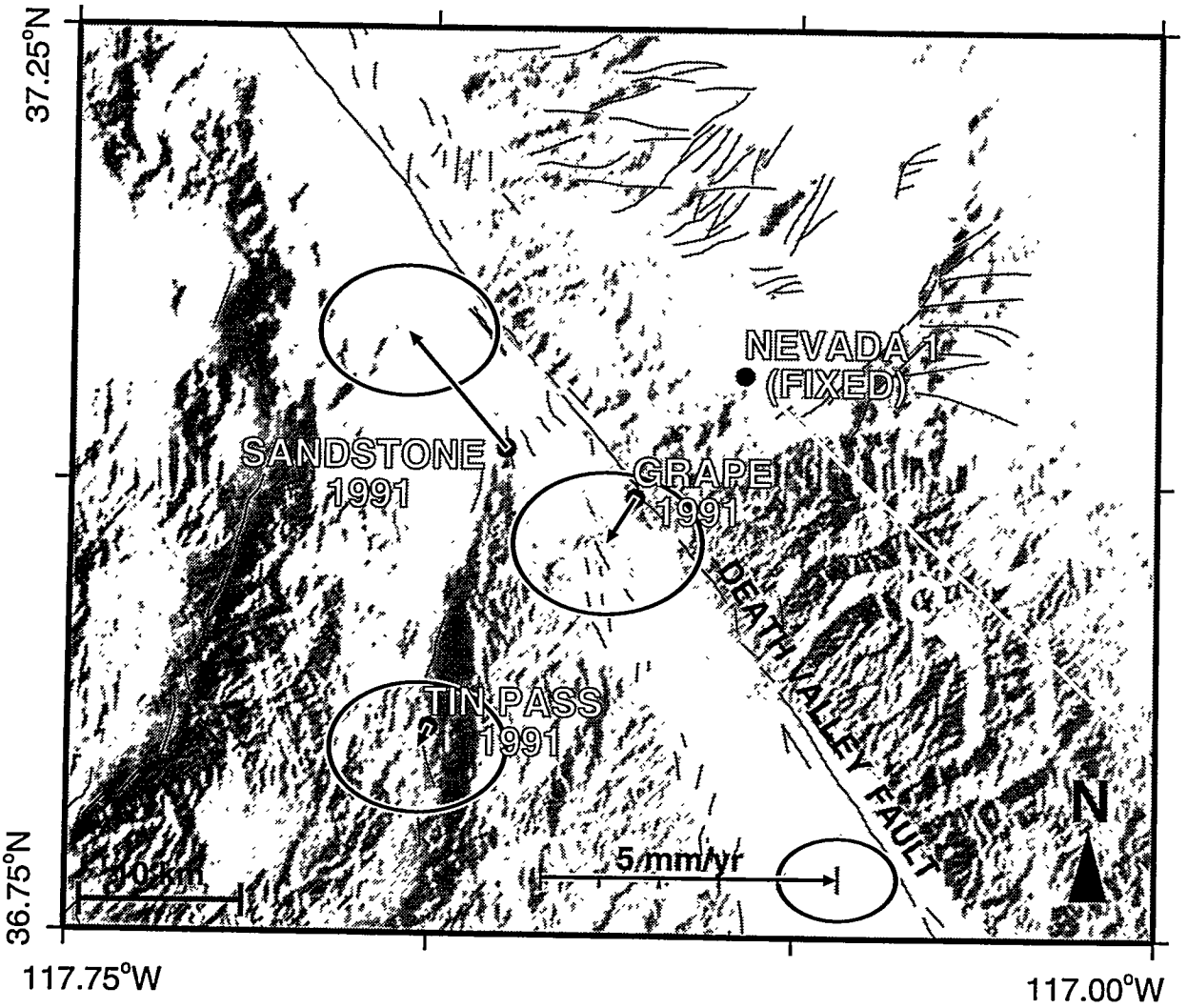

Figure 4-3. Maps showing relative motions based on the 1991, 1993, and 1994 Global Positioning System surveys within the Death Valley subnet. Ellipses show estimated 1σ errors.

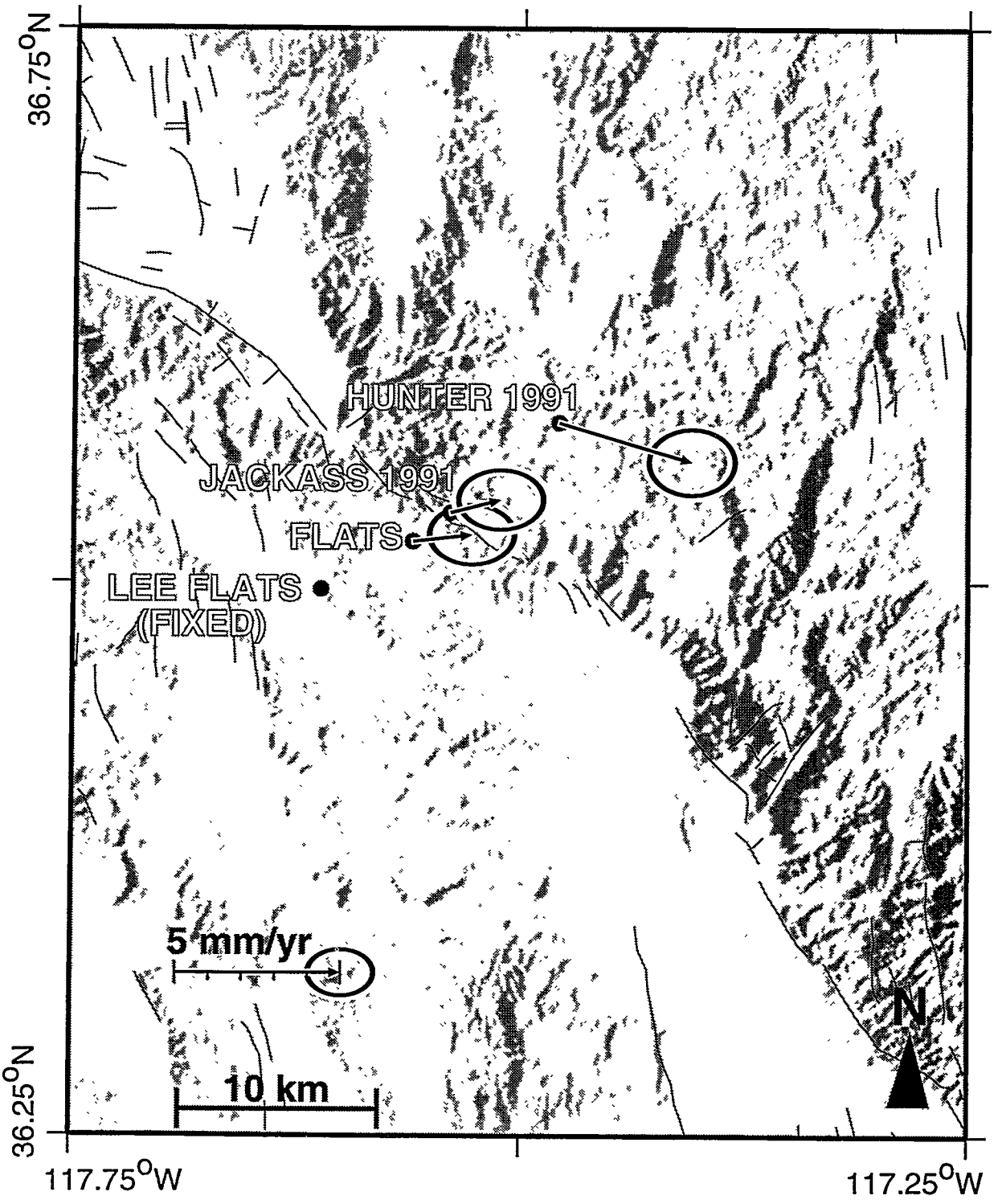

Figure 4-4. Map showing relative motions based on the 1991, 1993, and 1994 Global Positioning System surveys within the Hunter Mountain subnet. Ellipses show estimated 1σ errors.

4.3.2.2 The Death Valley Subnet

The Death Valley subnet (Figure 4-3), including sites Nevada 1, Grape, Sandstone, and Tin Pass, was designed to determine the rate of strain accumulation across the Northern Death Valley-Furnace Creek fault zone. The fault is essentially a pure right-lateral strike-slip fault where it lies closest to the repository (Brogan et al., 1991). The subnet includes two "narrow-aperture" sites (i.e., Grape and Sandstone), those near to the fault, and two "wide-aperture" sites (i.e., Nevada 1 and Tin Pass), those deployed farther from the fault, in this case at least 10 km away from and at right angles to the fault (Figure 4-3). This site configuration makes it possible to optimize the chances of determining the strain accumulating as a result of right-shear sense displacement along the fault zone—a pattern of deformation generally analogous to that along the San Andreas Fault (Brown, 1990). Ideally, the wide-aperture sites should record strain accumulating across the entire fault zone, while the narrow-aperture sites adjacent to the fault would give an indication of whether elastic strains are accumulating. If the wide-aperture sites are moving rapidly with respect to each other parallel to the fault in a right-shear sense, but the narrow-aperture sites are not, significant accumulation of elastic energy is indicated. To continue the analogy with the San Andreas Fault, this pattern would point to the similarity of the Northern Death Valley-Furnace Creek fault zone with the seismically hazardous "locked" segments of the San Andreas described by Thatcher (1990). On the other hand, if the narrow-aperture sites are moving just as rapidly as the wide-aperture, the fault is creeping and the probability of a major earthquake is far less, as in the case of the central "creeping" segment of the San Andreas Fault discussed by Thatcher (1990).

4.3.2.3 The Hunter Mountain Subnet

A strategy similar to that described for the Death Valley subnet was employed for the Hunter Mountain subnet (Figure 4-4), which includes sites Hunter, Jackass, Flats, and Lee Flats. The network was established across a portion of the fault determined to be in nearly pure right-shear (Burchfiel et al., 1987), with two narrow-aperture (i.e., Jackass and Flats) and two wide-aperture (i.e., Hunter and Lee Flats) stations.

4.3.3 1991 to 1994 Surveys

The network has been surveyed three times (October 1991, 1993, and 1994) using GPS equipment owned by the University NAVSTAR Consortium (UNAVCO). The surveys, conducted with UNAVCO equipment, also employed UNAVCO engineers who trained personnel in tripod set-up and proper use of the GPS receivers. The receiver used for the surveys has been the Trimble 4000 SSE with a "strip-type" antenna. The Trimble 4000 SSE is a dual (P-code) unit (see Leick, 1990, for discussion of P-code). Tracking specifications for the receiver are nine channels of L1/L2 P-code and full-cycle carrier phase or nine channels L1 C/A code, L1/L2 full-cycle carrier phase, and cross correlation of encrypted P-code. For a static survey, the best accuracy possible is considered to be as follows, based on information presented in the Trimble 4000 SSE operation manual (Trimble Navigation, Ltd., 1992), assuming at least five satellites tracked continuously using L1 and L2 signals at all sites: horizontal=5 mm+1 ppm times baseline length; vertical = 10 mm +1 ppm times baseline length.

It is known from continuous GPS surveys that a given day of measurement is repeatable to within about 1 mm in the horizontal and 4 mm in the vertical (Johansson et al., 1994) with a correlation time of about a week. Rates of motion of interest in the NRC/CalTech surveys appear to be in the range of 1 to 5 mm/yr. Thus, the total intersite motions in 3 yr are on the order of 3 to 15 mm, so that the

surveys are limited to observing only the more rapid motions over this relatively short time frame as elaborated in the following paragraphs of this section. Displacement rates measured for many stations in the network are within the range of uncertainty, due to the short period of the survey.

Another limiting factor on the results to date is that the solutions depend very strongly on the 1991 campaign results, since that campaign extends the period of measured strain accumulation to three yr. Three main difficulties are apparent from the 1991 survey. First, the satellite constellation was only about half what it is at the present time (i.e., about 12 satellites deployed instead of 24), so that the dilution of precision from constellation geometry was on the average higher than for the 1993 and 1994 surveys. Second, the International GPS Geodynamics Service network changed substantially after the 1991 survey, degrading the ability to provide an absolute frame for the 1991 occupation. This difficulty requires an assumption as to how to position the 1991 network relative to the other two, rather than directly measuring the 1991 network. There are a variety of methods by which this difficulty can be remedied, and each leads to determination of slightly different rates between the various survey sites. Third, the occupation schedule for the 1991 campaign tied the subnets together with a single day of data. Thus a substantial random error (e.g., a 2- to 3-mm error) on even one site translates into a significant error in the relative motions between the subnets. Aguereberry was not occupied during the 1991 campaign and is not included in the results at this time. In general, the relative motions within a given subnet are likely more accurate than the overall motions between the subnets.

With these caveats in mind, preliminary relative motions of the network are summarized in Table 4-1 and on Figure 4-1, excluding Aguereberry. The derived rates of Table 4-1 are given with respect to both a "centroid" reference frame (i.e., a frame with minimized net motion of the network), and with respect to Nevada 1 held fixed. The vectors plotted in Figure 4-1 show motions with Mile, the repository site location, held fixed. Error ellipses show 1σ errors, which are generally 1 mm/yr north-south and 1.5 mm/yr east-west. Representative residuals of the data from the centroid frame in Table 4-1 are shown in Figure 4-5 with 2σ error bars. In general, the rate uncertainty in the horizontal components is on average about ± 2 mm/yr at 2σ. Rate uncertainty, S, scales with observing interval, T, and the number of observing epochs, N, as

$$S < \text{proportional to} > 1/(T\sqrt{N}). \tag{4-1}$$

Thus, having obtained 2 mm/yr rate uncertainty with three observations spanning 3 yr, doubling the number of observations and the observation interval would yield an improvement by about a factor of three, or 0.7 mm/yr. An additional 6 yr would improve rate uncertainties down to about 0.4 mm/yr, and nine additional yr down to about 0.25 mm/yr.

The YM subnet (Figure 4-2) shows no significant horizontal intersite motions except for Wahomie, in agreement with the results of Savage et al., (1994). The large rate of Wahomie relative to Mile of 5 mm/yr southeast is clearly the result of the 1992 Little Skull Mountain earthquake, which was located very close to this survey site (Savage et al., 1994). Neither these results nor those of Savage et al., (1994) preclude relative horizontal motions as high as about 2 mm/yr in the vicinity of the repository. If such motions occur, a 20-m strain may accumulate across the network in 10,000 yr, which would be sufficient to produce as many as five to seven earthquakes in the 6.5 to 7.5 moment magnitude range. Alternatively, if intersite motions can be shown to be less than 0.3 mm/yr, events of this magnitude would be relatively improbable. Determining the number of the events of this size that could possibly occur has potentially substantial implications for assessment of repository performance. It could

Table 4-1. Components of relative site velocities

Centroid Reference Frame							Correlations		
	North		East		Up		NE	NU	EU
GRAP	−1.8	1.2	−3.4	1.6	−8.2	4.3	−0.038	−0.178	0.047
NEV1	−1.0	0.7	−2.9	0.9	0.8	3.4	−0.122	−0.191	0.143
TINP	−1.4	1.1	−3.1	1.5	8.4	4.3	−0.036	−0.205	0.055
SAND	1.0	1.1	−4.6	1.5	−10.5	4.3	−0.034	−0.213	0.108
FLAT	2.3	0.9	−0.5	1.3	−1.6	3.9	0.044	−0.153	0.107
JACK	2.5	0.9	−0.7	1.3	−2.6	3.9	0.027	−0.149	0.114
LEEF	2.1	0.7	−2.3	1.2	−1.0	3.7	0.016	−0.131	0.169
HUNT	0.9	1.0	1.7	1.3	4.4	4.0	−0.029	−0.169	0.140
BLAC	−0.5	0.6	2.0	1.0	−0.2	3.2	−0.028	−0.153	0.138
DANT	−2.8	1.1	3.2	1.6	4.9	5.2	−0.266	−0.132	0.215
67TJ	1.0	1.0	1.8	1.5	0.2	4.0	0.010	−0.199	0.055
CLAI	0.6	1.0	2.7	1.4	6.1	4.0	−0.047	−0.195	0.086
MILE	0.4	1.2	1.7	1.5	1.0	4.1	0.018	−0.192	0.038
WAHO	−3.3	1.0	4.3	1.6	−1.6	4.0	−0.010	−0.189	0.070

Nevada 1 Reference Frame							Correlations		
	North		East		Up		NE	NU	EU
GRAP	−0.9	1.1	−0.6	1.5	−9.0	3.1	−0.002	−0.197	−0.011
NEV1	0.0	0.0	0.0	0.0	0.0	0.0	0.000	0.000	0.000
TINP	−0.4	0.9	−0.2	1.4	7.6	3.1	0.015	−0.255	−0.011
SAND	2.0	1.0	−1.7	1.5	−11.4	3.2	0.014	−0.254	0.080
FLAT	3.3	0.9	2.4	1.3	−2.4	3.8	0.032	−0.155	0.109
JACK	3.5	0.9	2,1	1.3	−3.4	3.8	0.015	−0.151	0.116
LEEF	3.1	0.7	0.6	1.2	−1.8	3.6	0.006	−0.133	0.168
HUNT	1.9	1.0	4.5	1.3	3.6	3.9	−0.038	−0.171	0.141
BLAC	0.4	0.6	4.9	1.0	−1.0	2.9	0.003	−0.168	0.113
DANT	−1.8	1.0	6.1	1.6	4.1	5.2	−0.281	−0.132	0.218
67TJ	1.9	0.9	4.7	1.4	−0.6	3.5	0.028	−0.203	0.045
CLAI	1.6	0.9	5.6	1.3	5.3	3.5	−0.027	−0.196	0.075
MILE	1.3	1.1	4.6	1.3	0.2	3.6	0.039	−0.196	0.023
WAHO	−2.4	0.9	7.2	1.4	−2.4	3.5	0.004	−0.192	0.063

Solution Statistics: WRMS fit=2.1 mm; Chi-squared=0.561; total numbers of observation=144; velocity estimates and scaled standard deviations in mm/yr.

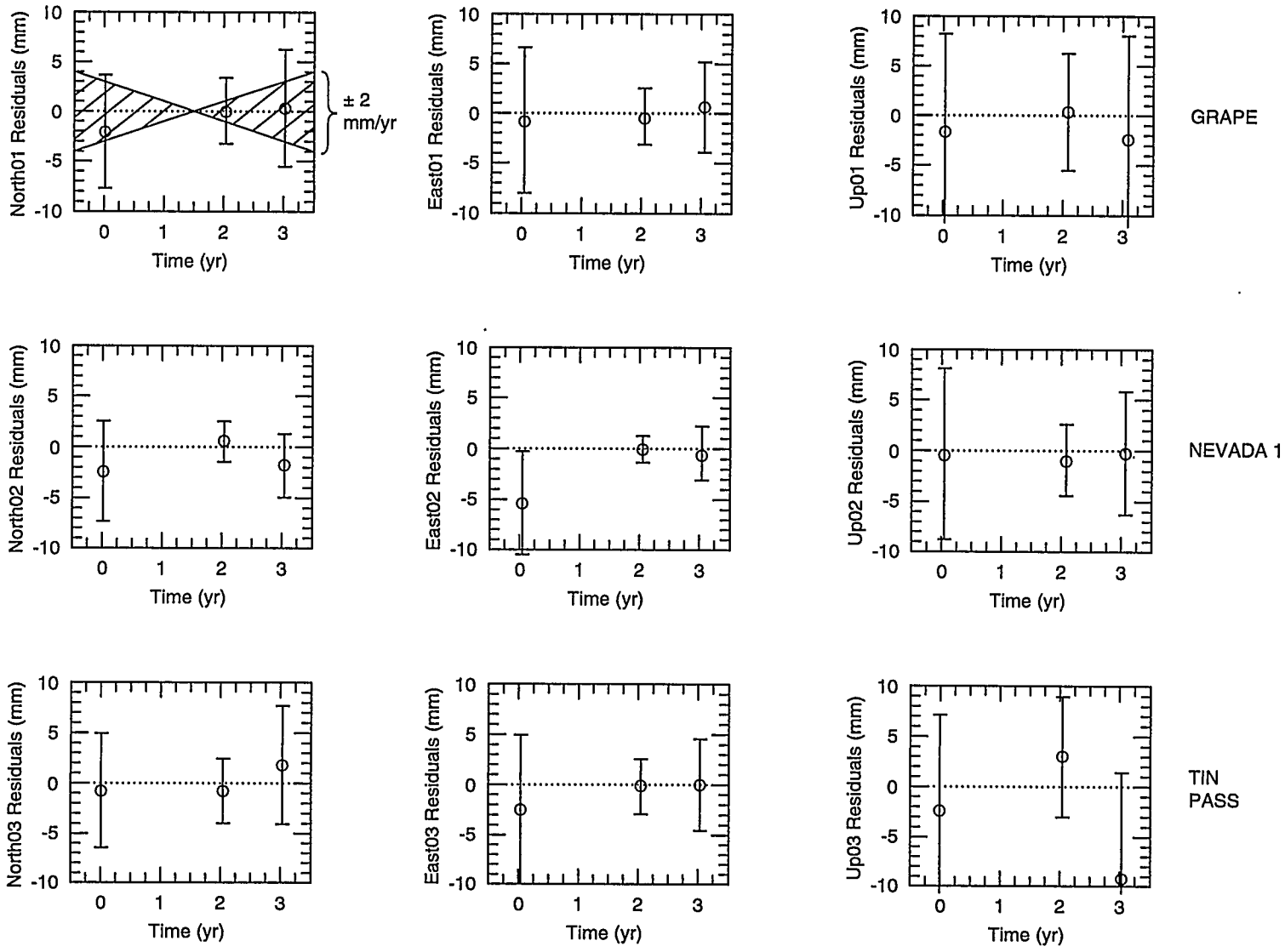

Figure 4-5. Representative time-series residuals based on centroid frame velocities (upper part of Table 4-1 for north, east, and up components of relative motion at sites Grape, Nevada, and Tin Pass. Errors are 2σ. Cross-hatched region in upper left frame shows error region of ± mm/yr.

mean the difference between licensing a repository that must withstand numerous earthquakes with ground accelerations exceeding 1 g and the possibility of ground rupture, versus a repository that need not be designed for such accelerations. Vertical motions are all well below 1σ, except for Claim, which appears to be rising relative to the other sites at about 5 ± 3.5 mm/yr.

Results from the Death Valley subnet show no significant intersite horizontal motions, except possibly for narrow-aperture site Sandstone (Figure 4-3), which is moving 2.8 ± 2 mm/yr northwestward relative to Nevada 1. However, motion of the other narrow-aperture site (i.e., Grape) is rather different, and the two wide-aperture sites (Nevada 1 and Tin Pass) do not show significant relative motion. It remains possible that a pattern of strain accumulation in right shear may emerge, but at present it does not appear that these motions will be particularly rapid. A noteworthy aspect of the preliminary solution in Table 4-1 is that sites Sandstone and Grape, at low elevations in Death Valley, show large subsidence of about 9 to 11 ± 3 mm/yr relative to Nevada 1. Tin Pass, located at a relatively high elevation, is moving upward at a rate of as much as 20 mm/yr relative to Sandstone and Grape. At face value, the data suggest the Northern Death Valley Fault is not accumulating strain as expected for a major strike-slip fault, but the large vertical motions are quite significant and are consistent with the obvious subsidence of the Death Valley basin relative to its flanks. The implications of such rapid vertical motions for the seismic hazard of the fault zone are not clear at present.

The Hunter Mountain subnet shows horizontal motions that are barely significant at 2σ, with site Hunter moving at 3.7 ± 2 mm/yr east-southeast relative to Lee Flats (Figure 4-4). The present solutions, while uncertain, do show the classical pattern of strain accumulation expected from right shear on a locked strike-slip fault, with the narrow-aperture stations (i.e., Jackass and Flats) moving at about the same rate, intermediate to that of the wide-aperture (i.e., Hunter and Lee Flats) stations. However, reduction of the rate uncertainty to less than 1 mm/yr will be required to conclude with certainty that the Hunter Mountain Fault is capable of large earthquakes. If the fault zone is moving at 3 to 4 mm/yr and fails over length scales of at least 100 km with events averaging 3 to 4 m of slip, approximately 10 earthquakes of moment magnitude 7.5 could be expected in the next 10,000 yr. Alternatively, slip could be accomplished by aseismic slip or many small-magnitude slip events. Intersite vertical motions are currently near or below 1σ for this subnet, as might be expected from the fact that the sites are all at about the same elevation on plateau-like topography.

Relative motions between the networks, including site Dante, are complex and largely counterintuitive at the present time (Figure 4-1). An overall pattern of large-scale right-oblique shear along a direction about N 30° W, as put forward by the widely accepted eastern California shear zone hypothesis (Dokka and Travis, 1990) is not consistent with these preliminary results. Relative to the repository, the Death Valley subnet is on the average moving rapidly southwestward at about 5 mm/yr, roughly orthogonal to the motion predicted by regional N 30° W, right-oblique shear. The Hunter Mountain network is on the average moving at a few mm/yr northwestward, in agreement with the hypothesis, except perhaps for Hunter. Most in conflict with regional right-oblique shear is the motion of Dante relative to Mile, which seems to be moving rapidly (4.5 ± 3 mm/yr, 2σ) southeast, precisely opposite the direction predicted by the hypothesis. Although it should be reiterated that the motion between the subnets is less certain than intersite motions within the subnets, nonetheless the pattern is likely to remain relatively complex as resolution improves.

Motion of the Death Valley subnet seems to reflect the opening of the valley orthogonal to its long dimension, considering the vertical motions. One hypothesis is that these motions represent a phase

in a cycle of alternating northwest right shear leading to failure of the strike-slip system, and southwest-directed stretching and subsidence related to continued deepening of Death Valley. This hypothesis implies that strain accumulation is partitioned in time, and that at present the Death Valley fault zone is not accumulating strain as a strike-slip fault. As a possibly analogous situation, Press and Allen (1995) have investigated patterns of seismic release along the San Andreas fault system in southern California and determined that this fault system also has not been accumulating and releasing strain as a strike-slip system over the last two decades. The southeastward motion of station Dante is much more difficult to explain. One possibility is that right shear is in a transient state of relaxation along that part of the system, even though strain is accumulating in the proper sense along the adjacent Hunter Mountain fault zone. These ideas must be considered rather speculative at this time, as it will require several more occupations to reduce the uncertainties.

4.4 CONCLUSIONS AND RECOMMENDATIONS FROM THE NUCLEAR REGULATORY COMMISSION/CALTECH/SMITHSONIAN SURVEY

GPS data being acquired during surveys in the NRC/CalTech network are critical for characterizing the present-day tectonic setting and analyzing the potential for future tectonic effects at YM. Preliminary GPS results derived from the surveys to date indicate two important trends in relation to contemporary strain patterns in the YMR. First, significant vertical and horizontal motions around the proposed repository site may be present and would be detectable with further monitoring. Second, significant horizontal and vertical strains are accumulating regionally along major fault zones within 50 to 100 km of the proposed repository, but the motions are only beginning to be measurable in this survey. Determining horizontal and vertical movement as precisely as possible is important since the motions have implications for assessment of repository performance. The motions bear directly on the interpretation of contemporary tectonic activity in the region containing YM; whether the repository area could experience surface or subsurface rupture from future tectonic events in the next 10,000 yr; and the degree and frequency of ground accelerations that could occur at the repository due to future large earthquakes.

Major improvement on rate uncertainty is readily attainable with further occupations of the existing network, with reductions by about a factor of 3 with only three additional occupations spread over a period of three yr. Therefore, it seems prudent that at least three more years of campaign-style GPS surveys be performed across the network. In addition, the surprising results from site Dante indicate more sites across the central Death Valley fault are needed to evaluate whether this part of the fault zone is moving in the "wrong" direction with respect to its slip history. New sites would include approximately three additional locations, two southeast of Dante and one near the bottom of Death Valley between Aguereberry and Dante. Serious consideration should be given to establishing continuously monitored stations, especially for the YM subnet, but up to and including the entire network. Continuous monitoring would allow determination of rates at least three to five times more rapidly than campaign-style monitoring because of the larger number of measurements. Thus, 1 yr of continuous data, conservatively, would achieve the same objective as another 3 to 5 yr of campaign-style monitoring. Improvement of precision and accuracy of survey results would substantially enhance the ability of the NRC staff to evaluate seismotectonic issues in the repository license application that the DOE is required to submit.

Data from other GPS surveys in the southwestern United States should be compiled in the CNWRA database and linked with the NRC/CalTech network results to provide the broadest information base for assessing contemporary strain history of YM and the surrounding region. This broad regional consideration is important in view of the potential for regional triggering of earthquakes, such as the

M5.6 Little Skull Mountain earthquake of June 29, 1992, which is thought to have been triggered by the M7.5 Landers, California earthquake (Anderson et al., 1992; Gomberg et al., 1992; Reasenberg et al., 1992) and was the largest Landers-triggered event (Reasenberg et al., 1992).

5 SLIP-TENDENCY ANALYSIS AND FAULT REACTIVATION

Earthquakes near the proposed HLW repository at YM represent considerable safety and performance risk during construction and operations, and after closure of the facility. Additionally, fault-slip within the repository could potentially cause direct disruption of waste packages. Several KTUs have been recognized related to potential for fault-slip in and around YM: (i) uncertainty in determining spatial and temporal patterns of seismicity, (ii) uncertainty in determining slip-history of faults, (iii) uncertainty in determining effects of structural deformation and tectonic processes on flow and transport of groundwater, (iv) uncertainty in determining magnitude of fault-slip and seismic shaking at surface and shallow subsurface locations, and (v) uncertainty in determining effects of structural deformation and tectonic processes on rock mass properties.

A new technique called slip-tendency analysis has been developed that allows for the assessment of slip potential from mapped and suspected faults in a known or inferred stress state (Ferrill et al., 1994a, b; Morris et al., 1994; Ferrill et al., 1995). The tendency of a surface to experience slip in a given stress state is related to its frictional characteristics, primarily rock type, and the ratio of shear to normal stress acting on the surface, here defined as slip tendency, and which is determined by the orientation of the surface and the state of stress. An interactive computer tool called "3DSTRESS" displays the stress tensor in terms of its associated slip-tendency distribution and the relative likelihood and direction of slip on surfaces of all orientations. The technique provides easy visualization and rapid evaluation of the potential slip significance of stress states, and individual surfaces within a stress state. It can be used to assess seismic risk from known or suspected faults, test for compatibility of geologic structures, focus exploration for high-risk and earthquake-prone blind faults, and interpret likely slipped faults from focal mechanism solutions.

5.1 SLIP TENDENCY

In most homogeneous stress states, two surfaces are optimally oriented for slip (Anderson, 1951). These surfaces intersect in the direction of the intermediate principal compressive stress (σ_2) and are symmetrical about the σ_1 axis (e.g., Jaeger and Cook, 1979). However, Wallace (1951) showed that the magnitude and orientation of the maximum resolved shear stress vector on any surface vary continuously with the orientation of the surface with respect to the 3D stress state (stress tensor) it experiences and the relative values of the principal stresses. Bott (1959) states explicitly: "...the maximum shearing stress within a ... plane of fracture ... may lie in every possible direction for a variable stress system of given orientation..." and concluded that principal stress rotations out of the vertical and horizontal planes are not necessary to explain oblique slip faults.

The distribution of surfaces with high resolved shear stress and the variability of the direction of the shear stress vector are expressed naturally in a number of ways. Natural fault systems, and those developed in analogue model materials, tend to be anastomosing networks of slip surfaces with variable orientations. Some slip surface orientations, those close to the "Andersonian" conjugate set (Anderson, 1951), tend to dominate, but many surfaces contribute to the overall deformation. Earthquakes and their associated aftershocks also occur on a variety of slip surfaces, and this phenomenon is utilized to determine the tectonic stress state responsible for the earthquake (McKenzie, 1969; Gephart and Forsyth, 1984).

Although well established, the principle of variation in the shear stress vector within and concomitantly with the stress tensor is difficult to visualize, and, in itself, is of limited utility. The likelihood that a surface will experience slip in a given stress state is a function of the frictional resistance to sliding on that surface, which is governed both by rock properties and the *ratio* of shear to normal stress acting on the surface. Thus, a more useful perspective for determining the population of surfaces that might reasonably experience slip in a stress system is to view the ratio of shear to normal stress as well as the directional component of the maximum resolved shear stress vector.

Slip is likely to occur on a surface when the resolved shear stress, τ, on that surface equals or exceeds the frictional resistance to sliding, F, which is proportional to the normal stress, σ_n, acting across that surface (Jaeger and Cook, 1979; Figure 5-1). Whether or not a surface will actually slip, depends on the coefficient of static friction for the surface, μ. At the instant of sliding, then:

$$F \leq \tau = \mu\sigma_n \tag{5-1}$$

The slip tendency (T_s) of a surface can be defined as the ratio of shear stress to normal stress acting on that surface:

$$T_S = \tau/\sigma_n \tag{5-2}$$

and, as such, depends solely on the stress state (stress tensor) and the orientation of the surface. The coefficient of static friction, μ, is the slip tendency that will cause slip on a surface and is often referred to as the "strength" of a fault in earthquake focal mechanism analysis (i.e., cohesion is assumed to be negligible). The implication of fault strength is that if slip occurs on a surface with a low slip tendency for the computed or assumed stress state, it must have a low value of μ and thus is "weak."

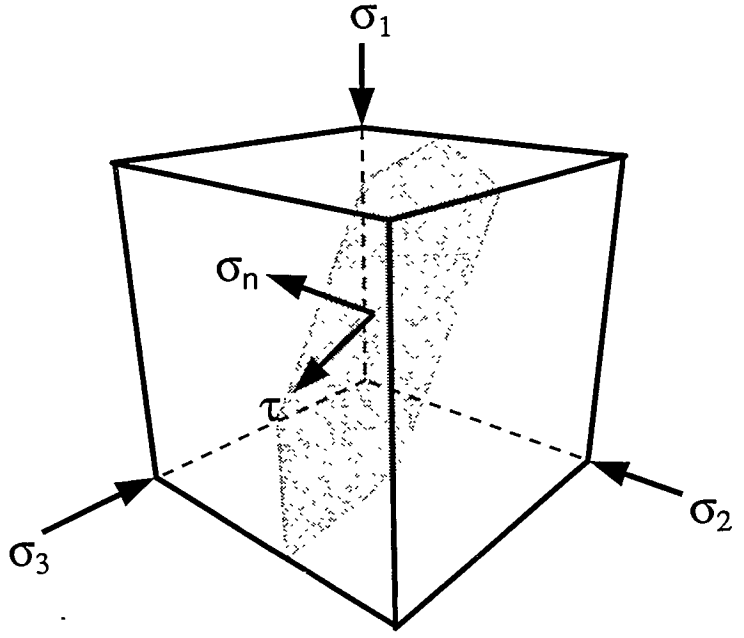

Figure 5-1. Normal stress, σ_n, and shear stress, τ, acting in an arbitrarily oriented surface within a stress state defined by the three principal compressive stresses σ_1, σ_2, and σ_3

5.2 SLIP TENDENCY AND THE STRESS TENSOR

In a homogeneous state of stress, a unique pair of surfaces usually experiences the maximum developable slip tendency (T_{SMAX}) for that stress state; this characteristic is the basis of "Andersonian" fault analysis (Anderson, 1951; Jaeger and Cook, 1979). Many other surfaces, however, have slip tendencies close to the maximum value. The distribution of slip tendency with orientation depends upon the relative values of the principal stresses (Wallace, 1951; Bott, 1959; Figure 5-2), and is very sensitive to the axial symmetry of the stress tensor. The "tightness" or aspect ratio of the distribution of surfaces experiencing high values of T_S is also determined by the relative values of the principal stresses, as σ_1/σ_3 increases, aspect ratio also increases [Figure 5-2(d)].

$$\text{Aspect ratio} = 1000 \times T_{SMAX}/N_{(0.5\ T_{sMAX})} \tag{5-3}$$

where $N_{(0.5\ TsMAX)}$ =number of surfaces experiencing $\geq 0.5 \times T_{sMAX}$ counted on a 5° net.

If the orientations and magnitudes of the principal stresses are known or assumed, it is possible to determine the state of stress on any surface experiencing that stress state (Bott, 1959; Ramsay, 1967). Three parameters are of special interest: (i) the normal stress, σ_n; (ii) the shear stress, τ; and (iii) the direction of the resolved shear-stress vector, $\vec{\tau}$, in the surface. The normal and shear stresses determine the slip tendency (τ/σ_n), and the shear-stress vector indicates the direction and sense of motion that is likely to occur.

The $\vec{\tau}$ field of the stress tensor has been most commonly exploited to determine stress states from earthquake data (McKenzie, 1969; Gephart, 1990) and paleoslip data (Angelier, 1979). In these applications, observed or computed slip directions are considered to reflect the orientations of $\vec{\tau}$ within a homogeneous stress tensor. The observed distribution is iteratively compared with the computed $\vec{\tau}$ fields of a wide variety of stress tensors to obtain an optimized best-fit. Friction is regarded as secondary in importance or is not considered, although Wesnousky and Jones (1994) examined paired-fault systems in the southern Great Basin for their synergistic qualities by computing states of friction for the faults under consideration.

It is interesting to consider the opposite perspective. We have developed an interactive computer tool that enables specification of the stress tensor by choosing values and orientations for the principal stresses and by calculating and displaying slip-tendency data for surfaces of all orientations. This display can then be interactively adjusted by modifying the magnitudes and orientations of the three principal stresses to investigate the slip tendency and slip vector $\vec{\tau}$ on any individual surface. We also link the slip-tendency data to fault-map traces, enabling investigation of various stress scenarios and their effects on known or suspected faults.

5.3 SLIP-TENDENCY DISTRIBUTION

The population of surfaces that experiences high slip tendencies (for example, 80 percent of T_{sMAX}) is variable and only approaches a simple bimodal distribution for certain stress configurations. Stress regimes can be defined in terms of K and R (the stress difference ratio), where:

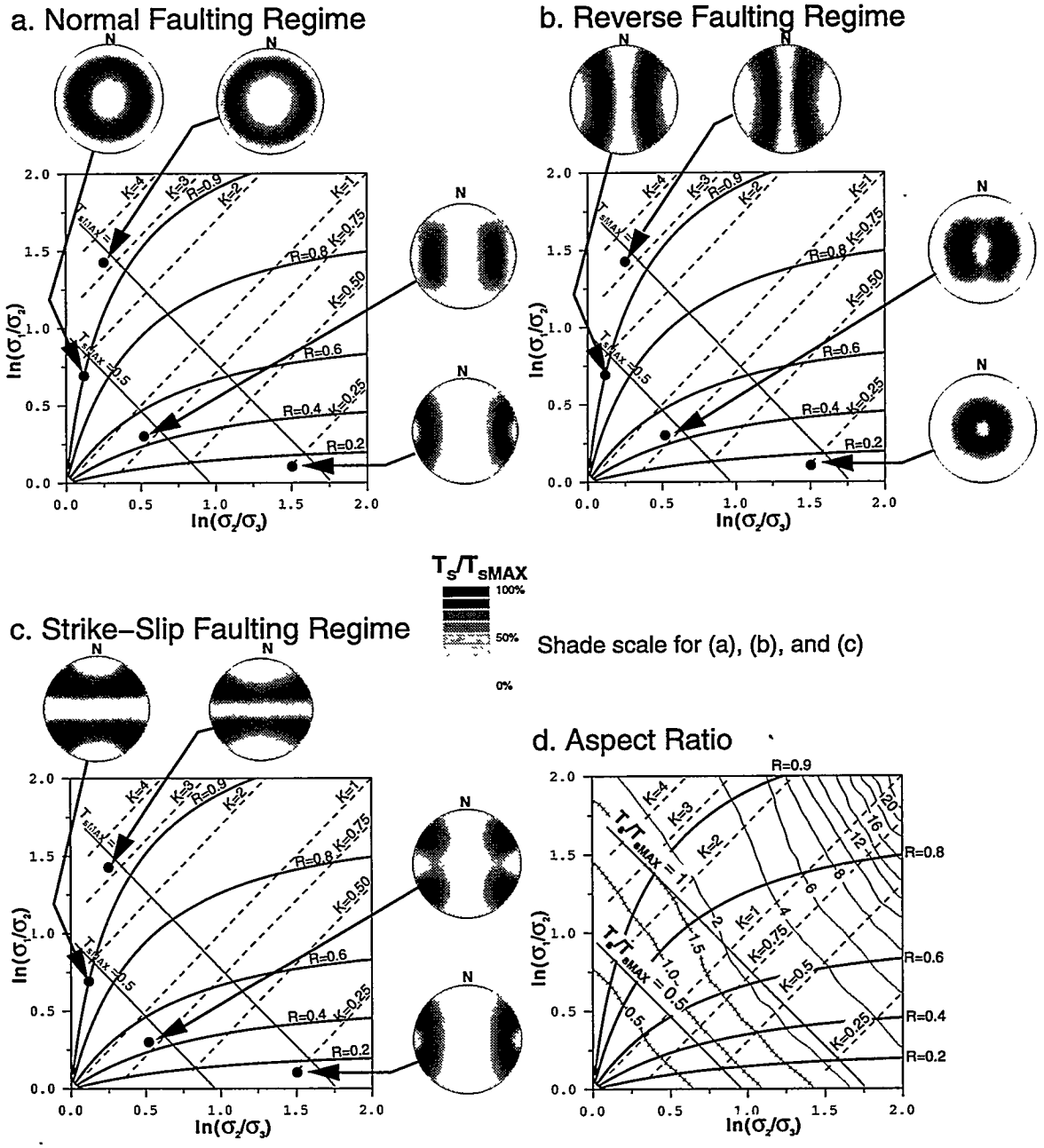

Figure 5-2. Graphs of $\log(\sigma_1/\sigma_2)$ versus $\log(\sigma_2/\sigma_3)$ with contours of R values (heavy solid lines), K values (dashed lines), and T_{sMAX} (light solid lines). For discussion of K and R, see text. The two contours of T_{sMAX} shown (0.5 and 1.0) bracket most realizable conditions of maximum stress for the Earh's crust (Byerlee, 1978). Figures (a) through (c): Selected slip tendency plots for four stress states are superimposed on the log/log graph; a slip tendency plot is a lower hemisphere, equal angle projection of poles to surfaces, poles are contoured with respect to the slip tendencies of the surfaces that they represent as a percentage of T_{sMAX} for that stress state (see shade scale). Three fault "regimes" are illustrated: (a) normal fault regime, σ_1, vertical, σ_2, north-south, σ_3, east-west; (b) reverse fault regime, σ_3, vertical, σ_2, north-south, σ_1, east-west; (c) strike-slip fault regime, σ_2, vertical, σ_1, north-south, σ_3, east-west. Figure (d) is contoured with respect to aspect ratio.

$$K = (\sigma_1/\sigma_2)/(\sigma_2/\sigma_3) = (\sigma_1\sigma_3)/\sigma_2^2 \quad (5\text{-}4)$$

$$R = (\sigma_1 - \sigma_2)/(\sigma_1 - \sigma_3) \quad (5\text{-}5)$$

Stress states for which $K \approx 1$ have strongly bimodal distributions of surfaces with high slip tendencies and fall along the (bottom left to top right) diagonal line in Figure 5-2. The distribution of high slip-tendency surfaces tends toward a girdle about the σ_3 axis where $K<1$ and about the σ_1 axis where $K>1$ (Figure 5-2).

5.4 PORE PRESSURE

The effect of varying pore pressure is to move the stress state (in a σ_1/σ_2 versus σ_2/σ_3 plot) along a locus of constant R (Figure 5-2). Increasing pore pressure causes no change to resolved shear stress but decreases all normal stresses by an amount equal to the pore pressure, which causes the stress state to evolve to a condition in which, eventually, hydraulic fracturing may occur (Secor, 1965). During this evolution, the stress state passes through conditions of increasing T_{sMAX} and if stress magnitudes are great enough, slip may occur before (and may inhibit) hydraulic fracturing.

5.5 APPLICATIONS

5.5.1 Fault Pattern Analysis at Yucca Mountain, Nevada

With the exception of mapping from 3D seismic surveys, it is only rarely possible to obtain full 3D data for the surface of a fault. However, it is common to have two-dimensional (2D) fault traces in map view with sparse dip information. Slip-tendency computations can be linked with fault-trace maps such that the stress state can be varied, and the effects of this variation on the slip tendencies of known faults can be viewed. The view can be "tuned" to specific fault dips or it can scan for strike trends alone. This capability provides a means for rapid assessment of the mutual compatibility of fault sets for various stress states. A consequence of this viewing technique is that faults can be semi-quantitatively assessed for their slip potential in any chosen stress state—a first step in determining seismic hazard on known or suspected faults.

Stock et al. (1985) provide the only published measurements of the *in situ* stress state at YM. At depths of between 1 and 1.3 km, their measurements indicate that:

σ_1 = vertical = 20.8 to 27.2 MPa

σ_2 = N 25° E to N 30° E = 12.8 to 17.9 MPa

σ_3 = N 60° W to N 65° W=10.6 to 14.8 MPa

and at depths of 1.2 km σ_3 is approximately 47 percent of σ_1. Assuming an average rock density of 2.7 gm/cm^3:

σ_1 = 130 MPa (conservatively)

σ_2 = 78 to 110 MPa

σ_3 = 63 MPa

at a depth of 5 km. Assuming a water table depth of 500 to 600 m (Stock et al., 1985) hydrostatic pressure at 5 km will be 45 MPa. Applying this effective stress state:

σ_1 = vertical = 85 MPa

σ_2 = N 25° E to N 30° E = 75 MPa

σ_3 = N 60° W to N 65° W = 18 MPa

to the faults near YM, Nevada, shows that both strike-slip and normal faults can coexist in the contemporary stress state (Figure 5-3). Moderately to steeply dipping faults with north-south to northeast-southwest strikes tend to have high slip tendencies (Figures 5-4 and 5-5). Although steeply dipping, northeast-southwest striking faults are expected to have the highest slip-tendency, oblique-slip and strike-slip faults in certain orientations have slip tendencies of >80 percent of the calculated maximum slip tendency (Figures 5-3 and 5-4). These conclusions agree with those of Stock et al. (1985). Although, assumption of a lower average rock densities (e.g., 2.5 g/cm^3) would slightly reduce estimated stresses, the overall pattern of slip-tendency would remain virtually unchanged.

Figure 5-5(b) illustrates the slip-tendency distribution for the probable current stress state at YM. Many faults are in orientations of relatively high slip tendency; however, several large NW-SE trending faults are in orientations of low slip tendency and are thus misoriented for contemporary slip. It is likely that these misoriented faults developed under different stress conditions and that the stress state at YM has evolved from some previous state similar to that illustrated in Figure 5-5(a).

Another important conclusion reached from this analysis at YM is that, although the patterns of faults experiencing high slip tendencies are very dependent on the orientation of σ_3, they are insensitive to small variations in the magnitudes and large variations in the orientations of σ_1 and σ_2, once σ_3 is known. For example, if σ_3 is horizontal, and trending N 90° E, almost all faults with dips of 70–90° at YM fall in the high slip-tendency category [Figure 5-5(a)], whereas if σ_3 is horizontal, and trending N 65° W, the pattern of faults with high slip tendencies is markedly different (Figure 5-5b).

In order to further evaluate the importance of the stress tensor (magnitudes and orientations) with respect to a fault, calculations of slip tendency were made for a fault similar in orientation to the Ghost Dance Fault. Calculations were made for two stress states and for a 35° range of possible strike and a 20° dip range (Figures 5-6 and 5-7). In the two modeled stress states, σ_1 is vertical (85 MPa), σ_3

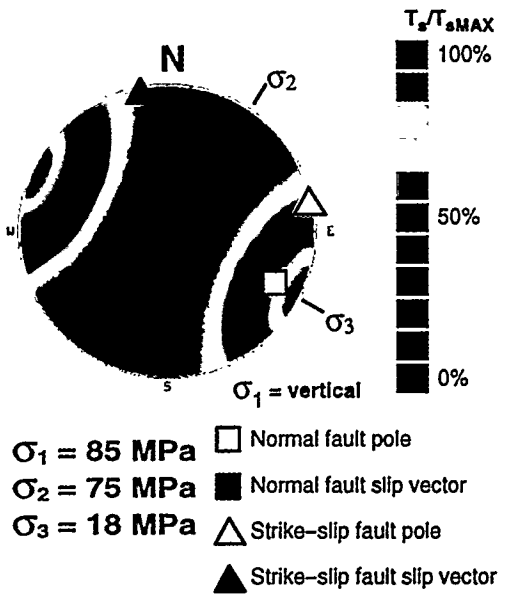

Figure 5-3. Slip-tendency plot showing that both dip-slip and strike-slip faults with certain orientation ranges experience high slip tendencies in the contemporary stress state at Yucca Mountain, Nevada

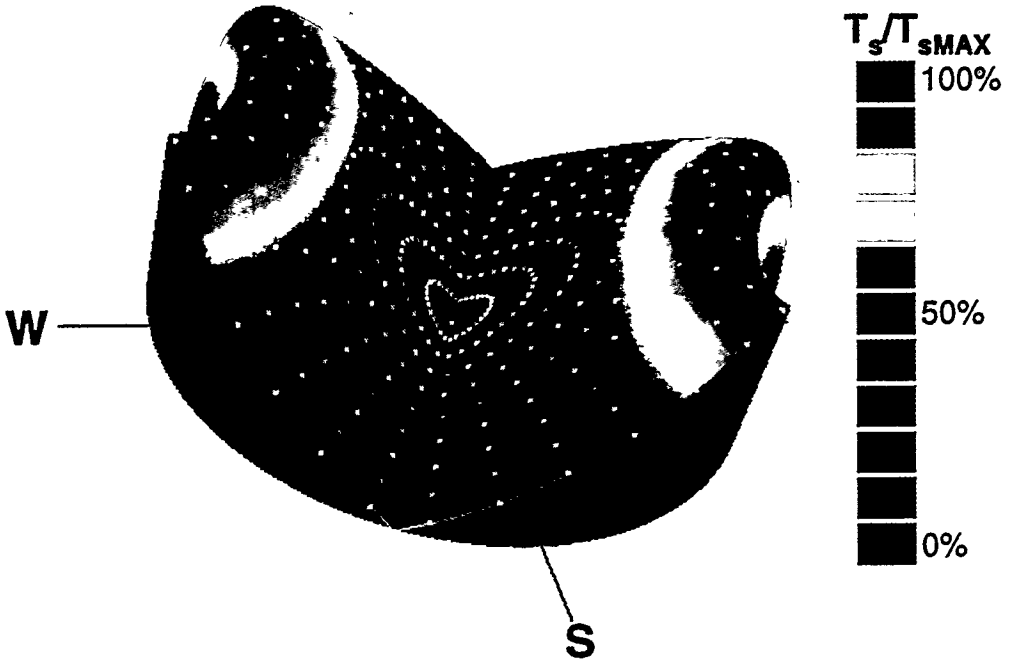

Figure 5-4. Oblique view of slip-tendency plot for the contemporary stress state at Yucca Mountain, Nevada, showing the "topography" of the slip tendency distribution. The height of the plot at any point is proportional to the ratio T_s/T_{sMAX} for the surface represented by the pole at that point. T_s/T_{sMAX} is the ratio of the calculated slip tendency to the maximum attainable slip-tendency in a given stress state. Aspect ratio is a measure of the sharpness of this topography.

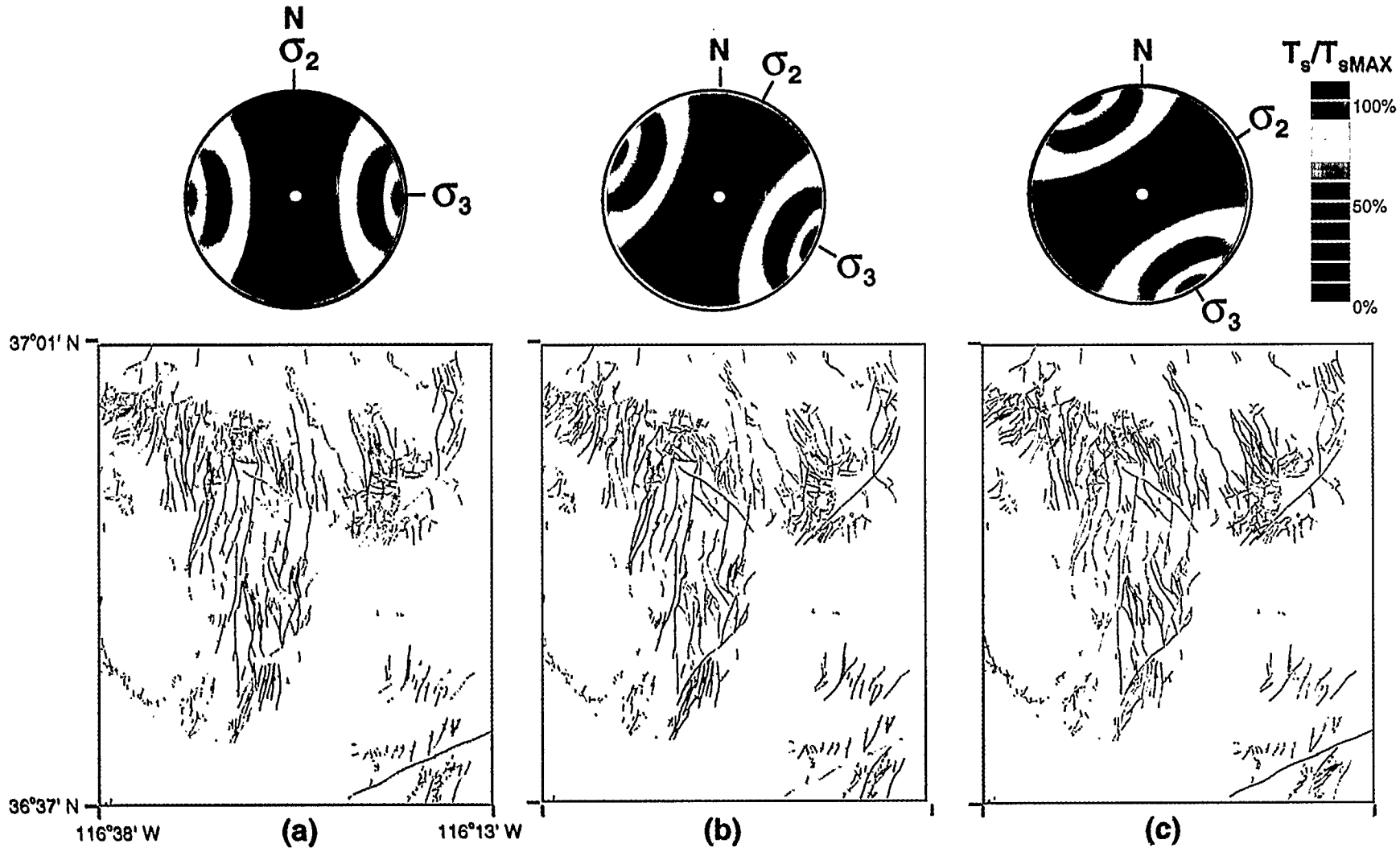

Figure 5-5. Slip-tendency plots and associated fault trace maps (after Frizzell and Shulters 1990) for three possible orientations of the contemporary stress magnitudes at Yucca Mountain, Nevada. The maps are color-coded according to the same scale as the slip-tendency plots. Faults are all assumed to have dips in the range 65 to 80°. Modeled stress magnitudes are those in Figure 5-3. Modeled stress orientations are as follows: σ_1=vertical, σ_2=north-south, σ_3=east-west; the preferred stress state σ_1=vertical, σ_2=N 25° E, σ_3=N 65° W; σ_1=vertical, σ_2=N 60° E, σ_3=N 30° W.

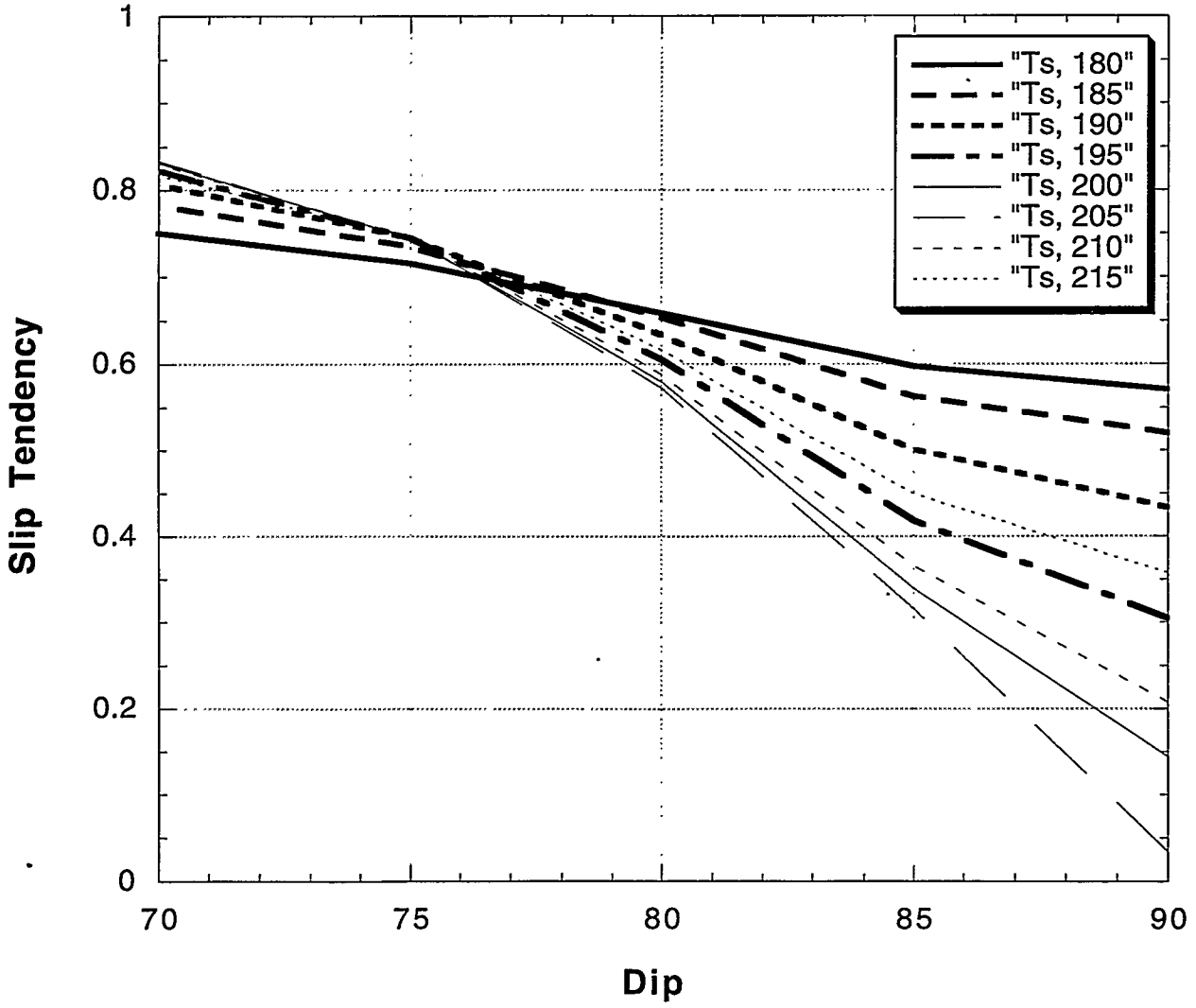

Figure 5-6. Graph of slip tendency (Ts) for a fault similar in orientation to that of the Ghost Dance Fault (strike=180–215°; dip=70–90° westward) in a stress state where: σ_1=vertical, 85 MPa; σ_2=horizontal with azimuth 025, 55 MPa; and σ_3= horizontal with azimuth 115, 18 MPa

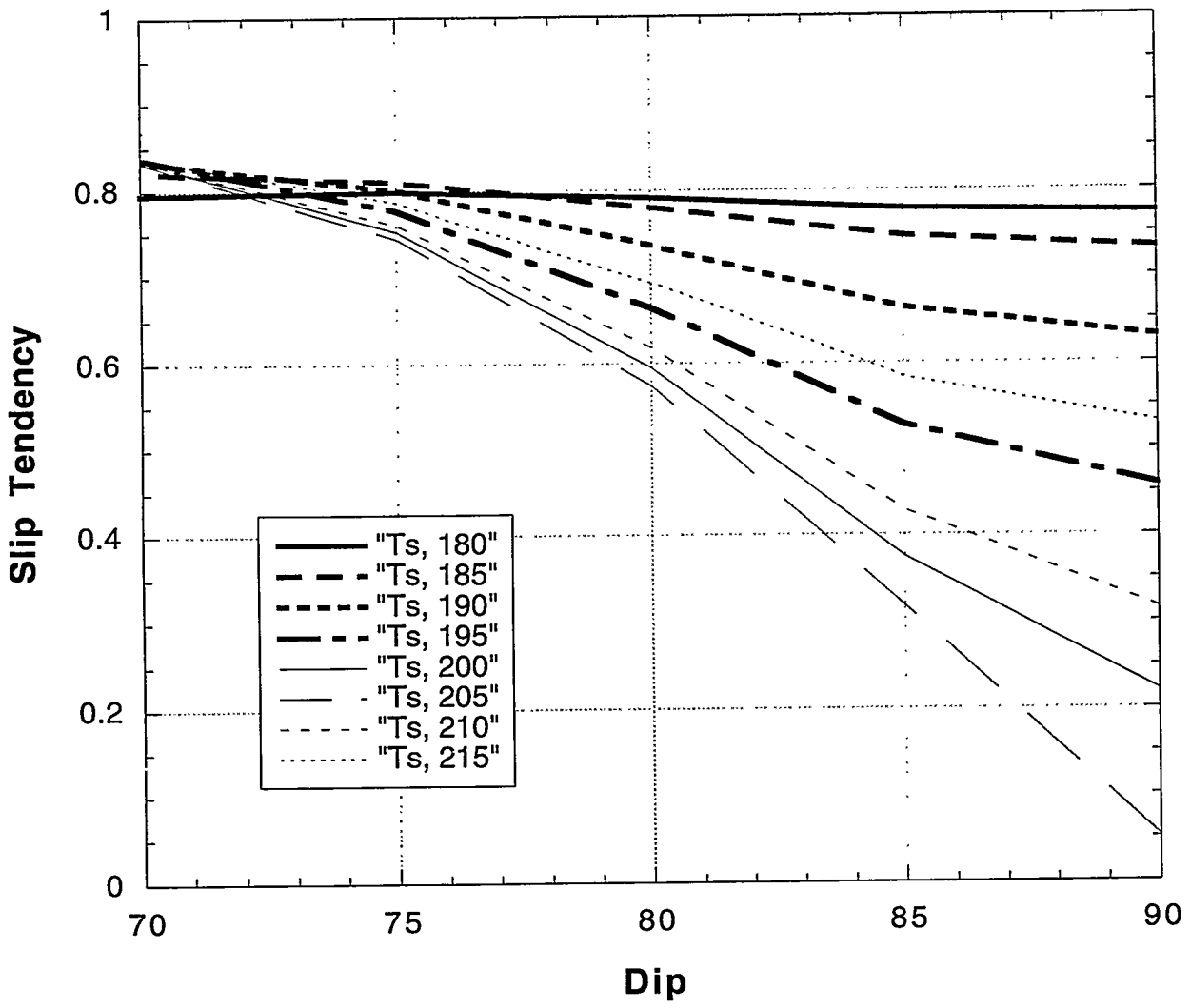

Figure 5-7. Graph of slip tendency (*Ts*) for a fault similar in orientation to that of the Ghost Dance Fault (strike=180 to 215°; dip=70 to 90° westward) in a stress state where: σ_1=vertical, 85 MPa; σ_2=horizontal with azimuth 025, 75 MPa; and σ_3= horizontal with azimuth 115, 18 MPa

is horizontal with azimuth 115 (18 MPa), and σ_2 is horizontal with azimuth 025 and is modeled at 55 MPa (Figure 5-6) and 75 MPa (Figure 5-7). For each of the strikes and stress states modeled, slip tendency tends to be higher for faults dipping at 70° and lowest (of calculated examples) where dip is vertical. It is also important to note that slip tendencies tend to be very sensitive to relatively minor changes in both strike and dip. This sensitivity is actually controlled by the relative orientations between the fault and the stress tensor. Therefore, the importance of knowing the orientation of the stress tensor is equal to the importance of knowing the fault orientation for estimation of slip tendency.

5.5.2 Assessment of Seismic Hazard

Knowledge of the *in situ* stress state in an area permits the evaluation of relative earthquake hazard for both known and suspected faults. The ability to predict the $\vec{\tau}$ component for a fault in a known stress state can further refine the assessment of seismic hazard, because ground motion resulting from an earthquake is a function of both magnitude and sense of fault slip (McGarr, 1984). Thus, knowledge of the likely slip orientation on a given fault provides information about ground accelerations that could result from an earthquake occurring on that fault.

5.5.3 Focal Mechanism Solutions

Focal mechanism solutions based on first-motion analysis for earthquakes with no surface break or other clear indication of orientation of the slip plane are inherently ambiguous—two possible fault planes explain the data. The choice of preferred nodal plane (the slip plane) automatically specifies the slip vector, which lies in the plane of choice, perpendicular to the line of intersection with the auxiliary plane. Thus, the choice is made by comparing the two possible slip vectors from first-motion analysis with the computed $\vec{\tau}$ for the two potential slip surfaces within the inferred stress state. The surface that gives less angular misfit is chosen as the preferred nodal plane. One commonly used stress inversion method for use with earthquake data, the Focal Mechanism Stress Inversion (FMSI) model (Gephart, 1990), specifically optimizes the focal mechanism slip vector data with the shear stress vector component ($\vec{\tau}$) of the assumed stress tensor and thus relies solely on the slip direction criterion to obtain a best-fit stress tensor. This approach can produce anomalous results in the form of assumed slip on misoriented surfaces (those with low values of slip tendency). Gephart (1990) suggests that a frictional criterion could be added to the model to eliminate such anomalies. Slip-tendency analysis could be incorporated into a model such as FMSI as an additional constraint in the optimization process.

5.5.4 Assessment of Fault Plane Solutions: The Little Skull Mountain Sequence

Earthquake data can be analyzed using slip-tendency analysis as a basis for selection of nodal planes from focal mechanism solutions. The Ms5.4 Little Skull Mountain earthquake occurred about 15 km southeast of YM on June 29, 1992, the day after the Ms 7.6 Landers earthquake. The Landers earthquake is thought to have triggered the Little Skull Mountain earthquake (Hill et al., 1993; Anderson et al., 1994; Bodin and Gomberg, 1994; Gomberg and Bodin, 1994; Ferrill et al., 1994a). Harmsen (1994) determined the tectonic stress field responsible for the Little Skull Mountain mainshock and aftershock sequence using Gephart's (1990) FMSI model. In order to obtain a "best-fit" stress tensor, the inversion technique used in FMSI matches the resolved shear stress vector ($\vec{\tau}$) field of the stress tensor against the slip directions determined from focal mechanism studies. No use is made of frictional criteria, although Gephart suggests that the frictional criteria can be superimposed as an additional

constraint. Slip-tendency analysis yields both frictional T_s, and slip direction ($\vec{\tau}$) information about the stress tensor and provides a semiquantitative means of assessing earthquake data. The FMSI solution for the Little Skull Mountain 1992 earthquake sequence gives orientations (bearing/plunge) for principal stresses as follows: σ_1=219°/69° , σ_2=024°/21° , σ_3=116°/05° , and $(\sigma_1-\sigma_2)/(\sigma_1-\sigma_3)$=0.35 (Harmsen, 1994). This section equates to the following stress approximations for a depth of 10 km (the approximate depth of the Little Skull Mountain mainshock): σ_1 =260 MPa, σ_2 =190 MPa, and σ_3 =70 MPa. Re-analysis of the FMSI results using the above stress state, and applying the T_s criterion to pick the preferred nodal planes, increases the mean slip tendency for faults active during the Little Skull Mountain sequence from 72 to 85 percent of T_{sMAX}, but also increases the angular misfit from 5 to 13°. The T_s criterion disagrees with the $\vec{\tau}$ criterion for 45 of the 86 Little Skull Mountain events cited by Harmsen (1994).

The FMSI model specifically optimizes the focal mechanism data with the shear-stress-vector component of the stress tensor, and thus relies solely on the slip direction criteria to obtain a best-fit stress tensor. The FMSI produces some anomalous results in the form of assumed slip on misoriented surfaces. Slip-tendency analysis provides a tool for the rapid identification and assessment of such anomalies, and could be incorporated into a model such as FMSI as an additional constraint in the optimization process. Application of this technique to evaluate earthquakes in the YM region may lead to significantly improved understanding of contemporary fault slip.

5.6 DISCUSSION AND SUMMARY

Slip-tendency analysis provides a means for assessment of relative risk of earthquakes and fault slip. In addition, it provides a test for compatibility of geologic structures thought to have developed in a single stress state focuses exploration for high risk and earthquake-prone blind faults, and serves as an alternative (to shear stress vector orientations) for interpretation of slipped faults from focal mechanism solutions.

Analysis of faults at YM, Nevada, indicates that the key uncertainty with respect to predicting which faults are likely to slip is the orientation of σ_3. Under the conditions that are currently thought to exist (e.g., Stock et al., 1985; Zoback, 1992; Zoback et al., 1992), faults with dips of 60 to 90° and strikes of N 0° E to N 30° E present the greatest risk of both strike-slip and normal dip-slip motion. However, if σ_3 were oriented west-east, virtually all mapped faults in the YM area would be potentially active, given appropriate magnitudes of the principal stresses.

Slip tendency yields information about *relative* magnitudes of T_s. Whether a fault will actually slip depends upon the absolute magnitudes of the principal stresses, and μ for that fault. To determine the likelihood that a fault will slip under conditions in which μ is known, the slip-tendency data must be calibrated by obtaining absolute magnitude data for one of the principal stresses. One method for estimating true stress magnitudes is to compute the likely vertical component of the stress tensor by equating it to lithostatic pressure (Stock et al., 1985). In order to assign a probability that a fault will slip, slip tendency must be calibrated using known active faults, 3D stress tensors, rock-strength data, and friction data.

6 CONCLUSIONS

Many of the potential tectonic hazards to preclosure and postclosure performance of the proposed HLW repository at YM are dependent on faults and fault activity. Fault zones and fault-related fracturing may provide barriers or pathways for groundwater flow and magma ascent. Slip on faults could cause direct disruption of a repository, and ground motion from seismic slip could cause damage during pre- and post-closure periods. From the critical review of tectonic data from the YM region and the surrounding tectonic provinces, several conclusions are drawn:

- Fault characteristics such as: (i) distributed faulting, (ii) blind earthquakes, (iii) blind aseismic slip, (iv) non-correlation across fault, and (v) inadequate characterization of fault-orientation and fault-slip direction may result in underestimation of fault activity from fault-trenching studies.

- Fault orientation and slip direction are critical to realistic estimates of fault slip-rate and magnitude. Fault orientation is also critical to realistic estimation of fault-slip tendency. Additional estimates of fault orientations (at depth) and slip directions in the YM are necessary in order to accurately estimate seismic hazards in the region.

- Apatite FTT results suggest that Quaternary slip on the BMF may have been at a rate of 0.28 mm/yr, significantly faster than the 0.015 mm/yr estimated from trenching in the Tarantula Canyon alluvial fan.

- Analyses of patterns and distribution of Quaternary alluvial fan sediments on the east and west sides of BM indicate that the BMF has been active through the Quaternary and into the Holocene. These studies also suggest a north to south increase in the rate of Quaternary slip on the BMF, with an approximate minimum in the vicinity of Tarantula Canyon.

- Spatial and temporal clusters of seismicity such as the Cedar Mountain/Excelsior Mountain sequence in the 1930's, the Rainbow Mountain/Fairview Peak/Dixie Valley sequence in the 1950's, and the Landers sequence in 1992 indicate a tendency for clusters of intense and unpredicted seismicity to occur near to, but outside of, previously recognized belts of seismicity. The historic record of seismicity in the YM region ($<$200 yr) may be too brief to define belts of seismic activity that are significant over a 10,000 yr period.

- A slip event on the DVFC fault system similar to the 1992 Landers sequence may be capable of causing stress changes in the YM region sufficient to trigger earthquakes on optimally oriented faults.

- Preliminary results from the NRC/CalTech GPS survey record southeastward displacement of site Wahomie with respect to the YM that is clearly related to the Little Skull Mountain earthquake. Survey results also suggest that site Claim, at the north end of BM, is rising with respect to YM.

- Preliminary results from Hunter Mountain subnet of the NRC/CalTech GPS are barely significant at 2σ, but appear to indicate the classical pattern of strain accumulation on a locked right-lateral strike slip fault. These preliminary results suggest a strong potential for seismicity on the Hunter Mountain fault.

- Preliminary results from the Death Valley subnet of the NRC/CalTech GPS are somewhat surprising in that a well-defined and consistent pattern of right-lateral strike-slip has not yet emerged. There is, however, a pattern of relative subsidence of Death Valley with respect to more distant stations (at higher elevation) in the subnet. The implications of this pattern of displacement for the seismic hazard of the DVFC fault zone are not yet clear.

- Slip-tendency analysis of YM faults indicates that many faults in the YM area are favorably oriented for slip in the contemporary stress state. Using the current estimates for the regional stress field, faults that strike between N 0° E and N 30° E with steep dips between 60 and 90° present the greatest risk of both strike-slip and normal dip-slip motion.

- A well constrained stress tensor (magnitudes and orientations) for the YM region would improve the ability to assess potential for slip on known or suspected faults, and their susceptibility to triggering due to minor stress changes. Other factors such as realistic estimates of the coefficient of static friction for faults and knowledge of fault orientation and shape are also needed to improve assessments of fault-slip potential.

7 REFERENCES

Anderson, E.M. 1951. *The Dynamics of Faulting*. London, UK: Oliver and Boyd, Ltd.

Anderson, J.G., J. Louie, J.N. Brune, D. dePolo, M. Savage, and G. Yu. 1992. Seismicity in Nevada apparently triggered by the Landers, California earthquake, June 28, 1992. *EOS, Transactions of the American Geophysical Union 1992 Fall Meeting Abstracts Supplement* 73(43): 393.

Anderson, J.G., J.N. Brune, J.N. Louie, Y. Zeng, M. Savage, G. Yu, Q. Chen, and D. dePolo. 1994. Seismicity in the western Great Basin apparently triggered by the Landers, California, earthquake, 28 June 1992. *Bulletin of the Seismological Society of America* 84(3): 863–891.

Angelier, J. 1979. Determination of the mean principal directions of stresses for a given fault population. *Tectonophysics* 56: T17–T26.

Arrowsmith, R.J., and D.D. Rhodes. 1994. Original forms and initial modifications of the Galway Lake Road scarp formed along the Emerson Fault during the 28 June 1992 Landers, California, Earthquake. *Bulletin of the Seismological Society of America* 84(3): 511–527.

Bean C.P., M.V. Doyle, and G. Entine. 1970. Etching of submicrons pores in irradiated mica. *Journal of Applied Physics* 141: 1,454–1,459.

Bevington, P. 1969. *Data Reduction and Error Analysis for the Physical Sciences*. New York, NY: McGraw Hill.

Bock, Y., R.I. Abbot, C.C. Counselman, S.A. Gourevitch, and R.W. King. 1985. Establishment of three-dimensional geodectic control by interferometry with the Global Positioning System. *Journal of Geophysical Research* 90(B9): 7,689–7,703.

Bodin, P., and J. Gomberg. 1994. Triggered seismicity and deformation between the Landers, California, and Little Skull Mountain, Nevada, earthquakes. *Bulletin of the Seismological Society of America* 84(3): 835–843.

Bott, M.H.P. 1959. The mechanics of oblique slip faulting. *Geological Magazine* 96: 109–117.

Brogan, G.E., K.S. Kellogg, D.B. Slemmons, and C.L. Terhune. 1991. *Late Quaternary faulting along the Death Valley-Furnace Creek Fault System, California and Nevada.* U.S. Geological Survey Open File Report 1991. Washington, DC: U.S. Government Printing Office: 23 p.

Brown, R.D., Jr. 1990. *The San Andreas Fault System—Quaternary Deformation in The San Andreas Fault System, California.* R.E. Wallace, ed. U.S. Geological Survey Professional Paper 1515. Washington, DC: U.S. Government Printing Office: 83–113.

Bull, W.B. 1964. *Geomorphology of segmented alluvial fans in western Fresno County, California.* U.S. Geological Survey Professional Paper 352-E: Washington, DC: U.S. Government Printing Office.

Bull, W.B. 1968. Alluvial fan. *Encyclopedia of Geomorphology*. Reinhold, New York, NY: Fairbridge ed. 7–10.

Burchfiel, B.C., K.V. Hodges, and L.H. Royden. 1987. Geology of Panamint Valley-Saline Valley pull-apart system, California—Palinspastic evidence for low-angle geometry of a Neogene range-bounding fault. *Journal of Geophysical Research* 92(B10): 10,422–10,426.

Byerlee, J.D. 1978. Friction of rocks. *Pure and Applied Geophysics* 116: 615–626.

Carr, W.J. 1984. *Regional Structural Setting of Yucca Mountain, Southwestern Nevada, and Late Cenozoic Rates of Tectonic Activity in Part of the Southwestern Great Basin, Nevada, and California.* U.S. Geological Survey Open-File Report 84-854, 109 p.

Carr, M.D., and S.A. Monsen. 1988. *A Field Trip Guide to the Geology of Bare Mountain.* Special Publication. D.L. Weide, and L.L. Faber, eds. Las Vegas, NV: University of Nevada at Las Vegas: Geoscience Department: 2: 50–57.

Carr, W.J., and L.D. Parrish. 1985. *Geology of Drill Hole USW-VH2, and Structure of Crater Flat, Southwestern, Nevada.* U.S. Geological Survey Open-File Report 85-475. Denver, CO: U.S. Geological Survey.

Connor, C.B., and B.E. Hill. 1995. Three nonhomogeneous Poisson models for the probability of basaltic volcanism: Application to the Yucca Mountain region, Nevada. *Journal of Geophysical Research* 100(B6): 10,107–10,125.

Darby, D.J., and C.M. Meertens. 1995. Terrestrial and GPS measurements of deformation across the Taupo back arc and Hikurangi fore arc regions in New Zealand. *Journal of Geophysical Research* 100(B5): 8,221–8,232.

Davis, J.L., W.H. Prescott, J.L. Svarc, and K.J. Wendt. 1989. Assessment of Global Positioning System measurements for studies of crustal deformation. *Journal of Geophysical Research* 94(B10): 13,635–13,650.

Denny, C.S. 1965. *Alluvial Fans in the Death Valley Region, California and Nevada.* Geological Survey Professional Paper 466. Washington, DC: U.S. Geological Survey.

Denny, C.S. 1967. Fans and pediments. *American Journal of Science* 265: 81–105.

Dohrenwend, J.C. 1982. Surficial Geologic *Map of the Walker Lake 1° by 2° Quadrangle, Nevada-California.* Scale 1:250,000. U.S. Geological Survey Miscellaneous Field Studies Map MF-1382-C. Reston, VA: U.S. Geological Survey.

Dohrenwend, J.C., and B.C. Moring. 1991a. *Reconnaissance Photogeologic Map of Young Faults in the Vya 1° by 2° Quadrangle, Nevada, Oregon, and California.* Scale 1:250,000. U.S. Geological Survey Miscellaneous Field Studies Map MF-2174. Reston, VA: U.S. Geological Survey.

Dohrenwend, J.C., and B.C. Moring. 1991b. *Reconnaissance Photogeologic Map of Young Faults in the Winnemucca 1° by 2° Quadrangle, Nevada, Oregon, and California.* Scale 1:250,000. U.S. Geological Survey Miscellaneous Field Studies Map MF-2175. Reston, VA: U.S. Geological Survey.

Dohrenwend, J.C., and B.C. Moring. 1991c. *Reconnaissance Photogeologic Map of Young Faults in the McDermitt 1° by 2° Quadrangle, Nevada, Oregon, and Idaho.* Scale 1:250,000. U.S. Geological Survey Miscellaneous Field Studies Map MF-2177. Reston, VA: U.S. Geological Survey.

Dohrenwend, J.C., M.A. McKittrick, and B.C. Moring. 1991a. *Reconnaissance Photogeologic Map of Young Faults in the Lovelock 1° by 2° Quadrangle, Nevada and California.* Scale 1:250,000. U.S. Geological Survey Miscellaneous Field Studies Map MF-2178. Reston, VA: U.S. Geological Survey.

Dohrenwend, J.C., M.A. McKittrick, and B.C. Moring. 1991b. *Reconnaissance Photogeologic Map of Young Faults in the Wells 1° by 2° Quadrangle, Nevada, Utah, and Idaho.* Scale 1:250,000. U.S. Geological Survey Miscellaneous Field Studies Map MF-2184. Reston, VA: U.S. Geological Survey.

Dohrenwend, J.C., C.M. Menges, B.A. Schell, and B.C. Moring. 1991c. *Reconnaissance Photogeologic Map of Young Faults in the Las Vegas 1° by 2° Quadrangle, Nevada, California, and Arizona.* Scale 1:250,000. U.S. Geological Survey Miscellaneous Field Studies Map MF-2182. Reston, VA: U.S. Geological Survey.

Dohrenwend, J.C., B.A. Schell, and B.C. Moring. 1991d. *Reconnaissance Photogeologic Map of Young Faults in the Elko 1° by 2° Quadrangle, Nevada and Utah.* Scale 1:250,000. U.S. Geological Survey Miscellaneous Field Studies Map MF-2179. Reston, VA: U.S. Geological Survey.

Dohrenwend, J.C., B.A. Schell, and B.C. Moring. 1991e. *Reconnaissance Photogeologic Map of Young Faults in the Lund 1° by 2° Quadrangle, Nevada and Utah.* Scale 1:250,000. U.S. Geological Survey Miscellaneous Field Studies Map MF-2180. Reston, VA: U.S. Geological Survey.

Dohrenwend, J.C., B.A. Schell, and B.C. Moring. 1991f. *Reconnaissance Photogeologic Map of Young Faults in the Ely 1° by 2° Quadrangle, Nevada and Utah.* Scale 1:250,000. U.S. Geological Survey Miscellaneous Field Studies Map MF-2181. Reston, VA: U.S. Geological Survey.

Dohrenwend, J.C., B.A. Schell, M.A. McKittrick, and B.C. Moring. 1992a. *Reconnaissance Photogeologic Map of Young Faults in the Goldfield 1° by 2° Quadrangle, Nevada and California.* Scale 1:250,000. U.S. Geological Survey Miscellaneous Field Studies Map MF-2183. Reston, VA: U.S. Geological Survey.

Dohrenwend, J.C., B.A. Schell, and B.C. Moring. 1992b. *Reconnaissance Photogeologic Map of Young Faults in the Millett 1° by 2° Quadrangle, Nevada.* Scale 1:250,000. U.S. Geological Survey Miscellaneous Field Studies Map MF- 2176. Reston, VA: U.S. Geological Survey.

Dokka, R.K. and C.J. Travis. 1990. Role of eastern California shear zone in accommodating Pacific-North American plate motion. *Geophysical Research Letters* 17: 1,323–1,326.

Donelick, R.A. 1993. Method of fission track analysis utilizing bulk chemical etching of apatite. United States Patent 5,267,274.

Dong, D., and Y. Bock. 1989. Global Positioning System network analysis with phase ambiguity resolution applied to crustal deformation studies in California. *Journal of Geophysical Research* 94(B4): 3,949–3,966.

Donnellan, A., B.H. Hager, R.W. King, and T.A. Herring. 1993. Geodetic measurement of deformation in the Ventura Basin, southern California. *Journal of Geophysical Research* 98(B12): 21,727–21,739.

Doser, D. 1986. Earthquake processes in the Rainbow Mountain-Fairview Peak-Dixie Valley, Nevada, region 1954-1959. *Journal of Geophysical Research* 91(B12): 12,572–12,586.

Dreger, D.S. 1994. Investigation of the rupture process of the 28 June 1992 Landers earthquake utilizing TERRAscope. *Bulletin of the Seismological Society of America* 84(3): 713–724.

Faulds, J.E., J.W. Bell, D.L. Feuerbach, and A.R. Ramelli. 1994. Geologic Map of the Crater Flat Area, Nevada. Nevada Bureau of Mines and Geology Map 101. Reno, NV: Nevada Bureau of Mines and Geology.

Feigl, K.L., D.C. Agnew, Y. Bock, D. Dong, A. Donnellan, B.H. Hager, T.A. Herring, D.D. Jackson, T.H. Jordan, R.W. King, S. Larsen, K.M. Larson, M.H. Murray, Z. Shen, and F.H. Webb. 1993. Space geodetic measurements of crustal deformation in central and southern California, 1984-1992. *Journal of Geophysical Research* 98(B12): 21,677–21,712.

Ferrill, D.A., S.R. Young, G.L. Stirewalt, A.P. Morris, and D.B. Henderson. 1994a. Tectonic processes in the central Basin and Range region. *NRC High-Level Radioactive Waste Research at CNWRA, January–June 1994.* CNWRA 94-01S. B. Sagar, ed. San Antonio, TX: Center for Nuclear Waste Regulatory Analyses: 139–160.

Ferrill, D.A., S.R. Young, A.P. Morris, D.B. Henderson, and R.H. Martin. 1994b. 3-dimensional stress domains interpreted from fault slip patterns in southern California and Nevada. *Geological Society of America Abstracts with Program—1994 Annual Meeting*. Boulder, CO: Geological Society of America 26(7): 185.

Ferrill, D.A., A.P. Morris, and D.B. Henderson. 1995. Kinematic models of fold-thrust belt curvature: Role of vertical-axis rotation. *EOS, Transactions of the American Geophysical Union* 76(17): S95.

Frizzel, V.A., Jr. and J. Shulters. 1990. *Geologic Map of the Nevada Test Site, Southern Nevada.* Scale 1: 100,000. U.S. Geological Survey Miscellaneous Investigations Series Map I-2046. Reston, VA: U.S. Geological Survey.

Gephart, J.W. 1990. Stress and the direction of slip on fault planes. *Tectonics* 9: 845–858.

Gephart, J.W., and D.W. Forsyth. 1984. An improved method for determining the regional stress tensor using earthquake mechanism data: Application to the San Fernando earthquake sequence. *Journal of Geophysical Research* 89(B11): 9,305–9,320.

Gilmore, T.D. 1992. *Geodetic Leveling Data Used to Define Historical Height Changes Between Tonopah Junction and Las Vegas, Nevada.* U.S. Geological Society Open-File Report 92-450. Menlo Park, CA: U.S. Geological Survey.

Goad, C.C. 1986. Precise Positioning with the Global Positioning System. *Proceedings of the Third International Symposium on Inertial Technology for Surveying and Geodesy.* Alberta, Canada: Surveying Engineering, University of Calgary: 6,005.

Gomberg, J., and P. Bodin. 1994. Triggering of the Ms=5.4 Little Skull Mountain, Nevada, earthquake with dynamic strains. *Bulletin of the Seismological Society of America* 84(3): 844–853.

Gomberg, J., P. Bodin, and S. Harmsen. 1992. Was the Little Skull Mountain, Nevada earthquake of June 29, 1992 triggered by the Landers, California earthquake? *EOS, Transactions of the American Geophysical Union 1992 Fall Meeting Abstracts Supplement* 73(43): 393.

Hahn, O., and F. Strassmann. 1939. Über den Nachweis und das Verhalten der bei Bestrahlung des Urans mittels Neutronen enstehenden Erdalkalimetalle. *Naturwissenschaften.* 27: 11–15.

Hamilton, W.B. 1988. Detachment faulting in the Death Valley Region, California and Nevada: Geologic and hydrologic investigations of a potential nuclear waste disposal site at Yucca Mountain, Southern Nevada. M.D. Carr and J.C. Yount, eds. *U.S. Geological Survey Bulletin* 1,790: 51–85.

Harmsen, S.C. 1994. The Little Skull Mountain, Nevada, earthquake of 29 June 1992: Aftershock focal mechanisms and tectonic stress field implications. *Bulletin of the Seismological Society of America* 84: 1,484–1,505.

Hart, E.W., W.A. Bryant, and J.A. Treiman. 1993. Surface faulting associated with the June 1992 Landers earthquake, California. *California Geology* 46(1): 10–16.

Heward, A.P. 1978. Alluvial fan sequence and megasequence models: With examples from Westphalian D-Stephanian B coal fields, Northern Spain fluvial sedimentology. A.D. Miall, ed. *Canadian Society of Petroleum Geologists Memoir* 5: 669–702.

Hill, D.P., P.A. Reasenberg, A. Michael, W.J. Arabaz, G. Beroza, D. Brumbaugh, J.N. Brune, R. Castro, S. Davis, D. dePolo, W.L. Ellsworth, J. Gomberg, S. Harmsen, L. House, S.M. Jackson, M.J.S. Johnston, L. Jones, R. Keller, S. Malone, L. Munguia, S. Nava, J.C. Pechmann, A. Sanford, R.W. Simpson, R.B. Smith, M. Stark, M. Stickney, A. Vidal, S. Walter, V. Wong, and J. Zollweg. 1993. Seismicity remotely triggered by the magnitude 7.3 Landers, California, earthquake. *Science* 260: 1,617–1,623.

Hofmann-Wellenhof, B., H. Lichtenegger, and J. Collins. 1993. *GPS—Theory and Practice.* Wien, Austria: Springer-Verlag: 326 p.

Holden, N.E. 1989. Total and spontaneous fission half-lives for uranium, plutonium, americium, and curium nuclides. *Pure and Applied Chemistry* 61.

Hooke, R.L. 1967. Processes on arid-region alluvial fans. *Journal of Geology* 75(4): 438–460.

Hooke, R.L. 1968. Steady-state relationships on arid-region alluvial fans in closed basins. *American Journal of Science* 266: 609–629.

Hooke, R.L. 1972. Geomorphic evidence for Late Wisconsin and Holocene tectonic deformation, Death Valley, California. *Geological Society of America Bulletin* 83: 2,073–2,098.

Hudnut, K.W., Y. Bock, M. Cline, P. Fang, Y. Feng, J. Freymuller, X. Ge, W.K. Gross, D. Jackson, M. Kim, N.E. King, J. Langbein, S.C. Larsen, M. Lisowski, Z.K. Shen, J. Svarc, and J. Zhang. 1994. Co-seismic displacements of the 1992 Landers earthquake sequence. *Bulletin of the Seismological Society of America* 84(3): 625–645.

Irvine, P.J., and R.L. Hill. 1993. Surface rupture along a portion of the Emerson Fault. *California Geology* 46(1): 23–26.

Jaeger, J.C., and N.G.W. Cook. 1979. *Fundamentals of Rock Mechanics.* 3rd ed. London, England: Chapman and Hall.

Jennings, C.W. 1992. *Preliminary Fault Activity Map of California.* DMG Open-File Report 92-03. The Resources Agency, California Department of Conservation, Division of Mines and Geology; 76.

Johansson, J.M., T.R. Carlsson, T.M. Carlsson, J.L. Davis, G. Elgered, P. Elosegui, R.T.K. Jaldehag, P.O.J. Jarlemark, J.X. Mitrovica, B.I. Nilsson, R.N. Pysklywec, B.O. Ronnang, H-G Scherneck, and I.I. Shapiro. 1994. Baseline inferences for Fennoscandian rebound observations, sea-level, and tectonics (BIFROST) - One year of GPS observations. *EOS, Transactions of the American Geophysical Union 1994 Fall Meeting Abstracts Supplement* 75(44): 178.

Kanamori, H. 1977. The Energy of Great Earthquakes. *Journal of Geophysical Research* 82(20: 2,981–2,987.

Kanamori, H., H.-K. Thio, D. Dreger, E. Hauksson, and T. Heaton. 1992. Initial investigation of the Landers, California, earthquake of 28 June 1992 using TERRAscope. *Geophysical Research Letters* 19(22): 2,267–2,270.

King, G.C.P., R.S. Stein, and J. Lin. 1994. Static stress changes and triggering of earthquakes. *Bulletin of the Seismological Society of America* 84(3): 935–953.

Klinger, R.E., and L.W. Anderson. 1994. Topographic profiles and their implications for late Quaternary activity on the Bare Mountain fault, Nye County, Nevada. *Geological Society of America Abstracts with Programs—1994 Annual Meeting*. Boulder, CO: Geological Society of America 26(2): 63.

Larson, K.M. 1993. Application of the Global Positioning System to crustal deformation measurements 3—Result from the southern California borderlands. *Journal of Geophysical Research* 98(B12): 21,713–21,726.

Larson, K.M., and D.C Agnew. 1991. Application of the Global Positioning System to crustal deformation measurement 1—Precision and accuracy. *Journal of Geophysical Research* 96(B10): 16,547–16,565.

Larson, K.M., F.H. Webb, and D.C. Agnew. 1991. Application of the Global Positioning System to crustal deformation measurement 2 — The influence of errors in orbit determination networks. *Journal of Geophysical Research* 96(B10): 16,567–16,584.

Laslett, G.M., P.F. Green, I.R. Duddy, and A.J.W. Gleadow. 1987. Thermal annealing of fission tracks in apatite: 2. A quantitative analysis. *Chemical Geology* (Isotope Geosciences Section) 65: 1–13.

Leeder, M.R. 1982. *Sedimentology*. London, England: George Allen and Unwin Ltd.

Leick, A. 1990. *GPS Satellite Surveying*. New York, NY: John Wiley and Sons: 352.

Maldonado, F. 1990. Structural geology of the upper plate of the Bullfrog Hills detachment fault system, southern Nevada: *Geological Society of America Bulletin* 102: 992–1,006.

McGarr, A. 1984. Scaling of ground motion parameters, state of stress, and focal depth. *Journal of Geophysical Research* 89: 6,969–6,979.

McKee, E.H. 1983. Reset K-Ar Ages—Evidence for Three Metamorphic Complexes, Western Nevada: *Isochron/West* (38): 17–20.

McKenzie, D.P. 1969. The relation between fault plane solutions for earthquakes and the directions of the principal stresses. *Bulletin of the Seismological Society of America* 59: 591–601.

Monastersky, R. 1993. Seismic Sunday. *Science News* 142(5): 72–74.

Monsen, S.A. 1983. *Structural Evolution and Metamorphic Petrology of the Precambrian-Cambrian Strata, Northwest Bare Mountain Nevada*: MS Thesis. Davis, CA: University of California at Davis: 66 p.

Monsen, S.A., M.D. Carr, M.C. Reheis, and P.A. Orkild. 1992. *Geologic Map of Bare Mountain, Nye County, Nevada*: U.S. Geological Survey Miscellaneous Investigations Series, Map I-2201. Reston, VA: U.S. Geological Survey.

Morris, A.P., D.A. Ferrill, and D.B. Henderson. 1994. Slip tendency analysis and fault reactivation. *EOS, Transactions of the American Geophysical Union* 75(44): 591.

Naeser, C.W., and N.D. Naeser. 1988. Fission-track dating of Quaternary Events. *Geological Society of America Special Paper* 227. Boulder, CO: Geological Society of America.

Nakata, J.K., C.M. Wentworth, and M.N. Machette. 1982. *Quaternary Fault Map of the Basin and Range and Rio Grande Rift Provinces, Western United States*. U.S. Geological Survey Open File Report 82-579. Washington, DC: U.S. Government Printing Office.

Nilsen, T.H. 1982. Alluvial fan deposits. *Sandstone Depositional Environments*. Tulsa, OK: American Association of Petroleum Geologists: 49–86.

Nuclear Regulatory Commission. 1994. *License Application Review Plan (LARP) for a Geologic Repository for Spent Nuclear Fuel and High-Level Radioactive Waste, Nevada.* NUREG-1323. Washington, DC: Nuclear Regulatory Commission: Office of Nuclear Material Safety and Safeguards.

Ofoegbu, G.I., and D.A. Ferrill. 1995. *Finite Element Modeling of Listric Normal Faulting*. CNWRA 95-008. San Antonio, TX: Center for Nuclear Waste Regulatory Analyses.

Oldow, J.S. 1992. Late Cenozoic displacement partitioning in the northwestern Great Basin. *Walker Lane Symposium: Structure, tectonics and mineralization of the Walker Lane.* Denver, CO: Geological Society of Nevada.

Pezzopane, S.K. 1995. *Preliminary Table of Characteristics of Known and Suspected Quaternary Faults in the Yucca Mountain Region*. U.S. Geological Survey Administrative Report. Denver, CO: U.S. Geological Survey.

Prescott, W.H., J.L. Davis, and J.L Svarc. 1989. Global Positioning System measurements for crustal deformation. *Science* 244: 1,337–1,340.

Press, F., and C. Allen. 1995. Patterns of seismic release in the southern California region. *Journal of Geophysical Research* 100(B4): 6,421–6,430.

Ramsay, J.G. 1967. *Folding and Fracturing of Rocks*. New York, NY: McGraw-Hill.

Ravenhurst, C.E., S.D. Willett, R.A. Donelick, and C. Beaumont. 1994. Apatite fission track thermochronometry from central Alberta: Implications for the thermal history of the Western Canada Sedimentary Basin. *Journal of Geophysical Research* (B10) 99: 20,023–20,041.

Reading, H.G. 1978. *Sedimentary Environments and Facies*. New York, NY: Elsevier.

Reasenberg, P.A., D.P. Hill, A.J. Michael, R.W. Simpson, W.L. Ellsworth, S. Walter, M. Johnson, R. Smith, S.J. Nava, W.J. Arabasz, J.C. Pechmann, J. Gomberg, J.N. Brune, D. DePolo, G. Beroza, S.D. Davis, and J. Zollweg. 1992. Remote seismicity triggered by the M7.5 Landers, California, earthquake of June 28, 1992. *EOS, Transactions of the American Geophysical Union 1992 Fall Meeting Abstracts Supplement* 73(43): 392.

Reheis, M.C. 1986. Preliminary Study of Quaternary faulting on the east side of Bare Mountain, Nye County, Nevada: *Geologic and Hydrologic Investigations of Yucca Mountain, Nevada*. U.S. Geological Survey Open-File Report 86-576: 103–111.

Reheis, M.C. 1988. Preliminary study of Quaternary faulting on the east side of Bare Mountain, Nye County, Nevada. Geologic and Hydrologic Investigations of a Potential Nuclear Waste Disposal Site at Yucca Mountain, Southern Nevada. M.D. Carr and J.C. Yount, eds. *U.S. Geological Survey Bulletin* 1,790: 103-112.

Reheis, M.C. 1994. Holocene faulting along the central Fish Lake Valley Fault Zone, California and Nevada. *Geological Society of America Abstracts with Programs-1994 Cordilleran Section Meeting*. Boulder, CO: Geological Society of America: 26(2): 83.

Reynolds, R.E. 1993. Road guide, Landers: *Earthquakes and aftershocks*. R.E. Reynolds, ed. San Bernardino County Museum Quarterly 40(1): 7–39.

Rogers, A.M., S.C. Harmsen, E.J. Corbett, K. Priestly, and D. dePolo. 1991. *The Seismicity of Nevada and Some Adjacent Parts of the Great Basin Neotectonics of North America*. D.B. Slemmons, E.R. Engdahl, M.D. Zoback, and D.D. Blackwell, eds. Boulder, CO: Geological Society of America 1: 153–184.

Roquemore, G.R., and G.W. Simila. 1994. Aftershocks from the June 28 1992 Landers earthquake: Northern Mojave Desert to the Coso Volcanic Field, California. *Bulletin of the Seismological Society of America* 84(3): 854–862.

Ruland, R., and A. Leick. 1985. Application of GPS to a high-precision engineering survey network. *Proceedings of the First International Symposium on Precise Positioning with the Global Positioning System, Positioning with GPS*. Rockville, MD: National Geodetic Information Center.

Savage, J.C., M. Lisowski, W.K. Gross, N.E. King, and J.L. Svarc. 1994. Strain accumulation near Yucca Mountain, Nevada, 1983-1993. *Journal of Geophysical Research* 99(B9): 18,103–18,107.

Sawyer, D.A., R.J. Fleck, M.A. Lanphere, R.G. Warren, D.E. Broxton, and M.R. Hudson. 1994. Episodic Caldera Volcanism in the Miocene Southern Nevada Volcanic Field: Revised stratigraphic framework, $^{40}Ar/^{39}Ar$ geochronology, and implications for magmatism and extension. *Geological Society of America Bulletin* 106(10): 1,304–1,318.

Scott, R.B. 1990. Tectonic setting of Yucca Mountain, southwest Nevada: Basin and Range extensional tectonics near the latitude of Las Vegas, Nevada. W.P. Wernicke, ed. *Geological Society of America Memoir* 176: 251–282.

Secor, D.T. 1965. Role of fluid pressure in jointing. *American Journal of Science* 263: 633–646.

Shen, Z., and D.D. Jackson. 1993. Global Positioning System reoccupation of early triangulation sites - Tectonic deforation of the southern Coast Ranges. *Journal of Geophysical Research* 96(B6): 9,931–9,946.

Sieh, K., L. Jones, E. Hauksson, K. Hudnut, D. Eberhart-Phillips, T. Heaton, S. Hough, K. Hutton, H. Kanamori, A. Lilje, S. Lindvall, S.F. McGill, J. Mori, C. Rubin, J.A. Spotila, J. Stock, H.K. Thio, J. Treiman, B. Wernicke, and J. Zachariasen. 1993. Near-field investigations of the Landers earthquake sequence, April to July 1992. *Science* 260: 171–176.

Slemmons, D.B. 1957. Geological effects of the Dixie Valley-Fairview Peak, Nevada, earthquakes of December 16, 1954. *Bulletin of the Seismological Society of America* 47: 353–375.

Smith, R.B., and W.J. Arabasz. 1991. Chapter 11—Seismicity of the intermountain seismic belt. *Neotectonics of North America*. D.B. Slemmons, E.R. Engdahl, M.D. Zoback, and D.D. Blackwell, eds. Boulder, CO: Geological Society of America 1: 185–228.

Snyder, D.B., and W.J. Carr. 1984. Interpretation of gravity data in a complex volcano-tectonic setting, south-western Nevada. *Journal of Geophysical Research* 89: 10,193–10,206.

Sowers, J.M., J.R. Unruh, W.R. Lettis, and T.D. Rubin. 1994. Relationship of the Kickapoo Fault to the Johnson Valley and Homestead Valley Faults, San Bernardino County, California. *Bulletin of the Seismological Society of America* 84(3): 528–536.

Stock, J.M., J.H. Healy, S.H. Hickman, and M.D. Zoback. 1985. Hydraulic fracturing stress measurements at Yucca Mountain, Nevada, and relationship to regional stress field. *Journal of Geophysical Research* 90 (B10): 8,691–8,706

Stock, J.M., J.H. Healy, J. Soitek, and L. Mastin. 1986. *Report on televiewer log and stress measurements in holes USW G-3 and UE-25p1, Yucca Mountain, Nye County, Nevada*. U.S. Geological Survey Open File Report 86-369. Washington, DC: U.S. Government Printing Office: 91.

Swadley, W.C., D.L. Hoover, J.N. Rosholt. 1984. *Preliminary Report on Late Cenozoic Faulting and Stratigraphy in the Vicinity of Yucca Mountain, Nye County, Nevada*: U.S. Geological Survey Open File Report 84-788: Reston, VA: U.S. Geological Survey: 42.

Swadley, W.C., and L.D. Parrish. 1988. *Surficial Geologic Map of the Bare Mountain Quadrangle, Nevada.* U.S. Geological Survey Miscellaneous Investigation Series Map I-1826. Denver, CO: U.S. Geologic Survey.

Thatcher, W. 1990. *The San Andreas fault system - Present-Day Crustal Movements and the Mechanics of Cyclic Deformation in The San Andreas Fault System, California.* Geological Survey Professional Paper 1515. Washington, DC. U.S. Government Printing Office: 189–205.

Toppozada, T.R. 1993. The Landers-Big Bear earthquake sequence and its felt effects. *Geology* 46(1): 3–9.

Trimble Navigation, Ltd. 1992. *Trimble Navigation 4000SSE Geodetic System Surveyor Operation Manual.* Part No. 20576-001. Sunnyvale, CA: Trimble Navigation Ltd.

Wagner, G., and P. Van Den Haute. 1992. *Fission-Track Dating*. Solid Earth Science Library. Boston, MA: Kluwer Academic Publishers: Vol. 6.

Wallace, R.E. 1951. Geometry of shearing stress and relationship to faulting. *Journal of Geology* 59: 118–130.

Wells, D., N. Beck, D. Delikaraoglou, A. Kleusberg, E.J. Krakiwsky, G. Lachapelle, R.B. Langley, M. Nakiboglu, K.P. Schwarz, J.M. Tranquilla, and P. Vanicek. 1987. Guide to GPS Positioning. Canadian GPS Associates. Fredericton, N.B., Canada: Canadian GPS Associates.

Wesnousky, S.G., and C.H. Jones. 1994. Oblique slip, slip partitioning, spatial and temporal changes in the regional stress field, and the relative strength of active faults in the Basin and Range, western United States. *Geology* 22: 1,031–1,034.

Wiemer, S., and Wyss, M. 1994. Seismic quiescence before the Landers (M=7.5) and Big Bear (M=6.5) 1992 earthquakes. *Bulletin of the Seismological Society of America* 84(3): 900–916.

Yada, K., T. Tanji, and I. Sunagawa. 1981. Application of lattice imagery to radiation damage investigations in natural zircon. *Physics of Chemistry and Minerals* 7: 47–52.

Young, S.R., and G.L. Stirewalt. 1994. Tectonics. *NRC High-Level Radioactive Waste Research at the Center for Nuclear Waste Regulatory Analyses, July-December 1993.* B. Sagar, ed. CNWRA 93-02S. San Antonio, TX: Center for Nuclear Waste Regulatory Analyses: 9-1 to 9-20.

Young, S.R., A.P. Morris, and G. Stirewalt. 1993a. Geometric analysis of alternative models of faulting at Yucca Mountain, Nevada: *Third Annual International High-Level Radioactive Waste Management Conference Proceedings.* La Grange Park, IL: American Nuclear Society 1: 1,818–1,825.

Young, S.R., G.L. Stirewalt, and A.P. Morris. 1993b. *Geometric Models of Faulting at Yucca Mountain. CNWRA 92-008.* San Antonio, TX: Center for Nuclear Waste Regulatory Analyses.

Zhang, P., D.B. Slemmons, and F. Mao. 1991. Geometric Pattern, Rupture Termination and Fault Segmentation of the Dixie Valley-Pleasant Valley active normal fault system, Nevada, USA. *Journal of Structural Geology* 13(2): 165–176.

Zoback, M.L. 1992. First- and second-order patterns of stress in the lithosphere: The World Stress Map Project. *Journal of Geophysical Research* 97 (B8): 11,703–11,728.

Zoback, M.L. and 36 Project participants. 1992. World Stress map maximum horizontal stress orientations. *Journal of Geophysical Research* 97(B8).

NRC FORM 335 (2-89) NRCM 1102, 3201, 3202

U.S. NUCLEAR REGULATORY COMMISSION

BIBLIOGRAPHIC DATA SHEET

(See instructions on the reverse)

1. REPORT NUMBER (Assigned by NRC, Add Vol., Supp., Rev., and Addendum Numbers, if any.)
NUREG/CR-6401
CNWRA 95-017

2. TITLE AND SUBTITLE
Faulting in the Yucca Mountain Region

Critical Review and Analyses of Tectonic Data from the Central Basin and Range

3. DATE REPORT PUBLISHED
MONTH: March
YEAR: 1996

4. FIN OR GRANT NUMBER
L2200

5. AUTHOR(S)
D.A. Ferrill, G.L. Stirewalt, D.B. Henderson, J. Stamatakos, A.P. Morris, K.H. Spivey, CNWRA
B.P. Wernicke, CIT

6. TYPE OF REPORT

7. PERIOD COVERED *(Inclusive Dates)*

8. PERFORMING ORGANIZATION – NAME AND ADDRESS *(If NRC, provide Division, Office or Region, U.S. Nuclear Regulatory Commission, and mailing address, if contractor, provide name and mailing address.)*
Center for Nuclear Waste Regulatory Analyses
Southwest Research Institute
6220 Culebra Road
San Antonio, TX 78228-0510

Division of Geological and Planetary Science
California Institute of Technology
Pasadena, CA 91125

9. SPONSORING ORGANIZATION – NAME AND ADDRESS *(If NRC, type "Same as above"; if contractor, provide NRC Division, Office or Region, U.S. Nuclear Regulatory Commission, and mailing address.)*
Division of Regulatory Applications
Office of Nuclear Regulatory Research
U.S. Nuclear Regulatory Commission
Washington, DC 20555-0001

10. SUPPLEMENTARY NOTES
E. O'Donnell, NRC Project Manager

11. ABSTRACT *(200 words or less)*

Yucca Mountain, Nevada, has been proposed as the potential site for a high-level waste (HLW) repository. The tectonic setting of Yucca Mountain presents several potential hazards for a proposed repository, such as potential for earthquake seismicity, fault disruption, basaltic volcanism, magma channeling along pre-existing faults, and faults and fractures that may serve as barriers or conduits for ground water flow. Characterization of geologic structures and tectonic processes will be necessary to assess compliance with regulatory requirements for the proposed HLW repository. In this report, we specifically investigate fault slip, seismicity, contemporary stain, and fault-slip potential in the Yucca Mountain region with regard to Key Technical Uncertainties outlined in the License Application Review Plan (Sections 3.2.1.5 through 3.2.1.9 and 3.2.2.8). These investigations center on (i) alternative methods of determining the slip history of the Bare Mountain Fault, (ii) cluster analysis of historic earthquakes, (iii) crustal strain determinations from Global Positioning System measurements, and (iv) three-dimensional slip-tendency analysis. The goal of this work is to assess uncertainties associated with neotectonic data sets critical to the Nuclear Regulatory Commission and the Center for Nuclear Waste Regulatory Analyses' ability to provide prelicensing guidance and perform license application review with respect to the proposed HLW repository at Yucca Mountain.

12. KEY WORDS/DESCRIPTORS *(List words or phrases that will assist researchers in locating the report.)*
faulting, analyses, tectonic data, hazards, high-level waste (HLW) repository, Yucca Mountain, Bare Mountain Fault, earthquakes

13. AVAILABILITY STATEMENT
unlimited

14. SECURITY CLASSIFICATION
(This Page) unclassified
(This Report) unclassified

15. NUMBER OF PAGES

16. PRICE

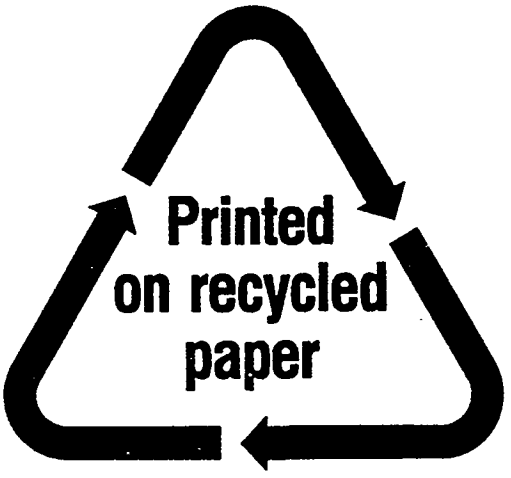

Federal Recycling Program

DISCLAIMER